

Electronic Supporting Information

A new family of luminescent $[\text{Pt}(\text{pbt})_2(\text{C}_6\text{F}_5)\text{L}]^{n+}$ ($n = 1, 0$) Complexes: Synthesis, Optical and Cytotoxic Studies.

David Gómez de Segura,^a Nora Giménez,^a David Rincón-Montón,^a M. Teresa Moreno,^{*a} José G. Pichel,^{b, c} Icíar P. López^{*b} and Elena Lalinde^{*a}

^a D. Gómez de Segura, Dr. N. Giménez, D. Rincón, Prof. Dr. M. T. Moreno, Prof. Dr. E. Lalinde. Departamento de Química-Centro de Síntesis Química de La Rioja, (CISQ), Universidad de La Rioja, 26006, Logroño, Spain. E-mail: elenalalinde@unirioja.es; teresa.moreno@unirioja.es

^b Dr. I. P. López, Dr. J. G. Pichel.

Lung Cancer and Respiratory Diseases Unit (CIBIR), Fundación Rioja Salud, 26006, Logroño, Spain. E-mail: iplgarcia@riojasalud.es

^c Dr. J. G. Pichel.

Spanish Biomedical Research Networking Centre in Respiratory Diseases (CIBERES), ISCIII, E-28029, Madrid, Spain. <https://www.ciberes.org>.

Contents:	Page
1.- Experimental Section.....	S2
2.- NMR Spectra.....	S7
3.- Crystal Structures.....	S20
4.- Photophysical Properties and Theoretical calculations.....	S25
5.- Biological Studies.....	S48

1.- Experimental Section

General Comments. All reactions were carried out under an atmosphere of dry argon, using standard Schlenk techniques. Solvents were obtained from a solvent purification system (M-BRAUN MS SPS-800). Elemental analyses were carried out with a Carlo Erba EA1110 CHNS/O microanalyzer. Mass spectra were recorded by electrospray ionization on an interphase ESI/APCI Bruker MicrOTOF-Q spectrometer with positive ion mode, with MeOH/H₂O 90/10 and 0.1% formic acid as a mobile phase. IR spectra were obtained on a Fourier Transform Perkin Elmer Spectrum UATR Two spectrophotometer, with the diamond crystal ATR attachment, which covers the region between 4000 and 450 cm⁻¹; data processing was carried out with Omnic. NMR spectra were recorded on a Bruker AVANCE ARX 400 spectrometer at 298 K. Chemical shifts are reported in parts per million (ppm) relative to external standards (SiMe₄ for ¹H and ¹³C{¹H}, CFCl₃ for ¹⁹F{¹H} and H₃PO₄ for ³¹P{¹H})) and all coupling constants are given in hertz (Hz). The UV-VIS absorption spectra were measured with a Hewlett Packard 8453 spectrophotometer. Excitation and emission spectra were obtained with a Shimadzu RF-60000 and Edimburg FLS 1000 spectrofluorimeters. Lifetime measurements were performed with a Jobin Yvon Horiba Fluorolog 3-22 Tau-3 spectrofluorimeter operating in the phosphorimeter mode (with an F1-1029 lifetime emission PMT assembly, using 450 W Xe lamp) or with a Datastation HUB-B with a nanoLED (the nanoLEDs employed for lifetime measurements were of 390 or 370 nm with pulse lengths of 0.8-1.4 ns) controller and software DAS6 and with Edimburg FLS 1000 spectrofluorimeter with μF2 pulse lamp (Power: 100 W, Fuse: 3.15 Amp A/S). Quantum Yields were measured with Hamamatsu Absolute PL Quantum Yield Measurement System. The complex *fac*-[Pt(pbt)₂(C₆F₅)Cl]¹ and the ligands pybt² and bpybt³ were prepared according to the published procedure. Other commercially available reagents were used as received.

Synthesis of *fac*-[Pt(pbt)₂(C₆F₅)(4-Mepy)](PF₆) (**1**)

4-methylpyridine (49 μL, 0.503 mmol), TiPF₆ (0.117 g, 0.335 mmol) and KClO₄ (excess) were added to a suspension of *fac*-[Pt(pbt)₂(C₆F₅)Cl] (0.144 g, 0.168 mmol) in 20 mL of 1,2-dichloroethane. The white suspension was refluxed for 5 h and evaporated to dryness. Then, 30 mL of CH₂Cl₂ were added and the mixture was filtered through celite. The filtrate was evaporated to dryness and treated with Et₂O (~10 mL) to give **1** as white solid (0.148 g, 83%). ESI (+): *m/z* (%) 875 [M-PF₆]⁺ (100), 782 [{M-(4-Mepy)}-

$\text{PF}_6]^+$ (95). Anal. calcd for $\text{C}_{38}\text{H}_{23}\text{N}_3\text{PPtS}_2$ (1020.78): C, 44.71; H, 2.27; N, 4.12; S, 6.28. Found: 45.00; H, 2.68; N, 4.31; S, 6.09 (%). IR (ATR) (cm^{-1}): $\nu(\text{C}-\text{F}_{\text{C}_6\text{F}_5})$ 1074 (m), 968 (m); $\nu(\text{C}_6\text{F}_5)_{\text{X-sens}}$ 758(m). Conductivity ($\text{cm}^2 \cdot \text{mol}^{-1} \cdot \Omega^{-1}$ in MeOH): 82.4. ^1H NMR (400 MHz, CD_3COCD_3): δ 8.77 (d, 2H, $^3J_{\text{H-H}} = 5$, $^3J_{\text{Pt-H}} = 16$, H^{14}), 8.45 (d, $^3J_{\text{H-H}} = 8$, H^4), 8.26 (d, $^3J_{\text{H-H}} = 8$, H^7'), 8.05 (d, $^3J_{\text{H-H}} = 7.5$, H^8), 7.80 (m, $^3J_{\text{H-H}} \approx J_{\text{H-oF}} = 6$, $^3J_{\text{Pt-H}} = 40$, H^{11}), 7.78-7.71 (m, $^3J_{\text{H-H}} = 8$, 2H, $\text{H}^{8',5}$), 7.69-7.61 (m, 2H, $\text{H}^{6,7}$), 7.58-7.52 (m, 2H, $\text{H}^{9,10}$), 7.49-7.48 (m, 3H, $\text{H}^{6,15}$), 7.20-7.09 (m, 3H, $\text{H}^{5',9',10'}$), 6.88 (t, $^3J_{\text{H-H}} \approx J_{\text{H-oF}} = 6$, $^3J_{\text{Pt-H}} = 40$, $\text{H}^{11'}$), 6.47 (d, $^3J_{\text{H-H}} = 8.5$, $\text{H}^{4'}$), 2.45 (s, 3H, CH_3 (4-Mepy)). $^{13}\text{C}\{\text{H}\}$ NMR (100.6 MHz, CD_3COCD_3): δ 181.5 (s, $^2J_{\text{Pt-C}} = 71$, $\text{C}^{2/2'}$), 181.2 (s, $^2J_{\text{Pt-C}} = 58$, $\text{C}^{2/2'}$), 155.2 (s, C^{16}), 152.4 (s, C^{14}), 151.2 (d, $J_{\text{C-oF}} = 2$, $^2J_{\text{Pt-C}} = 13$, C^{7a}), 147.7 (s, $^3J_{\text{Pt-C}} = 21$, $\text{C}^{3a'}$), 138.3 (d, $J_{\text{C-oF}} = 1.5$, C^{12}), 137.7 (s, $\text{C}^{13'}$), 137.5 (s, C^{13}), 135.3 (m, $\text{C}^{11'}$), 135.1 (s, $\text{C}^{9/10}$), 134.5 (d, $J_{\text{C-oF}} = 3$, $^2J_{\text{Pt-C}} = 45$, C^{11}), 133.5 (s, $\text{C}^{10'}$), 133.2 (s, C_{pbt}), 133.1 (s, C_{pbt}), 130.0 (s, $\text{C}^{9'/5'}$), 129.4 (s, C^6), 129.2 (s, C^8), 129.1 (s, $\text{C}^{5/8'}$), 129.0 (s, C^6'), 128.9 (s, $\text{C}^{5/8'}$), 128.6 (s, $\text{C}^{9/10}$), 128.3 (s, $\text{C}^{9'/5'}$), 128.2 (s, C_{pbt}), 128.1 (s, C^{15}), 125.9 (s, C^7'), 125.2 (s, C^4), 122.4 (d, $J_{\text{C-oF}} = 14$, C^7), 117.7 (s, $\text{C}^{4'}$), 21.3 (s, CH_3 (4-Mepy)). $^{19}\text{F}\{\text{H}\}$ NMR (376.5 MHz, CD_3COCD_3): δ -72.6 (d, $^1J_{\text{F-P}} = 707$, PF_6), -113.9 (dm, $^3J_{\text{Pt-oF}} = 113.5$, $1o\text{-F}_{\text{C}_6\text{F}_5}$), -116.4 (dm, $^3J_{\text{Pt-oF}} = 100.6$, $1o\text{-F}_{\text{C}_6\text{F}_5}$), -158.9 (t, $p\text{-F}_{\text{C}_6\text{F}_5}$), -163.0 (m, $1m\text{-F}_{\text{C}_6\text{F}_5}$), -163.8 (m, $1m\text{-F}_{\text{C}_6\text{F}_5}$). $^{31}\text{P}\{\text{H}\}$ NMR (161.9 MHz, CD_3COCD_3): δ -144.1 (sept, $^1J_{\text{P-F}} = 707$, PF_6).

Synthesis of *fac*-[Pt(pbt)₂(C₆F₅)(pybt)](PF₆) (2)

Complex **2** was obtained as a white solid (0.088 g, 60%) following a similar procedure as **1**, refluxing for 15 h a mixture of *fac*-[Pt(pbt)₂(C₆F₅)Cl] (0.120 g, 0.147 mmol), 4-pyridylbenzothiazole (0.093 g, 0.438 mmol), TiPF₆ (0.102 g, 0.292 mmol) and excess of KClO₄ (~1:30). ESI (+): *m/z* (%) 994 [M-PF₆]⁺ (100), 782 [{M-PF₆}⁻-pybt]⁺ (65). Anal. calcd for $\text{C}_{44}\text{H}_{24}\text{F}_{11}\text{N}_4\text{PtS}_3\text{P}$ (1139.92): C, 46.36; H, 2.12; N, 4.92; S, 8.44. Found: C, 46.35; H, 2.18; N, 6.62; S, 10.31 %. IR (ATR) (cm^{-1}): $\nu(\text{C}-\text{F}_{\text{C}_6\text{F}_5})$ 1078 (w), 976 (m); $\nu(\text{C}_6\text{F}_5)_{\text{X-sens}}$ 758 (m). Conductivity ($\text{cm}^2 \cdot \text{mol}^{-1} \cdot \Omega^{-1}$ in MeOH): 82.4. ^1H NMR (400 MHz, CD_3COCD_3): δ 9.10 (d, $^3J_{\text{Pt-H}} = 25$, H^{14}), 8.44 (d, $^3J_{\text{H-H}} = 9$, H^4), 8.26 (m, 2H, $\text{H}^{7',15}$), 8.18 (d, $^3J_{\text{H-H}} = 8$, H^{22}), 8.11 (d, $^3J_{\text{H-H}} = 8$, H^{19}), 8.04 (m, H^8), 7.91-7.80 (m, 2H, $\text{H}^{11,20/21}$), 7.77 (dd, $^3J_{\text{H-H}} = 8$, $^4J_{\text{H-H}} = 1$, $\text{H}^{8'}$), 7.73 (td, $^3J_{\text{H-H}} = 8$, $^4J_{\text{H-H}} = 1$, H^5), 7.69-7.48 (m, 6H, $\text{H}^{6,7,9,10,6',20/21}$, pybt), 7.22-7.09 (m, 3H, $\text{H}^{5',9',10'}$), 6.88 (t, $^3J_{\text{H-H}} \approx J_{\text{H-oF}} = 7$, $^3J_{\text{Pt-H}} = 41$, $\text{H}^{11'}$), 6.47 (d, 1H, $^3J_{\text{H-H}} = 9$, $\text{H}^{4'}$). $^{13}\text{C}\{\text{H}\}$ NMR (100.6 MHz, CD_3COCD_3): δ 181.8 (s, $\text{C}^{2/2'}$), 181.2 (s, $\text{C}^{2/2'}$), 163.3 (s, $\text{C}^{6'/16}$), 154.9 (s, C^{21}), 154.1 (s, C^{14}), 151.3 (s, C^{7a}), 147.7 (s, $\text{C}^{3a'}$), 145.2 (s, C^6), 138.3 (s, C^{12}), 137.7 (s, $\text{C}^{13'}$), 137.6 (s, C^{13}), 137.0 (s, $\text{C}^{12'}$), 135.3

(s, C^{11'}), 135.1 (s), 135.0 (s, C^{20/21}), 134.4 (d, $J_{C-F} = 2$, C¹¹), 133.6 (s, C^{10'}), 133.3 (s, C^{7a'}), 130.2 (s), 129.7 (s, C⁸), 129.5 (s), 128.8 (s, C^{8'}), 128.5 (s), 128.3 (s), 126.0 (s, C¹⁵), 125.4 (s, C⁴), 123.6 (s, C⁷), 122.6 (d, $J_{C-F} = 13$, C⁷), 117.8 (s, C^{4'}). ¹⁹F{¹H} NMR (376.5 MHz, CD₃COCD₃): δ -72.6 (d, $^1J_{F-P} = 705$, PF₆), -114.0 (dm, $^3J_{Pt-oF} = 97$, 1o-F_{C6F5}), -116.2 (dm, $^3J_{Pt-oF} = 97$, 1o-F_{C6F5}), -158.8 (t, p-F_{C6F5}), -162.9 (m, 1m-F_{C6F5}), -163.6 (m, 1m-F_{C6F5}). ³¹P{¹H} NMR (161.9 MHz, CD₃COCD₃): δ -144.2 (sept., $^1J_{P-F} = 705$, PF₆).

Synthesis of *fac*-[Pt(pbt)₂(C₆F₅)(4,4'-bpy)](PF₆) (3)

To a suspension of *fac*-[Pt(pbt)₂(C₆F₅)Cl] (0.105 g, 0.128 mmol) in deoxygenated 1,2-dichloroethane (20 mL), 4,4'-bipyridine (0.099 g, 0.633 mmol), TiPF₆ (0.104 g, 0.298 mmol) and excess of KClO₄ (~1:30) were added. After refluxed for 15 h, the solvent was evaporated to dryness. Then, the yellow residue was dissolved in CH₂Cl₂ (~25 mL), filtered through celite and evaporated to dryness. The residue was treated with Et₂O (~20 mL), filtered and then evaporated to dryness. The residue was treated with iPrOH (~5 mL) to obtain complex **3** as a white solid (0.088 g, 66%). ESI (+): *m/z* (%) 938 [M-PF₆]⁺ (100), 782 [{M-PF₆}·4,4'-bipy]⁺ (65). Anal. calcd for C₄₂H₂₄F₁₁N₄PPtS₂ (1083.84): C, 46.54; H, 2.23; N, 5.17; S, 5.92. Found: C, 45.67; H, 2.55; N, 6.43; S, 7.66%. IR (ATR) (cm⁻¹): ν(C-F_{C6F5}) 1071 (m), 974 (m); ν(C₆F₅)_{X-sens} 757 (m). Conductivity (cm²·mol⁻¹·Ω⁻¹ in MeOH): 90. ¹H NMR (400 MHz, CD₃COCD₃): δ 9.06 (d, $^3J_{Pt-H} = 23$, H¹⁴), 8.73 (s, H¹⁹), 8.44 (d, $^3J_{H-H} = 8$, H⁴), 8.26 (d, $^3J_{H-H} = 8$, H^{7'}), 8.06-8.04 (m, H^{8,15}), 7.85 (t, $^3J_{H-H} \sim J_{H-oF} = 6$, $^3J_{Pt-H} = 43$, H¹¹), 7.77-7.63 (m, H^{5,6,7,18}), 7.63 (d, $^3J_{H-H} = 8$, H^{8'}), 7.56-7.48 (m, H^{9,10,6'}), 7.20-7.10 (m, H^{5',9',10'}), 6.87 (t, $^3J_{H-H} \approx J_{H-oF} = 6$, $^3J_{Pt-H} = 41$, H^{11'}), 6.50 (d, $^3J_{H-H} = 8$, H⁴). ¹³C{¹H} NMR (100.6 MHz, CD₃COCD₃): δ 181.6 (s, C^{2/2'}), 181.1 (s, C^{2/2'}), 153.7 (s, C¹⁴), 151.9 (s, C¹⁹), 150.8 (s, C^{7a}), 147.6 (s, C^{3a'}), 143.2 (s), 138.2 (d, $J_{C-F} = 2$, C¹²), 137.5 (s, C^{13'/13}), 135.2 (s, C^{9/10}), 134.9 (d, $J_{C-F} = 8$, C¹¹), 134.4 (s, C^{11'}), 133.5 (s, C^{10'}), 133.1 (s, C^{7a'}), 130.0 (s, C^{5'}), 129.5 (s, C^{9/10}), 129.3 (s, C⁸), 128.6 (s, C^{6'}), 128.4 (s, C^{9'}), 128.1 (s, C⁶), 125.8 (s, C^{7'}), 125.1 (s, C⁴), 122.3 (d, $J_{C-F} = 15$, C⁷), 117.8 (s, C^{4'}). ¹⁹F{¹H} NMR (376.5 MHz, CD₃COCD₃): δ -72.6 (d, $^1J_{F-P} = 690$, PF₆), -114.0 (dm, $J_{Pt-oF} = 100$, 1o-F, C₆F₅), -116.3 (dm, $^3J_{Pt-oF} = 101$, 1o-F_{C6F5}), -158.8 (m, p-F_{C6F5}), -162.9 (m, 1m-F_{C6F5}), -163.7 (m, 1m-F_{C6F5}). ³¹P{¹H} NMR (161.9 MHz, CD₃COCD₃): δ -144.3 (sept., $^1J_{P-F} = 705$, PF₆).

Synthesis of *fac*-[Pt(pbt)₂(C₆F₅)(bpe)](PF₆) (4)

1,2-bis-(4-pyridyl)ethylene (0.067 g, 0.368 mmol), TiPF₆ (0.085 g, 0.243 mmol) and excess of KClO₄ (~1:30) were added to a suspension of *fac*-[Pt(pbt)₂(C₆F₅)Cl] (0.100 g,

0.122 mmol) in deoxygenated 1,2-dichloroethane (20 mL) and the mixture was refluxed for 10 h in absence of light. Then, the solvent was evaporated to dryness. The residue was dissolved in CH₂Cl₂ (~25 mL), filtered through celite and evaporated to dryness. The treatment of the residue with Et₂O (~10 mL) and MeOH (~5 mL) gives **4** as a white solid (0.065 g, 45%). ESI (+): *m/z* (%) 964 [M-PF₆]⁺ (82), 782 [{M-bpe}-PF₆]⁺ (100). Anal. calcd for C₄₄H₂₆F₁₁N₄PPtS₂ (1109.88): C, 47.62; H, 2.36; N, 5.05; S, 5.78. Found: C, 47.39; H, 2.45; N, 5.04; S, 5.55%. IR (ATR) (cm⁻¹): ν (C-F_{C₆F₅}) 1077 (m), 972 (m); ν (C₆F₅)_{X-sens} 757 (m). Conductivity (cm²·mol⁻¹·Ω⁻¹ in MeOH): 90. ¹H NMR (400 MHz, CD₃COCD₃): δ 8.90 (d, 2H, ³J_{H-H} = 5, ³J_{Pt-H} = 15, H¹⁴), 8.61 (d, 2H, ³J_{H-H} = 5, H²¹), 8.46 (d, ³J_{H-H} = 8, H⁴), 8.27 (d, ³J_{H-H} = 8, H^{7'}), 8.06 (d, ³J_{H-H} = 7, H⁸), 7.84 (d, 2H, ³J_{H-H} = 6, H¹⁵), 7.80-7.63 (m, 5H, H^{6,5,10,11,8'}), 7.57-7.49 (m, 6H, H^{6',9,17,18,20}), 7.21-7.10 (m, 4H, H^{5',10',9',7'}), 6.89 (t, ³J_{H-H} ≈ J_{H-oF} = 7, ³J_{Pt-H} = 40, H^{11'}), 6.50 (d, ³J_{H-H} = 8, H^{4'}). ¹⁹F{¹H} NMR (376.5 MHz, CD₃COCD₃): δ -72.6 (d, ¹J_{F-P} = 708, PF₆), -114.0 (dm, ³J_{Pt-oF} = 103, 1o-F_{C₆F₅}), -116.4 (dm, ³J_{Pt-oF} = 102, 1o-F_{C₆F₅}), -158.9 (t, 1p-F_{C₆F₅}), -163.0 (m, 1m-F_{C₆F₅}), -163.8 (m, 1m-F_{C₆F₅}). ³¹P{¹H} NMR (161.9 MHz, CD₃COCD₃): δ -144.3 (sept, ¹J_{F-P} = 708, PF₆).

Synthesis of *fac*-[Pt(pbt)₂(C₆F₅)(bpyb)](PF₆) (**5**)

Compound **5** was obtained as a white solid (0.118 g, 86%) following the same procedure as **2** starting from *fac*-[Pt(pbt)₂(C₆F₅)Cl] (0.100 g, 0.122 mmol), 1,4-bis-(pyridyl)-butadiyne (bpyb) (0.075 g, 0.359 mmol), TiPF₆ (0.096 g, 0.276 mmol) and excess of KClO₄ (~1:30). ESI (+): *m/z*, 986 [M-PF₆]⁺ (55), 782 [{M-bpyb}-PF₆]⁺ (100). Anal. calcd for C₄₆H₂₄F₁₁N₄PPtS₂ (1131.89): C, 48.81; H, 2.14; N, 4.95; S, 5.66. Found: C, 49.09; H, 2.43; N, 6.60; S, 7.51%. IR (ATR) (cm⁻¹): ν (C≡C) 2222 (w), ν (C-F_{C₆F₅}) 1076 (d), 971 (d); ν (C₆F₅)_{X-sens} 751 (m). Conductivity (cm²·mol⁻¹·Ω⁻¹ in MeOH): 72.1. ¹H NMR (400 MHz, CD₃COCD₃): δ 9.03 (d, 2H, ³J_{Pt-H} = 25, H¹⁴), 8.67 (d, 2H, ³J_{H-H} = 6, H²³), 8.46 (d, ³J_{H-H} = 8, H⁴, pbt), 8.26 (d, ³J_{H-H} = 9, H^{7'}), 8.06 (dd, ³J_{H-H} = 7, ⁴J_{H-H} = 2, H⁸), 7.90-7.63 (m, 7H, H^{5,6,7,11,8',15}), 7.59-7.46 (m, 5H, H^{9,10,6',22}), 7.20-7.09 (m, 3H, H^{5',9',10'}), 6.88 (t, ³J_{H-H} ≈ J_{H-oF} = 13, ³J_{Pt-H} = 42, H^{11'}), 6.47 (d, ³J_{H-H} = 9, H^{4'}). ¹³C{¹H} NMR (100.6 MHz, CD₃COCD₃): δ 181.8 (s, C^{2/2'}), 181.2 (s, C^{2/2'}), 153.4 (s, C¹⁴), 151.4 (s, C²²), 151.3 (s, C^{7a}), 147.7 (s, C^{3a'}), 138.3 (d, J_{C-F} = 2, C¹²), 137.7 (s, C^{13'}), 137.6 (s, C¹³), 135.4 (s, C^{9/10}), 135.2 (s, C_{pbt}), 135.1 (s, C^{11'}), 134.6 (d, J_{C-F} = 2, C¹¹), 133.7 (s, C^{10'}), 133.3 (s, C^{7a'}), 131.0 (s, C_{pbt}), 130.9 (s, C¹⁵), 130.2 (s, C^{5'}), 129.8 (s, C^{9/10}), 129.6 (s, C^{5/8'}), 129.5 (s, C⁸), 129.0 (s, C^{5/8'}), 128.9 (s, C^{6'}), 128.6 (s, C^{9'}), 128.3 (s, C⁶), 127.0 (s, C²²), 125.0 (s, C^{7'}), 125.4

(s, C⁴), 122.5 (d, $J_{C-F} = 14$, C⁷), 117.8 (s, C^{4'}), 84.0 (s, C²⁰), 82.1 (s, C¹⁸), 81.2 (s, C¹⁹), 79.1 (s, C¹⁷), 77.1 (s, C^{16/21}), 76.4 (s, C^{16/21}). ¹⁹F{¹H} NMR (376.5 MHz, CD₃COCD₃): δ -72.6 (d, $^1J_{F-P} = 710$, PF₆), -114.1 (dm, $^3J_{Pt-oF} = 102$, 1o-F_{C6F5}), -116.4 (dm, $^3J_{Pt-oF} = 102$, 1o-F_{C6F5}), -158.7 (t, p-F_{C6F5}), -162.9 (m, 1m-F_{C6F5}), -163.5 (m, 1m-F_{C6F5}). ³¹P{¹H} NMR (161.9 MHz, CD₃COCD₃): δ -144.2 (sept, $^1J_{P-F} = 710$, PF₆).

Synthesis of *fac*-[Pt(pbt)₂(C₆F₅)(OCOCF₃)] (6)

Compound **6** was obtained as a white solid (0.185 g, 84%) by refluxing for 6 h a mixture of *fac*-[Pt(pbt)₂(C₆F₅)Cl] (0.201 g, 0.246 mmol) and silver trifluoroacetate (0.060 g, 0.271 mmol) in acetone (20 mL). Then, the suspension was filtered through celite, evaporated to dryness and treated with Et₂O (5 mL). ESI (+): *m/z*, 782 [M-OCOCF₃]⁺ (100). Anal. calcd for C₄₆H₂₄F₁₁N₄PPtS₂ (1131.89): C, 45.59; H, 1.80; N, 3.13; S, 7.16. Found: C, 43.64; H, 2.13; N, 3.1; S, 6.06%. IR (ATR) (cm⁻¹): ν (C-F_{C6F5}) 1072 (d), 970 (d); ν (C₆F₅)_{X-sens} 753 (m). ¹H NMR (400 MHz, CD₃COCD₃): δ= 8.60 (t, $^3J_{H-H} = 7$, H⁷), 7.93 (d, $^3J_{H-H} = 7$, H⁴), 7.65 (d, $^3J_{H-H} = 8$, H^{7'}), 7.52 (d, $^3J_{H-H} = 7.5$, H⁸), 7.29 (d, $^3J_{H-H} = 6.3$, H^{5/6}), 7.27 (d, $^3J_{H-H} = 6.3$, H^{5/6}), 7.22 (d, $^3J_{H-H} = 8$, H^{8'}), 7.12 (dd, $^3J_{H-H} = 8$, $J_{H-oF} = 4$, $^3J_{Pt-H} = 38$, H¹¹), 7.02 (t, $^3J_{H-H} = 7.5$, H⁹), 6.92 (t, $^3J_{H-H} = 7$, H¹⁰), 6.87 (t, $^3J_{H-H} = 8$, H^{6'}), 6.65 (t, $^3J_{H-H} = 7.5$, H^{9'}), 6.55 (t, $^3J_{H-H} = 7$, H^{10'}), 6.51 (t, $^3J_{H-H} = 8$, H^{4'}), 6.22 (dd, $^3J_{H-H} = 8$, $J_{H-oF} = 4$, $^3J_{Pt-H} = 48$, H^{11'}), 5.93 (d, $^3J_{H-H} = 8.5$, H^{4'}). ¹⁹F{¹H} NMR (282.4 MHz, CD₃COCD₃): δ= -75.3 (s, $^4J_{Pt-F} = 4.1$, CF₃), -118.3 (dt, $^3J_{F-F} = 23.7$, $J_{H-F} \approx 4J_{F-F} = 6$, $^3J_{Pt-oF} = 115.1$, 1o-F_{C6F5}), -118.6 (dt, $^3J_{F-F} = 24.3$, $J_{H-F} = 6$, $^3J_{Pt-oF} = 97.6$, 1o-F_{C6F5}), -161.2 (tt, $^3J_{F-F} = 20.3$, $^4J_{F-F} = 10$, p-F_{C6F5}), -165.1 (m, m-F_{C6F5}), -165.8 (m, m-F_{C6F5}).

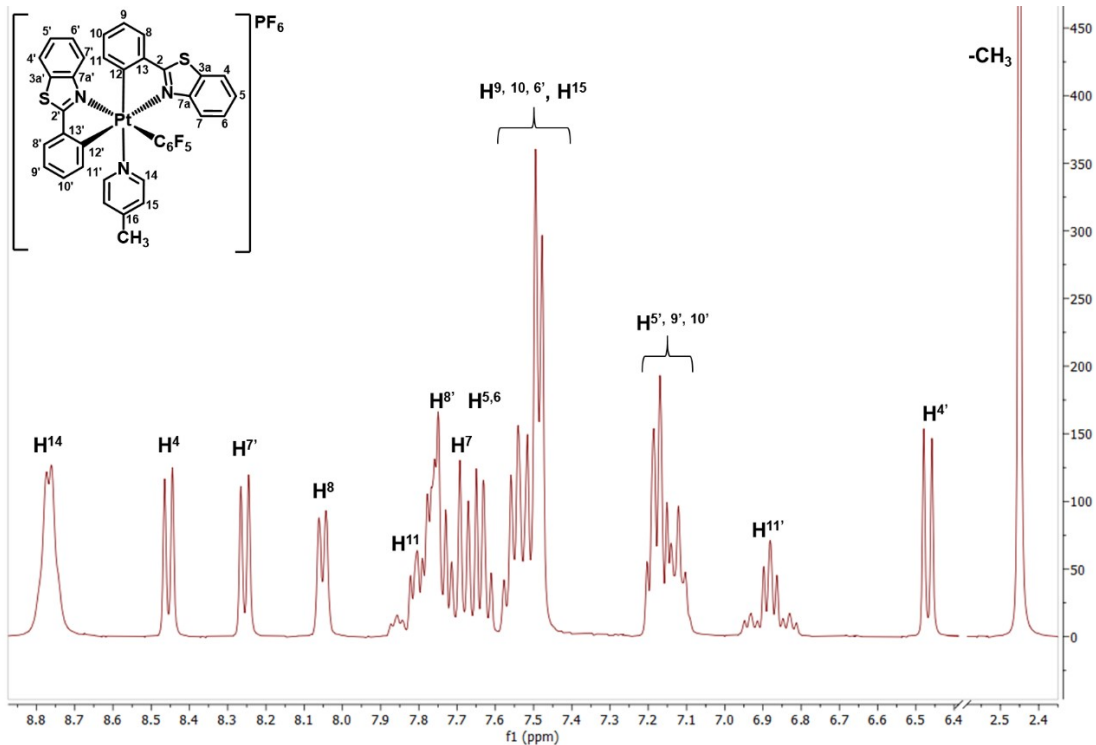
Synthesis of *fac*-[Pt(pbt)₄(C₆F₅)₂(μ-bpyb)](PF₆)₂ (7)

1,4-bis-(pyridyl)-butadiyne (0.014 g, 0.065 mmol), TlPF₆ (0.163 g, 0.393 mmol) and excess of KClO₄ (~1:30) were added to a deoxygenated 1,2-dichloroethane suspension (20 mL) of *fac*-[Pt(pbt)₂(C₆F₅)Cl] (0.100 g, 0.122 mmol), and the mixture refluxed for 6 h. The brown suspension was evaporated to dryness and the residue treated with 10 mL of toluene to give a brown solid, which was filtered (0.115 g). This solid was treated with CH₂Cl₂ (5 mL) and filtered. Addition of *n*-hexane (10 mL) and keeping 12 h at 298 K give **7** as a white solid (0.071 g, 28%). ESI (+): *m/z* 1913 [M-PF₆]⁺ (0.6), 782 [Pt(pbt)₂(C₆F₅)]⁺ (100), 986 [Pt(pbt)₂(C₆F₅)(bpyb)]⁺ (55). Anal. calcd for C₇₈H₄₀F₂₂N₆Pt₂S₄P₂ (2059.54): C, 45.49; H, 1.96; N, 4.08; S, 6.23. Found: C, 42.00; H, 2.19; N, 5.53; S, 7.79%. IR (ATR) (cm⁻¹): ν (C≡C) 2156 (w); ν (C-F, C₆F₅) 1074 (m), 972

(m); $\nu(\text{C}_6\text{F}_5)_{\text{X-sens}}$ 753 (m). Conductivity ($\text{cm}^2 \cdot \text{mol}^{-1} \cdot \Omega^{-1}$ in MeOH): 182.7. ^1H NMR (400 MHz, CD_3COCD_3): δ 9.02 (d, 2H, $^3J_{\text{Pt-H}} = 27$, H¹⁴), 8.46 (d, $^3J_{\text{H-H}} = 8$, H⁴), 8.25 (d, $^3J_{\text{H-H}} = 9$, H^{7'}), 8.05 (dd, $^3J_{\text{H-H}} = 7$, $^4J_{\text{H-H}} = 2$, H⁸), 7.87-7.64 (m, 7H, H^{5, 6, 7, 11, 8', 15}), 7.58-7.47 (m, 3H, H^{9, 10, 6'}), 7.20-7.10 (m, 3H, H^{5', 9', 10'}), 6.86 (t, $^3J_{\text{H-H}} \approx J_{\text{H-oF}} = 7$, $^3J_{\text{Pt-H}} = 41$, H^{11'}), 6.46 (d, $^3J_{\text{H-H}} = 9$, H^{4'}). $^{13}\text{C}\{\text{H}\}$ NMR (100.6 MHz, CD_3COCD_3): δ 181.6 (s, C^{2/2'}), 181.0 (s, C^{2/2'}), 153.3 (s, C¹⁴), 151.1 (s, C^{7a}), 147.6 (s, C^{3a}), 138.1 (s C¹²), 137.5 (s, C^{13'}), 137.4 (s, C¹³), 135.2 (s, C^{9/10}), 134.9 (s, C¹¹), 134.3 (d, $J_{\text{C-F}} = 7$, C^{11'}), 133.5 (s, C^{10'}), 133.1 (s, C^{7a}), 130.8 (s, C¹⁵), 130.0 (s, C^{5'}), 129.5 (s, C^{9/10}), 129.3 (s, C⁸), 128.7 (s, C^{6'}), 128.4 (s, C^{9'}), 128.1 (s, C⁶), 125.8 (s, C^{7'}), 125.2 (s, C⁴), 122.3 (d, $J_{\text{C-F}} = 14$, C⁷), 117.6 (s, C^{4'}), 81.3 (s, C¹⁸), 80.8 (s, C¹⁷). $^{19}\text{F}\{\text{H}\}$ NMR (376.5 MHz, CD_3COCD_3): δ -72.7 (d, $^1J_{\text{F-P}} = 710$, PF₆), -114.1 (dm, $^4J_{\text{Pt-oF}} = 102$, 1o-F_{C6F5}), -116.5 (dm, $^4J_{\text{Pt-oF}} = 99$, 1o-F_{C6F5}), -158.7 (m, p-F_{C6F5}), -162.8 (m, 1m-F_{C6F5}), -163.6 (m, 1m-F_{C6F5}). $^{31}\text{P}\{\text{H}\}$ NMR (161.9 MHz, CD_3COCD_3): δ -144.3 (sept, $^1J_{\text{P-F}} = 710$, PF₆).

2.- NMR spectra

a)



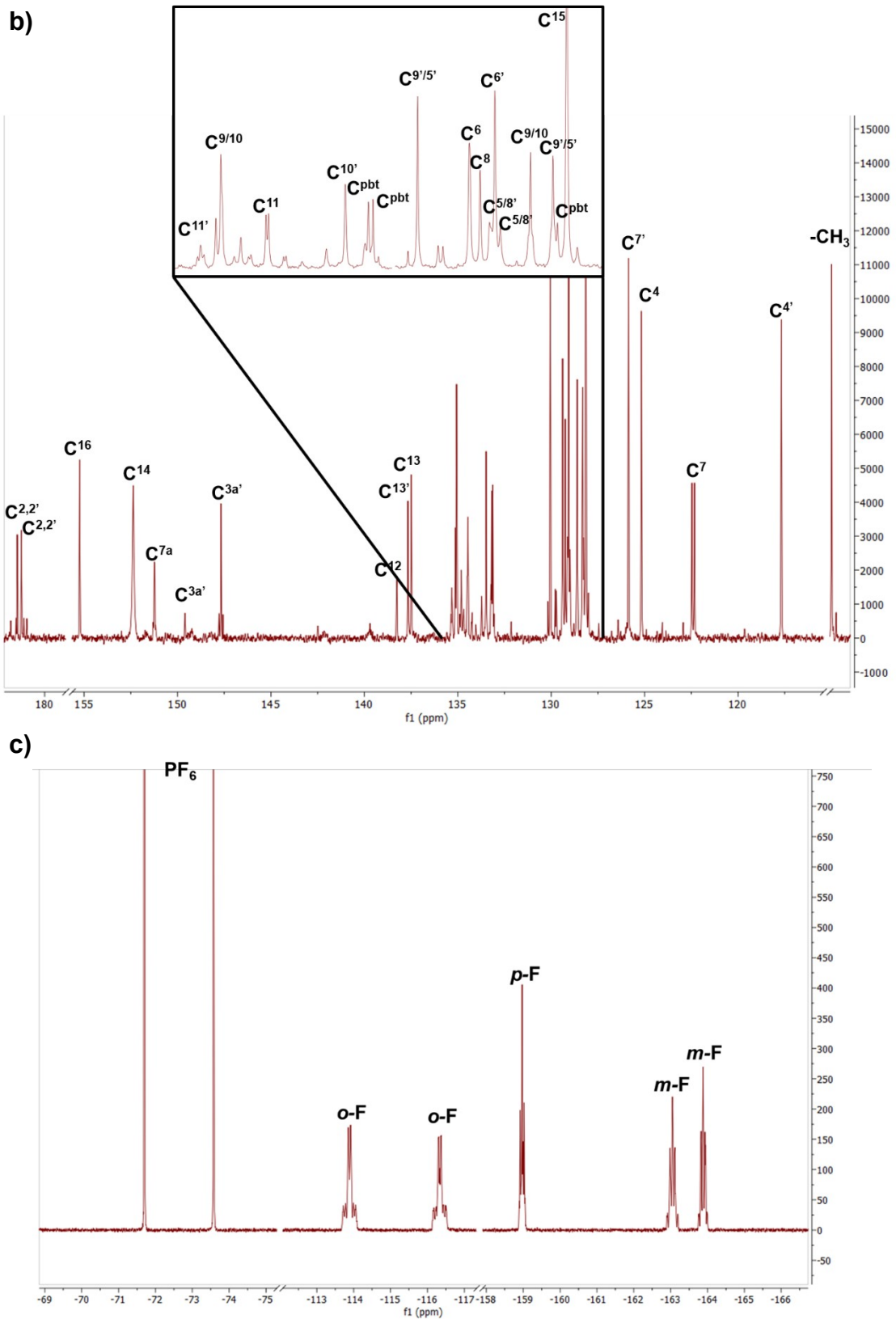
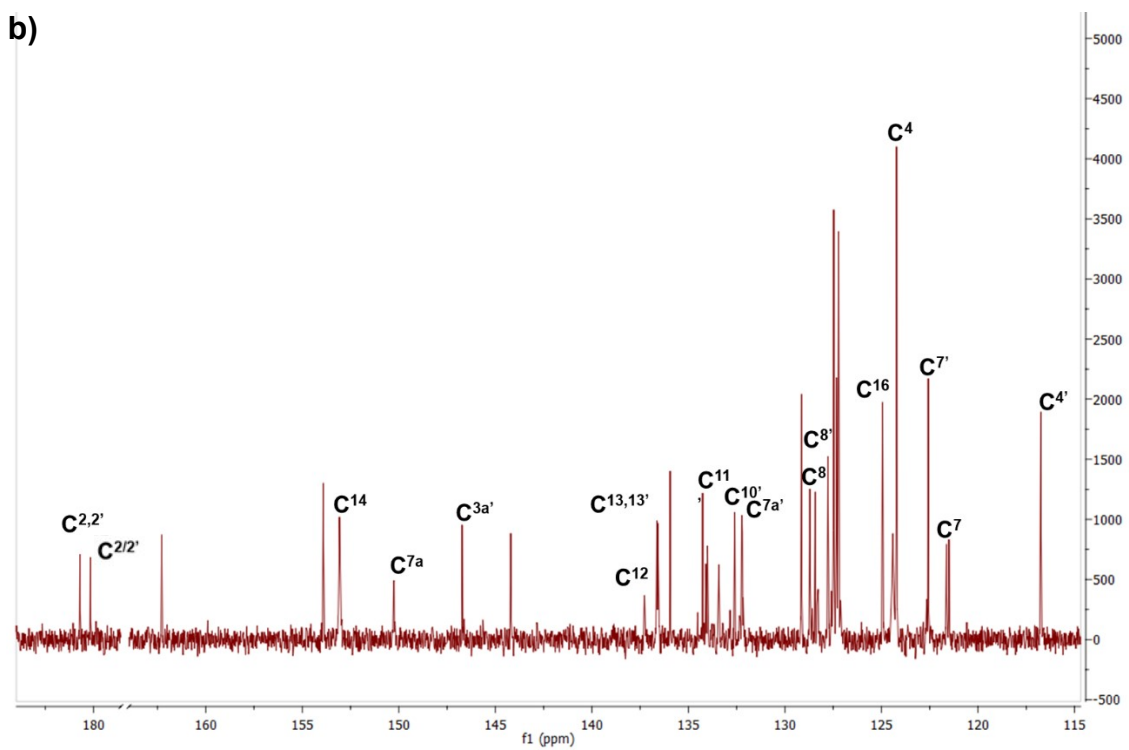
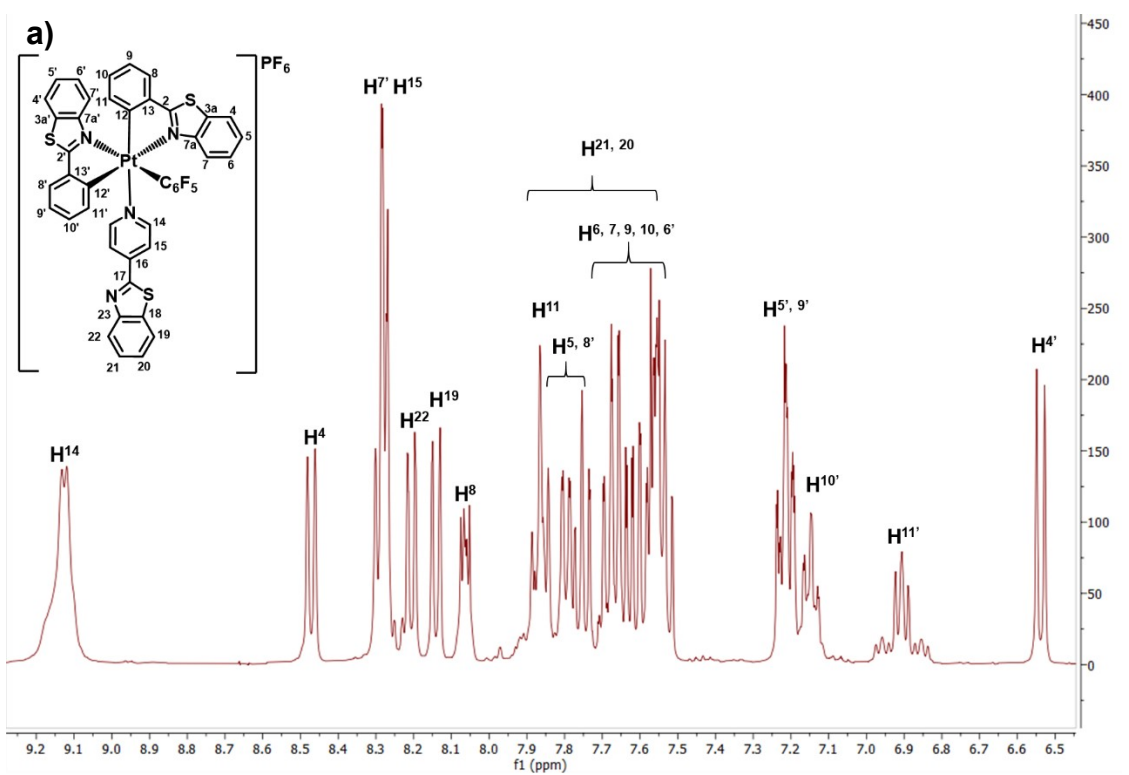


Fig. S1 NMR spectra of **1** in CD_3COCD_3 at 298 K a) ^1H , b) $^{13}\text{C}\{^1\text{H}\}$, c) $^{19}\text{F}\{^1\text{H}\}$.



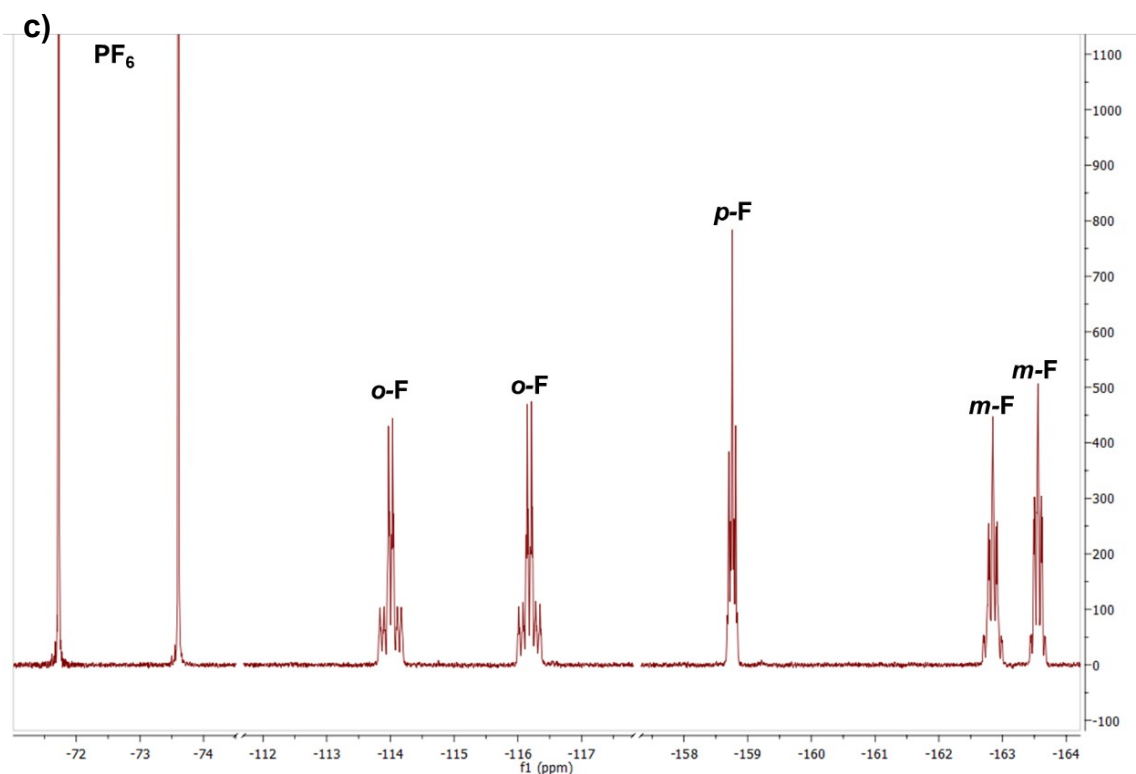
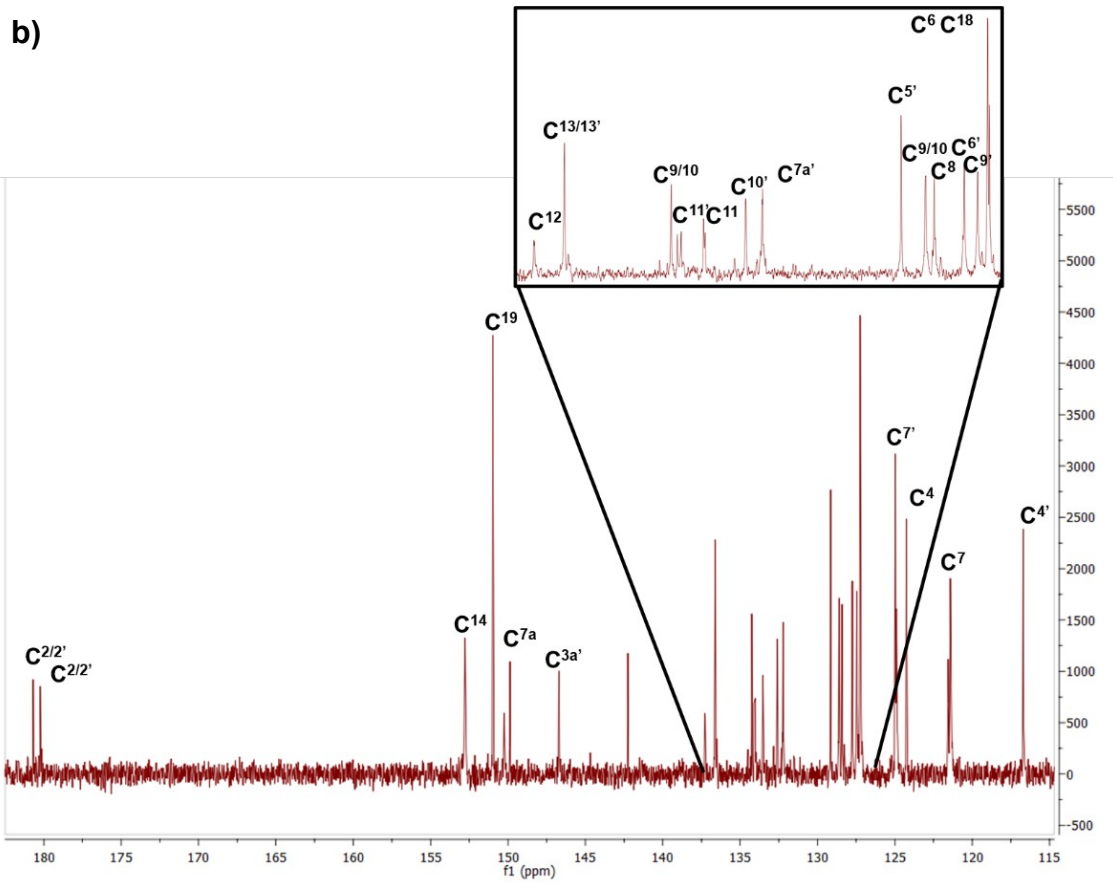
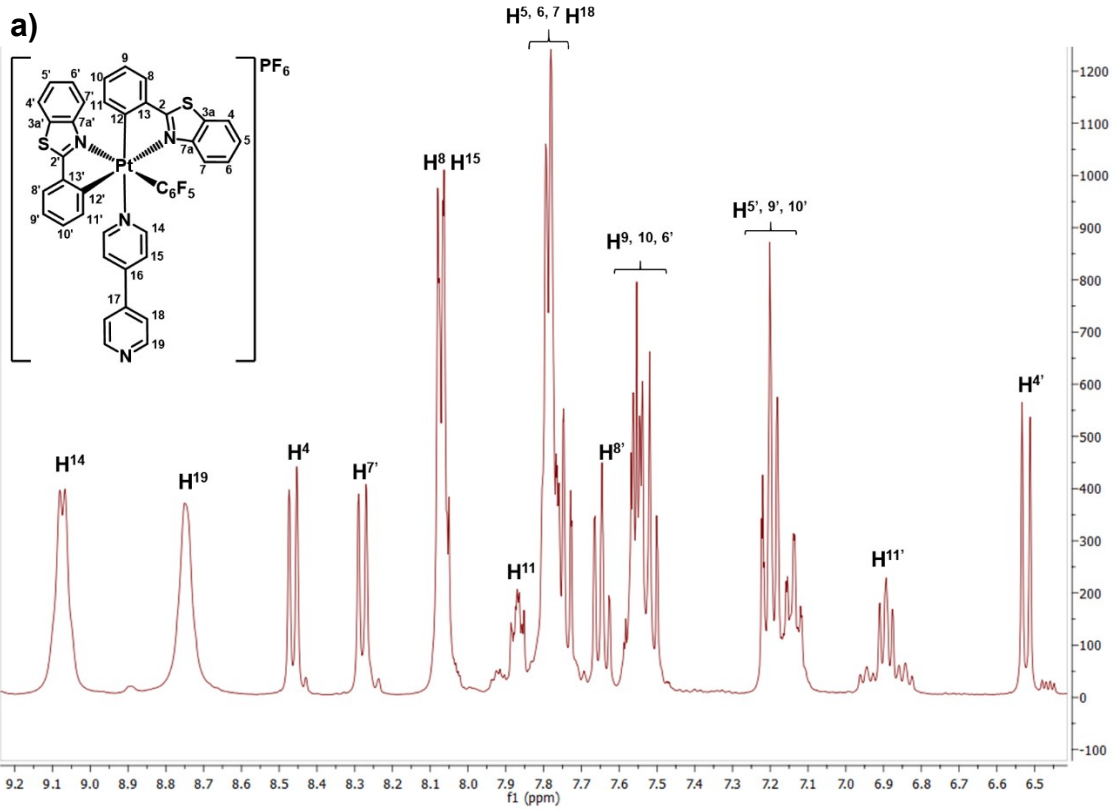


Fig. S2 NMR spectra of **2** in CD_3COCD_3 at 298 K a) ^1H , b) $^{13}\text{C}\{^1\text{H}\}$, c) $^{19}\text{F}\{^1\text{H}\}$.



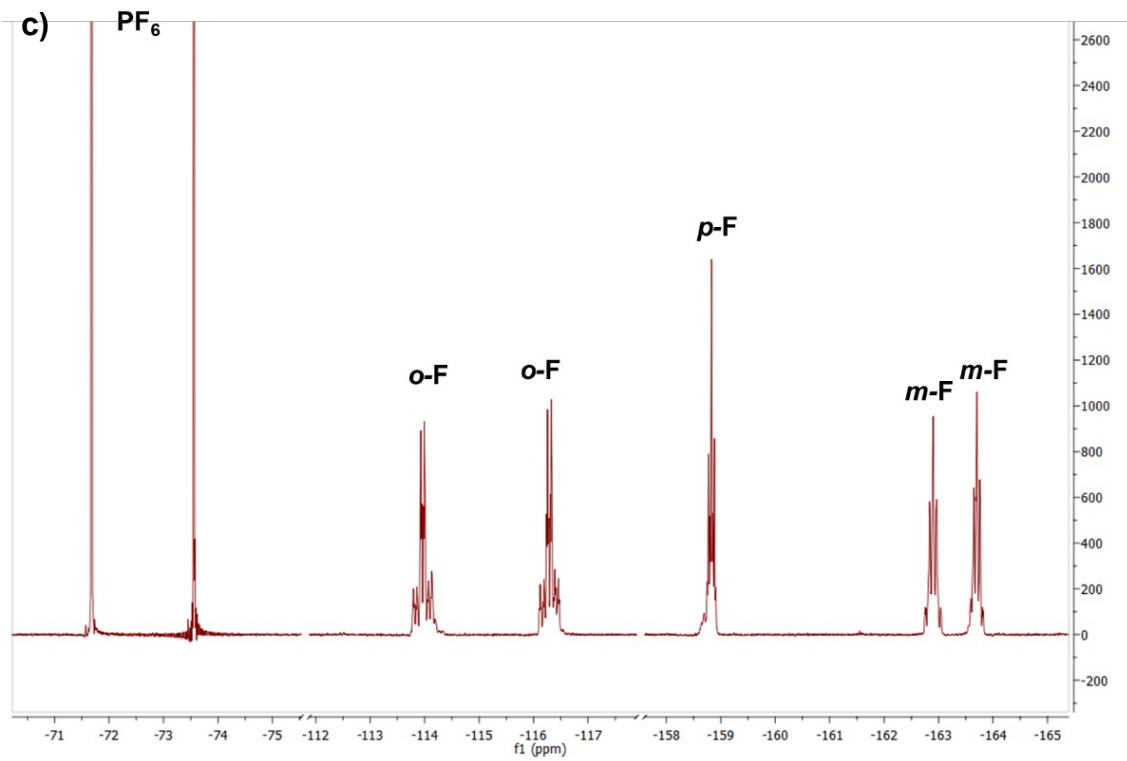


Fig. S3 NMR spectra of **3** in CD₃COCD₃ at 298 K a) ¹H, b) ¹³C{¹H}, c) ¹⁹F{¹H}.

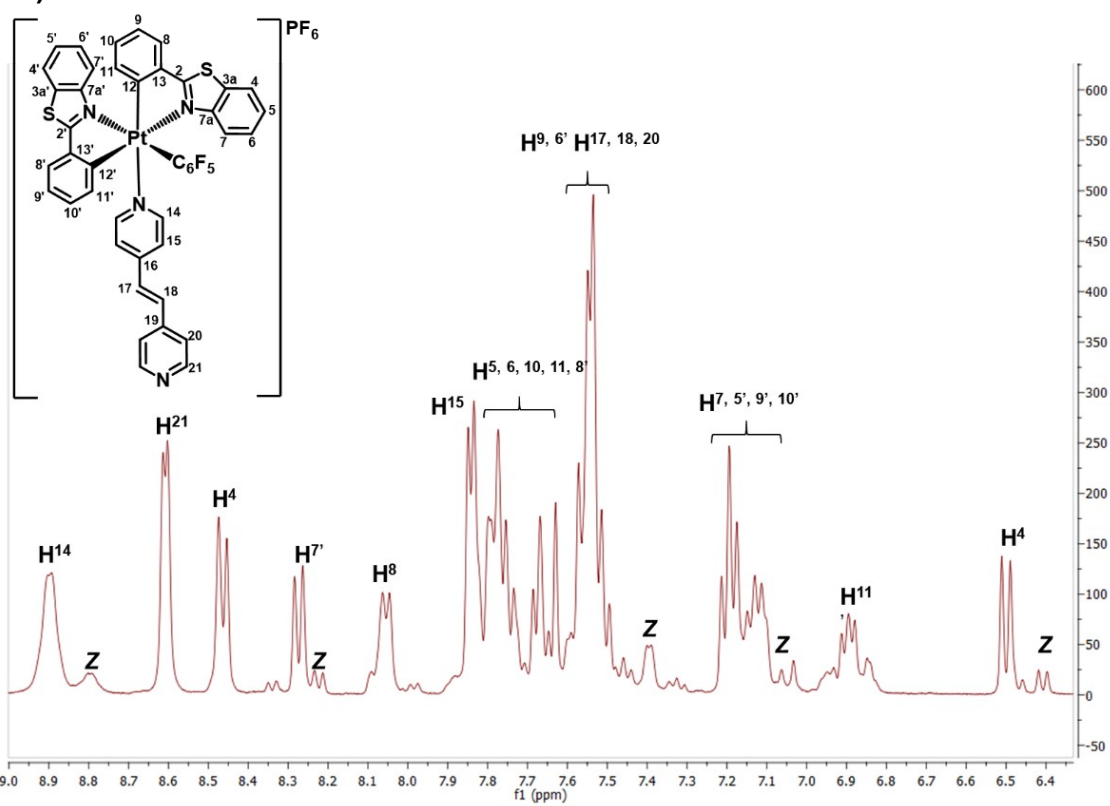
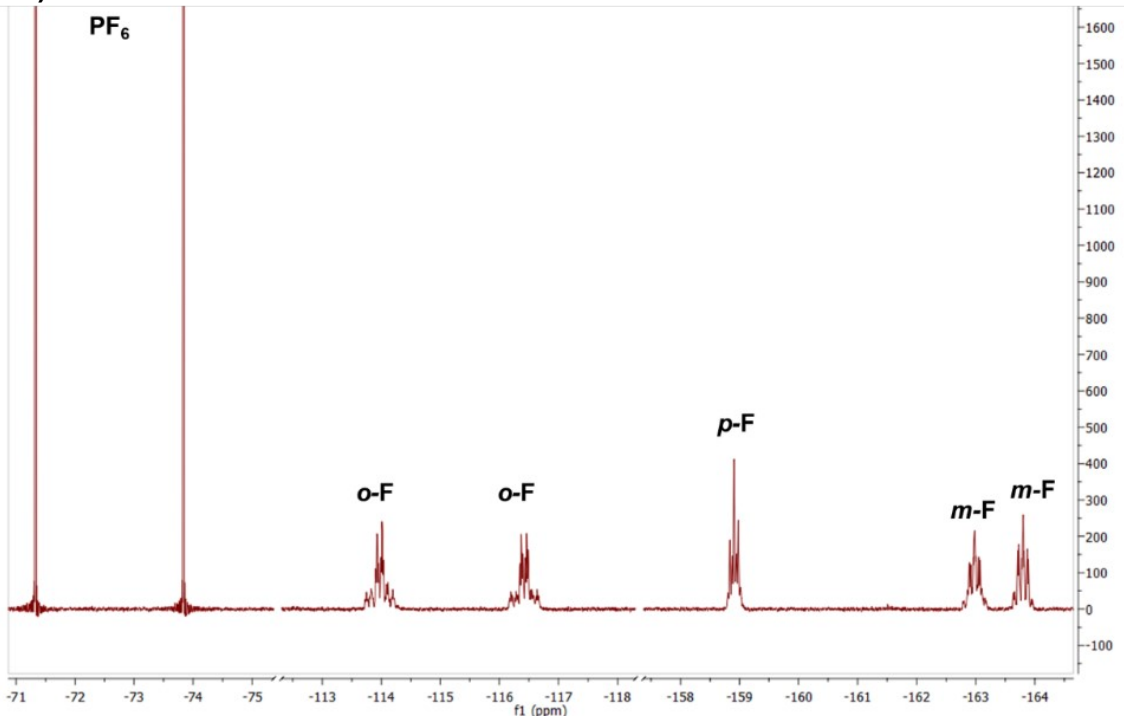
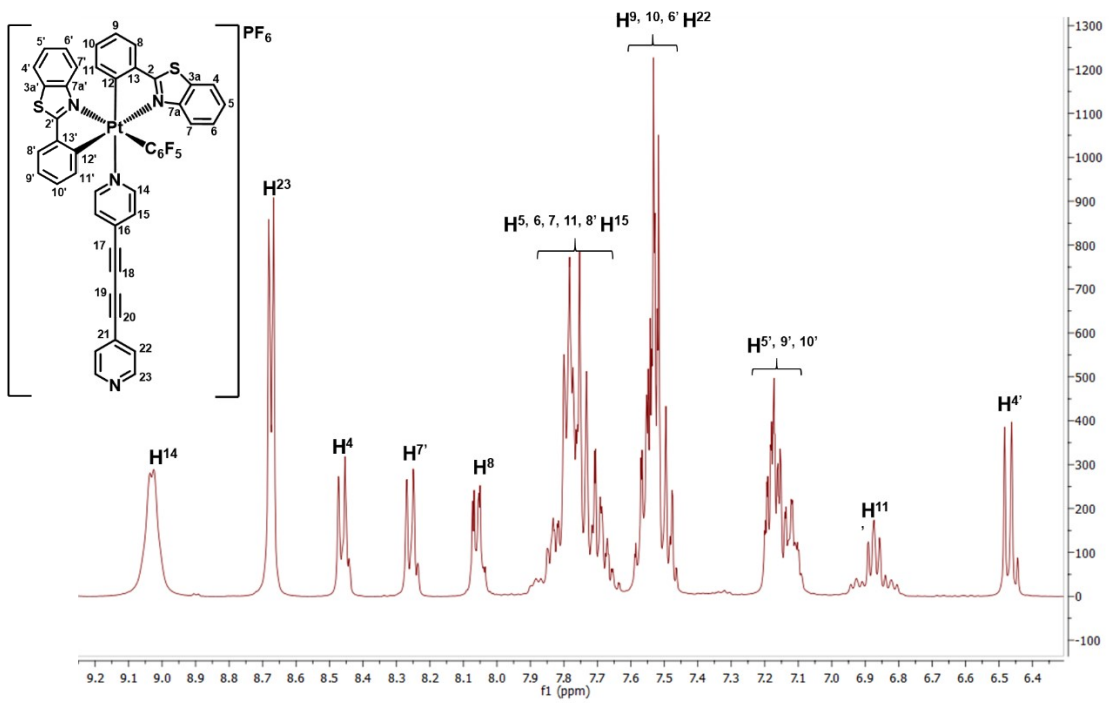
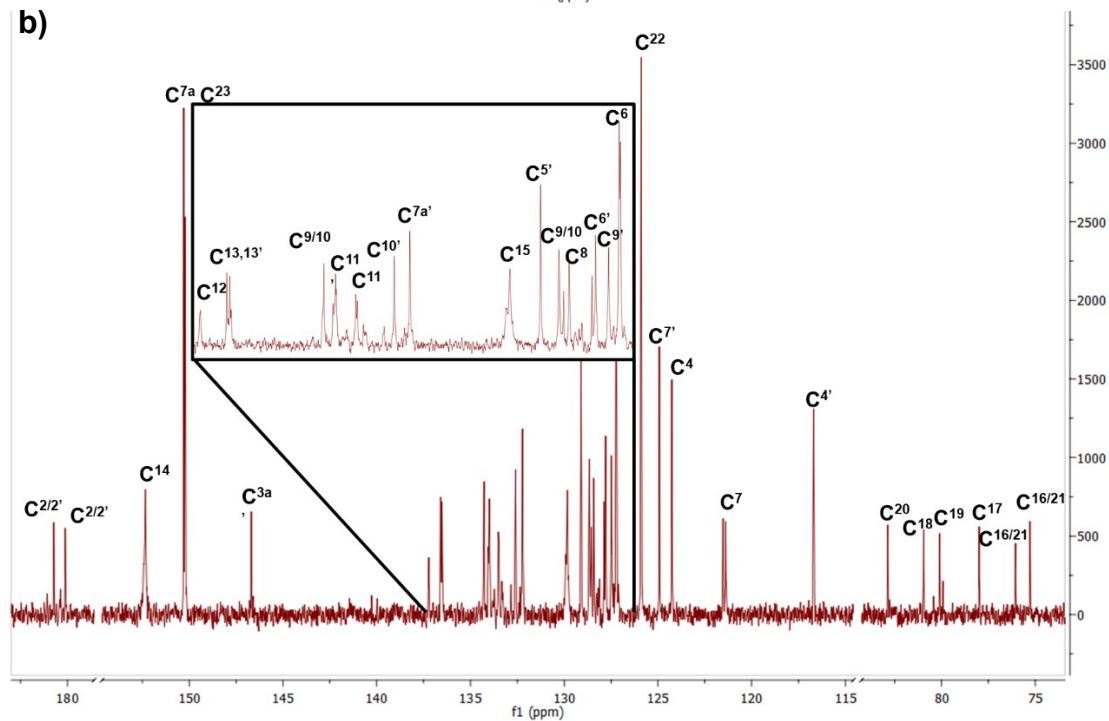
a)**b)**

Fig. S4 NMR spectra of **4** in CD_3COCD_3 at 298 K a) ^1H , b) $^{19}\text{F}\{\text{H}\}$.

a)



b)



c)

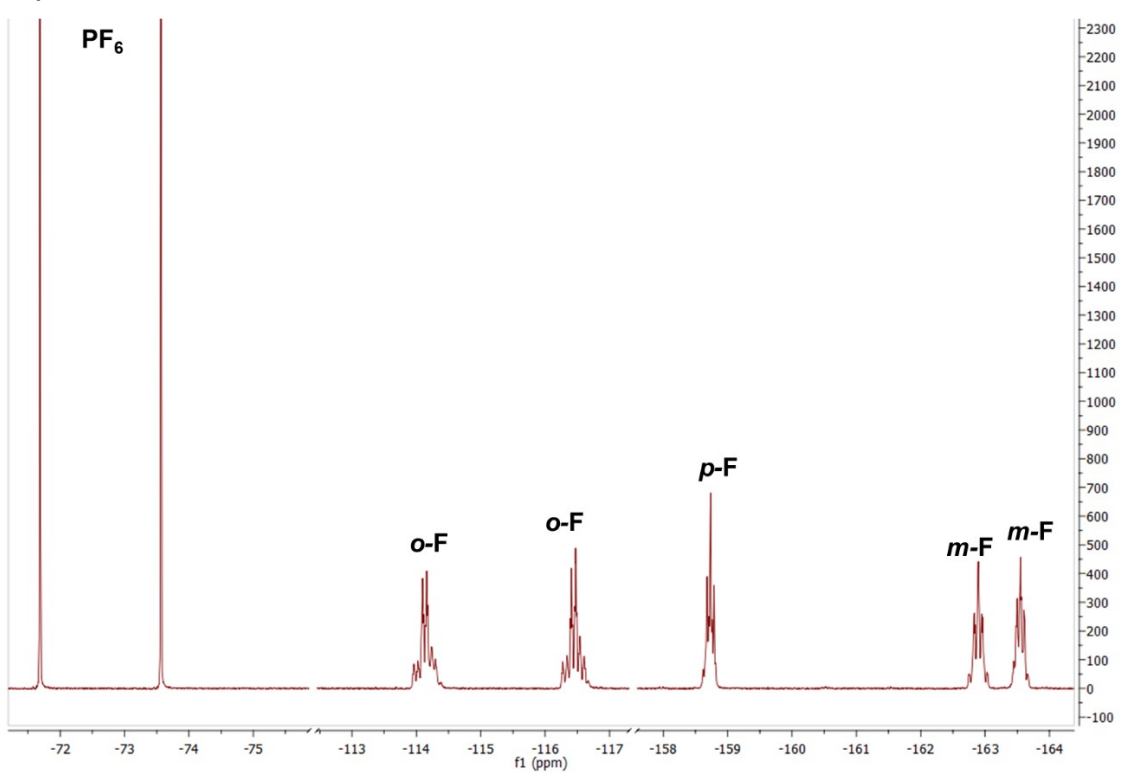


Fig. S5 NMR spectra of **5** in CD_3COCD_3 at 298 K a) ^1H , b) $^{13}\text{C}\{^1\text{H}\}$, c) $^{19}\text{F}\{^1\text{H}\}$.

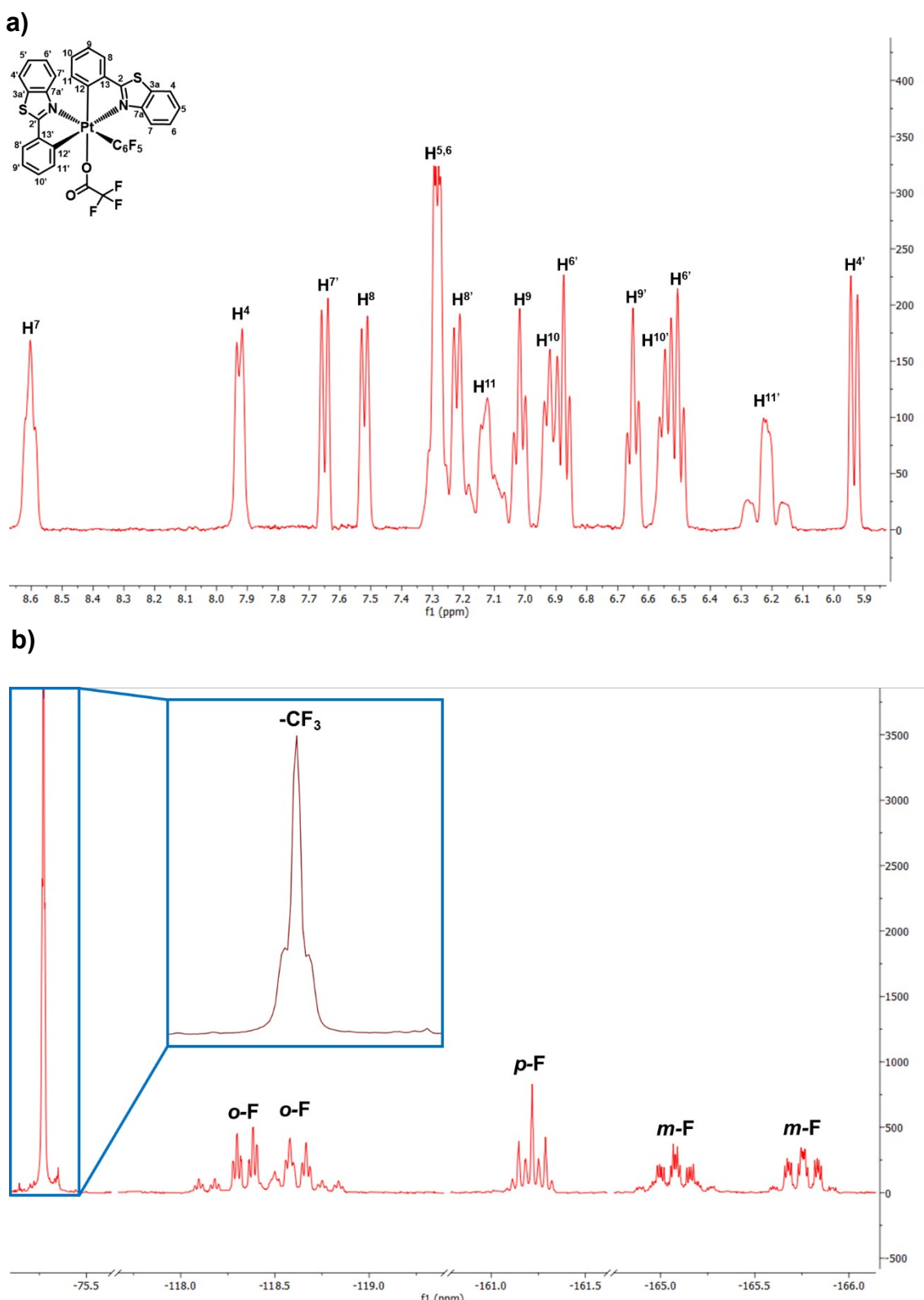
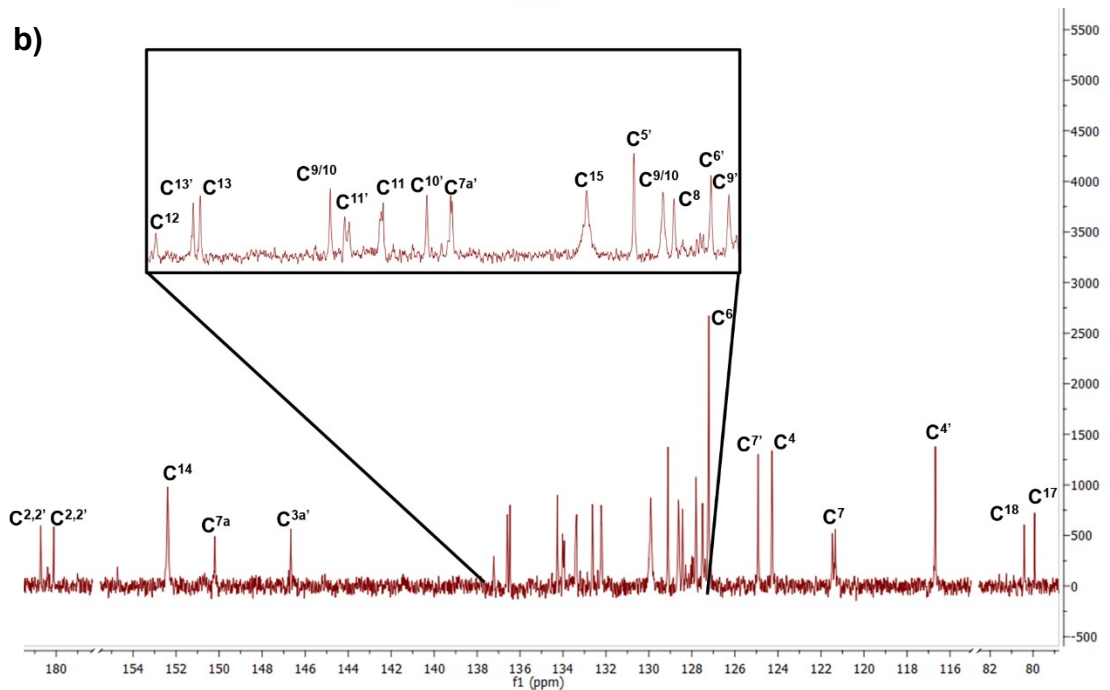
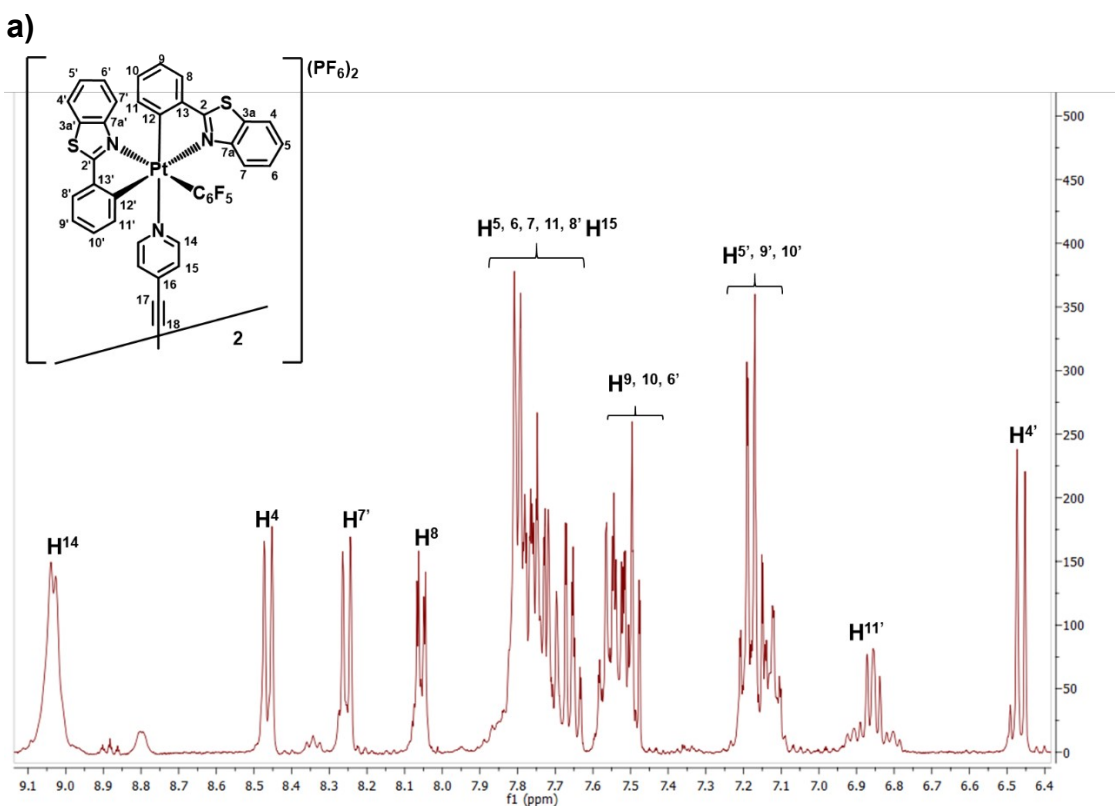


Fig. S6 NMR spectra of **6** in CD_3COCD_3 at 298 K a) ^1H , b) $^{19}\text{F}\{\text{H}\}$.



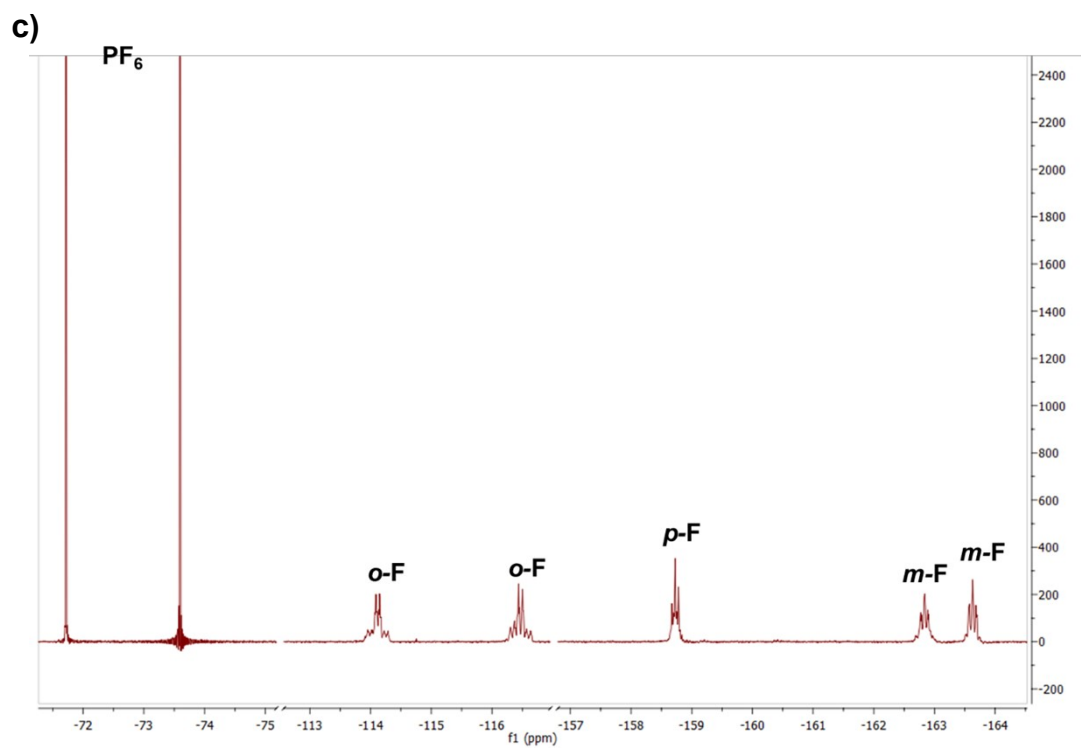


Fig. S7 NMR spectra of **7** in CD₃COCD₃ at 298 K a) ¹H, b) ¹³C{¹H}, c) ¹⁹F{¹H}.

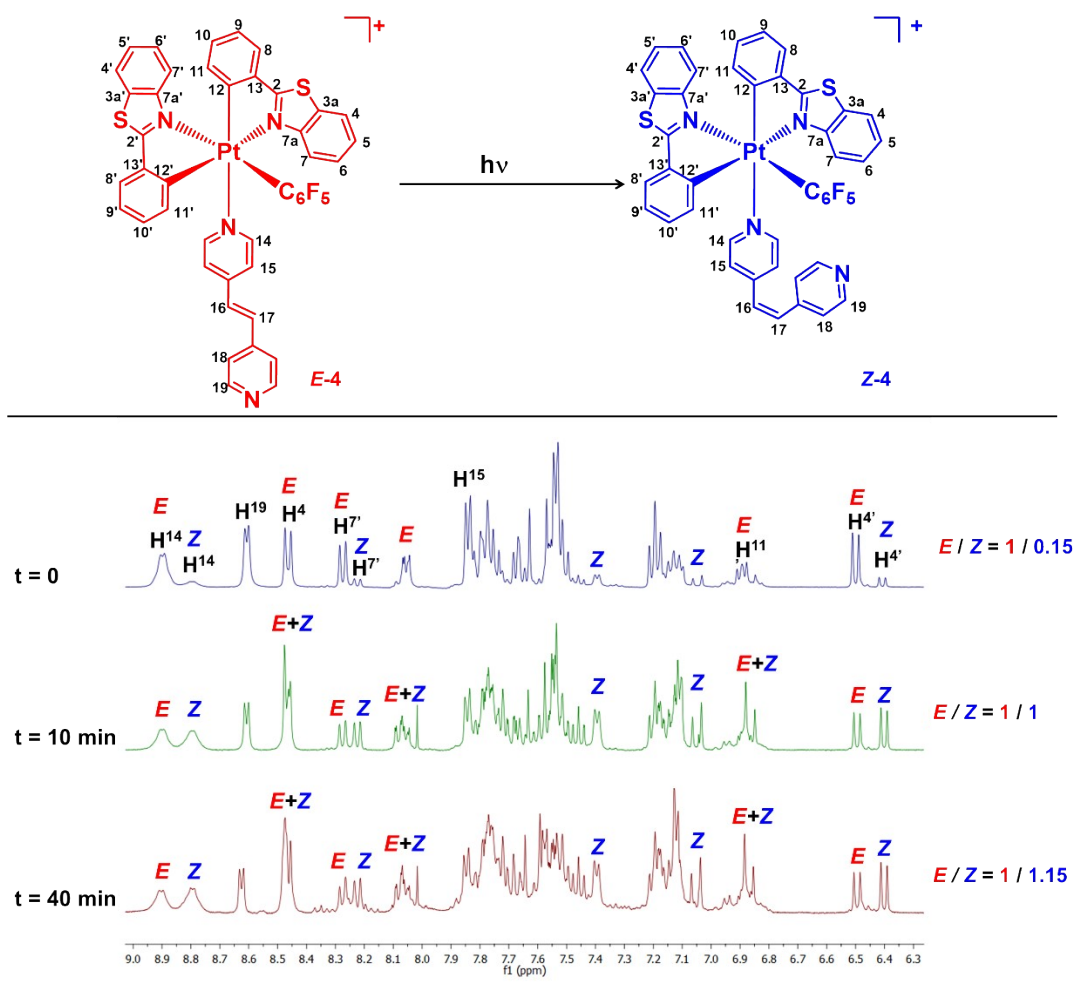


Fig. S8 Control by ^1H NMR spectroscopy of the irradiation of **4** in CD_3COCD_3 (Hg lamp, 125 W, $t = 0, 10, 40 \text{ min}$), showing the formation of the isomer Z.

3.- Crystal Structures

X-ray structure determinations. X-ray crystallographic data and selected bond lengths and angles for **1**·CH₃COCH₃, **4**·2CH₃COCH₃ and **6** are summarized in Tables S1 and S2. Yellow crystals of **1**·CH₃COCH₃, **4**·2CH₃COCH₃ and **6** were obtained by slow diffusion of *n*-hexane into a solution of the corresponding complex in acetone at room temperature. X-ray intensity data were collected using Molybdenum graphite monochromatic (Mo-K_α) radiation with Nonius- κ CCD diffractometer at a temperature of 173 K with an Oxford Cryosystem temperature controller for **1** and at 298 K for **4** using the DENZO and SCALEPACK suite programs or with a Bruker APEX-II diffractometer at 298 K for **6** using the APEX-II software. Structures were solved by Intrinsic Phasing using SHELXT⁴ with the WinGX graphical user interface.⁵ Multi-scan absorption corrections were applied to all the data sets and refined by full-matrix least squares on F^2 with SHELXL.⁶ hydrogen atoms were positioned geometrically, with isotropic parameters $U_{iso} = 1.2 U_{eq}$ (parent atom) for aromatic hydrogens and CH₂ and $U_{iso} = 1.5 U_{eq}$ (parent atom) for methyl groups. These complexes crystallized in a centrosymmetric group, so must be aquiral. Thus, both configurations (Λ and Δ) in a 50:50 ratio were found in the unit cell. Finally, the structures show some residual peaks greater than 1 e Å⁻³ in the vicinity of the iridium atoms but with no chemical meaning.

Table S1. X-ray Crystallographic data for **1**·CH₃COCH₃, **4**·2CH₃COCH₃ and **6**.

	1 ·CH ₃ COCH ₃	4 ·2CH ₃ COCH ₃	6
Empirical formula	C ₄₁ H ₂₉ F ₁₁ N ₃ OPtS ₂	C ₄₇ H ₃₂ F ₁₁ N ₄ OPtS ₂	C ₃₄ H ₁₆ F ₈ N ₂ O ₂ PtS ₂
Molecular weight	1078.85	1169.96	895.70
T (K)	173(1)	293(2)	298(2)
Wavelength (Å)	0.71076	0.71073	0.71076
Crystal system	Triclinic	Triclinic	Orthorhombic
Space group	P-1	P-1	Pbca
Crystal size (mm)	0.5 x 0.25 x 0.2	0.3 x 0.1 x 0.05	0.470 x 0.222 x 0.130
a (Å)	10.8839(3)	10.7410(6)	18.7733(12)
b (Å)	13.1414(4)	14.9263(9)	16.9829(11)
c (Å)	14.5947(5)	15.9697(10)	19.3989(13)
α (°)	79.0260(10)	63.406(3)	90
β (°)	85.881(2)	81.042(3)	90
γ (°)	75.335(2)	79.846(3)	90
V (Å³)	1981.93(11)	2245.0(2)	6184.9(7)
Z	2	2	8
Density (calculated) (Mg/cm³)	1.808	1.731	1.924
Absorption coefficient (mm⁻¹)	3.776	3.342	4.758
F(000)	1056	1152	3456
θ range for data collection (°)	2.817 to 25.680 -13<=h<=13, -15<=k<=16, -17<=l<=17	1.431 to 27.480 -13<=h<=12, -19<=k<=19, -20<=l<=20	3.020 to 27.930 -23<=h<=23, -21<=k<=21, -24<=l<=24
Index ranges			
Reflections collected	26935	35632	268677
Independent reflections	7471 [R(int) = 0.0419]	10198 [R(int) = 0.0872]	6313 [R(int) = 0.0473]
Data / restraints / parameters	7471 / 0 / 541	10198 / 0 / 604	6313 / 0 / 436
Goodness-of-fit on F2	1.054	1.109	1.179
Final R indices [I>2σ(I)]^[a]	R1 = 0.0279, wR2 = 0.0735	R1 = 0.0513, wR2 = 0.1298	R1 = 0.0498, wR2 = 0.0903
R indices (all data)^[a]	R1 = 0.0296, wR2 = 0.0748	R1 = 0.0790, wR2 = 0.1494	R1 = 0.0657, wR2 = 0.1005
Largest diff. peak and hole (e Å⁻³) (dmin/dmax)	1.369 and -1.752	1.362 and -1.928	1.168 and -1.588

^[a] $R_1 = \sum(|F_o| - |F_c|)/\sum|F_o|$; $wR2 = [\sum w(F_o^2 - F_c^2)^2/\sum wF_o^2]^{1/2}$; goodness of fit = $\{\sum[w(F_o^2 - F_c^2)^2]/(N_{obs} - N_{param})\}^{1/2}$; $w = [\sigma^2(F_o) + (g_1P)^2 + g_2P]^{-1}$; $P = [\max(F_o^2; 0 + 2F_c^2)]/3$.

Table S2. Selected distances (Å) and angles (°) for complexes **1**·CH₃COCH₃ **4**·2CH₃COCH₃ and **6**.

1 ·CH ₃ COCH ₃			
Distances (Å)		Angles (°)	
Pt(1)-N(1)	2.210(3)	C(27)-Pt(1)-N(1)	88.24(13)
Pt(1)-N(2)	2.127(3)	N(1)-Pt(1)-N(2)	95.03(12)
Pt(1)-C(26)	2.037(4)	C(26)-Pt(1)-N(2)	80.59(14)
Pt(1)-C(27)	2.045(4)	C(26)-Pt(1)-C(27)	95.51(15)
Pt(1)-C(13)	2.041(4)	C(13)-Pt(1)-N(1)	80.15(14)
Pt(1)-N(3)	2.170(3)	C(13)-Pt(1)-N(2)	85.52(13)
C(7)-C(8)	1.449(6)	C(13)-Pt(1)-C(26)	91.91(15)
C(20)-C(21)	1.443(5)	C(13)-Pt(1)-C(27)	90.16(14)
H(12)···F(5)	2.675	N(3)-Pt(1)-N(1)	100.98(11)
H(2)···F(1)	2.422	N(3)-Pt(1)-N(2)	90.86(11)
H(25)···F(5)	2.669	N(3)-Pt(1)-C(26)	86.72(13)
		N(3)-Pt(1)-C(27)	93.39(13)
4 ·2CH ₃ COCH ₃			
Distances (Å)		Angles (°)	
Pt(1)-N(1)	2.225(6)	C(27)-Pt(1)-N(1)	85.6(2)
Pt(1)-N(2)	2.133(5)	N(1)-Pt(1)-N(2)	98.1(2)
Pt(1)-C(26)	2.036(7)	C(26)-Pt(1)-N(2)	80.8(2)
Pt(1)-C(27)	2.061(6)	C(26)-Pt(1)-C(27)	95.2(3)
Pt(1)-C(13)	2.042(7)	C(13)-Pt(1)-N(1)	79.7(3)
Pt(1)-N(3)	2.172(6)	C(13)-Pt(1)-N(2)	87.8(2)
C(7)-C(8)	1.471(10)	C(13)-Pt(1)-C(26)	93.1(3)
C(20)-C(21)	1.437(10)	C(13)-Pt(1)-C(27)	90.6(3)
H(12)···F(5)	2.860	N(3)-Pt(1)-N(1)	102.4(2)
H(2)···F(1)	2.465	N(3)-Pt(1)-N(2)	89.0(2)
H(25)···F(5)	2.592	N(3)-Pt(1)-C(26)	84.8(2)
		N(3)-Pt(1)-C(27)	92.5(2)
6			
Distances (Å)		Angles (°)	
Pt(1)-N(1)	2.165(6)	C(27)-Pt(1)-N(1)	87.8(2)
Pt(1)-N(2)	2.135(5)	N(1)-Pt(1)-N(2)	96.6(2)
Pt(1)-C(26)	2.039(7)	C(26)-Pt(1)-N(2)	80.8(3)
Pt(1)-C(27)	2.056(7)	C(26)-Pt(1)-C(27)	94.6(3)
Pt(1)-C(13)	2.011(7)	C(13)-Pt(1)-N(1)	80.3(3)
Pt(1)-O(1)	2.146(5)	C(13)-Pt(1)-N(2)	88.9(2)
C(7)-C(8)	1.451(11)	C(13)-Pt(1)-C(26)	95.7(3)
C(20)-C(21)	1.436(10)	C(13)-Pt(1)-C(27)	90.0(3)
H(12)···F(5)	2.756	O(1)-Pt(1)-N(1)	94.9(2)
H(2)···F(1)	2.707	O(1)-Pt(1)-N(2)	84.2(2)
H(25)···F(5)	2.505	O(1)-Pt(1)-C(26)	88.7(2)
		O(1)-Pt(1)-C(27)	97.4(2)

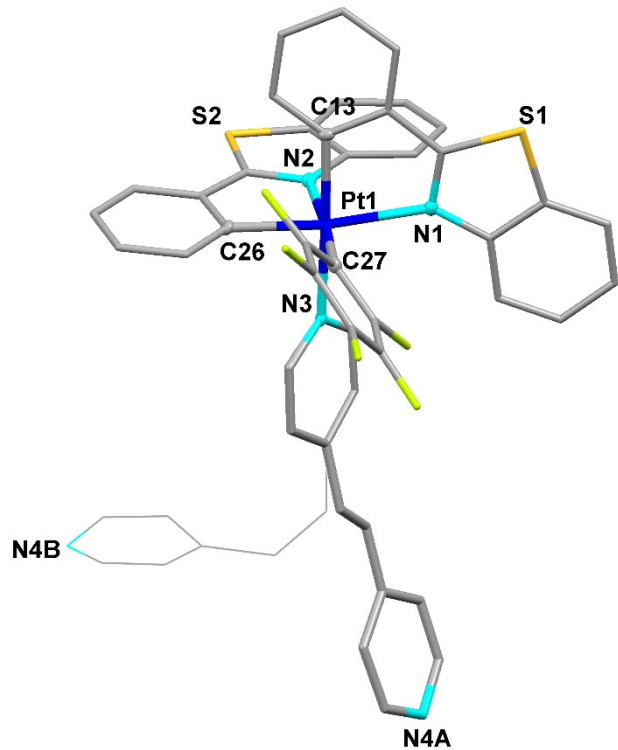


Fig. S9 Molecular structure of the cation $[\text{Pt}(\text{pbt})_2(\text{C}_6\text{F}_5)(\text{bpe})]^+$ in 4 (crystals grown under light ambient) showing the two disordered positions: *E* (thick line) and *Z* (thin line).

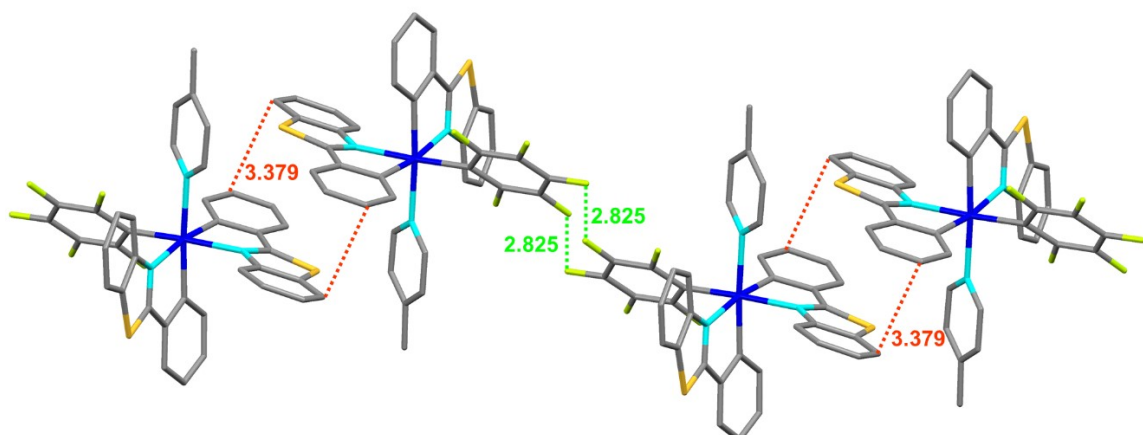


Fig. S10 Crystal packing of $\mathbf{1}\cdot\text{CH}_3\text{COCH}_3$ showing the intermolecular contacts.

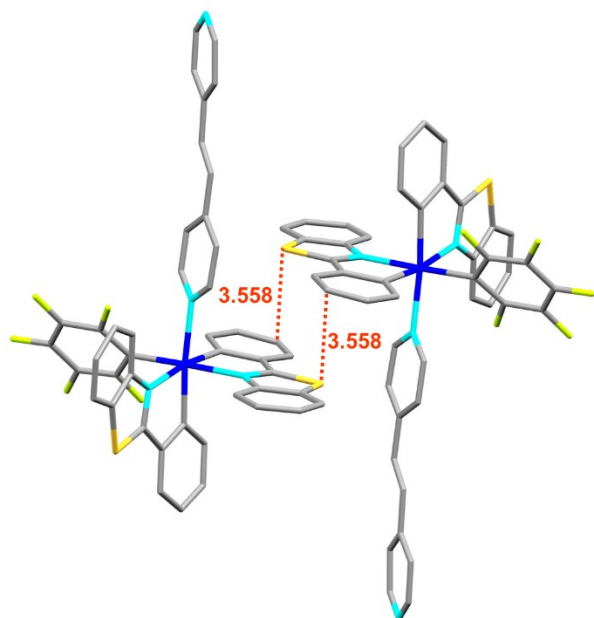


Fig. S11 Crystal packing of **4**·2CH₃COCH₃ showing the intermolecular contacts.

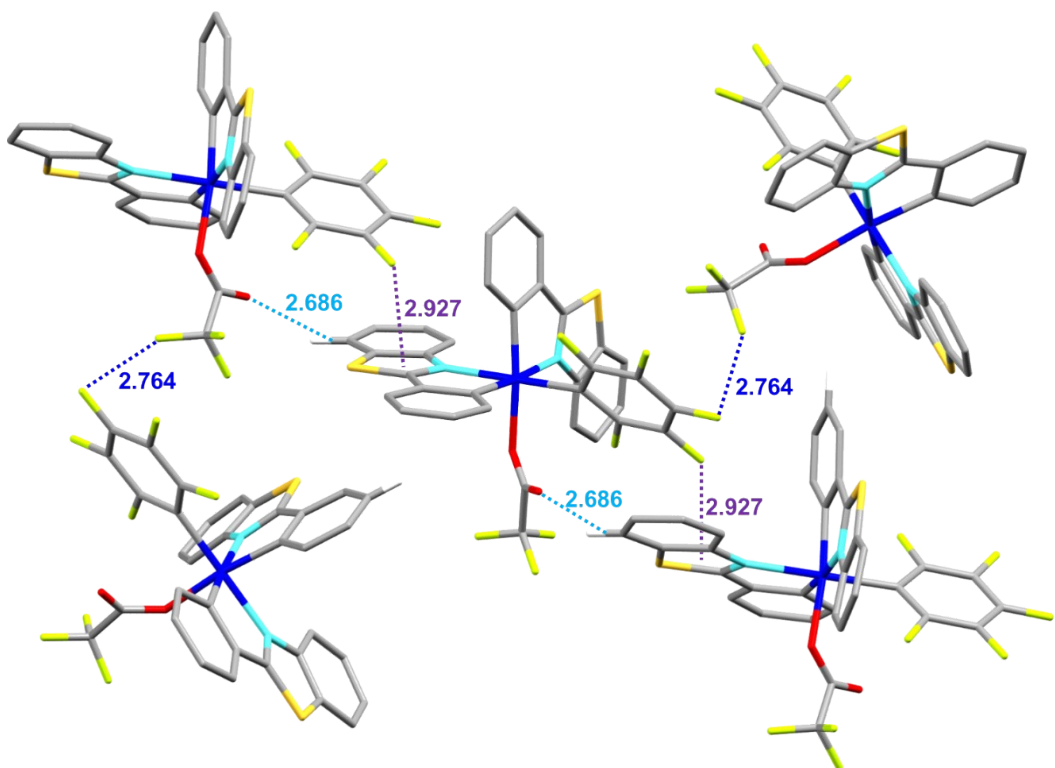


Fig. S12 Crystal packing of **6** showing the intermolecular contacts.

4.- Photophysical Properties and TD-DFT/SCRF Theoretical Calculations

Theoretical Calculations. Calculations were carried out with the Gaussian 16 package⁷ for **1-7**, using Becke's three-parameter functional combined with Lee-Yang-Parr's correlation functional (B3LYP).⁸ Optimizations on the singlet state (S_0) were performed using as a starting point the molecular geometry obtained through X-ray diffraction analysis for complex **1** and simulated structures for **2-7**. No negative frequency was found in the vibrational frequency analysis of the final equilibrium geometries. The basis set used was the LanL2DZ effective core potential for Pt and 6-31G(d,p) for the ligand atoms.⁹ DFT and TD-DFT calculations were carried out using the polarized continuum model approach¹⁰ (PCM) implemented in the Gaussian 16 software, in the presence of CH_2Cl_2 . The predicted emission wavelengths were obtained by energy difference between the triplet state at its optimized geometry and singlet state at the triplet geometry. The results were visualized with GaussView 6. Overlap populations between molecular fragments were calculated using the GaussSum 3.0 software.¹¹

Compound	$\lambda_{\text{abs}}/\text{nm}$ ($\epsilon \times 10^{-3}/\text{M}^{-1}\text{ cm}^{-1}$)
<i>fac</i> -[Pt(pbt) ₂ (C ₆ F ₅)(4-Mepy)](PF ₆) 1	207 (37.6), 258 (21.4), 264 (19.0), 306 (24.7), 320 (29.4), 338 (30.8), 354 (21.8)
<i>fac</i> -[Pt(pbt) ₂ (C ₆ F ₅)(pybt)](PF ₆) 2	222 (79), 256 (25), 263 (25), 320 (47), 335 (51), 356 (36)
<i>fac</i> -[Pt(pbt) ₂ (C ₆ F ₅)(4,4'-bipy)](PF ₆) 3	220 (65.3), 260 (29.8), 265 (30.6), 290 (28.6), 306 (38.2), 326 (49), 339 (42.3), 350 (41.4)
<i>fac</i> -[Pt(pbt) ₂ (C ₆ F ₅)(bpe)](PF ₆) 4	231 (21), 258 (11), 265 (11), 307 (28), 317 (29), 332 (23), 356 (10)
<i>fac</i> -[Pt(pbt) ₂ (C ₆ F ₅)(bpyb)](PF ₆) 5	219 (39), 257 (20), 265 (18), 297 (18), 304 (20), 321 (25), 340 (21), 355 (12)
<i>fac</i> -[Pt(pbt) ₂ (C ₆ F ₅)(OCOCF ₃)] 6	232 (32.0), 256 (16.5), 263 (15.8), 307 (23.0), 321 (26.9), 339 (25.2), 357 (17.2)
<i>fac</i> -[{Pt(pbt) ₂ (C ₆ F ₅) ₂ } ₂ (μ-bpyb)](PF ₆) ₂ 7	221 (65), 264 (31), 287 (28), 306 (38), 325 (49), 347 (42), 357 (28)

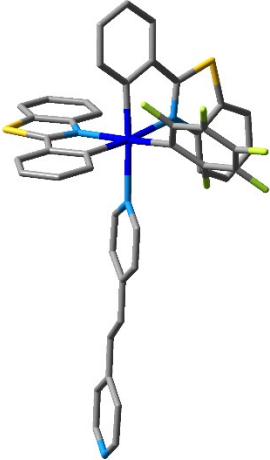
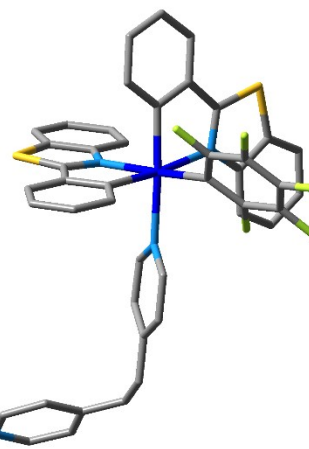
Table S3. Absorption data for compounds **1 – 7** in CH_2Cl_2 (5×10^{-5} M)

Table S4. DFT optimized geometries for ground state and triplet state (in CH₂Cl₂)**1⁺**

	S ₀	T ₁	
	X-Ray	S ₀	T ₁
Pt(1)-N(1)	2.210(3)	2.286	2.294
Pt(1)-N(2)	2.127(3)	2.204	2.181
Pt(1)-C(26)	2.037(4)	2.042	2.036
Pt(1)-C(27)	2.045(4)	2.064	2.068
Pt(1)-C(13)	2.041(4)	2.047	2.045
Pt(1)-N(3)	2.170(3)	2.275	2.293
C(7)-C(8)	1.449(6)	1.450	1.450
C(20)-C(21)	1.443(5)	1.448	1.377
H(12)···F(5)	2.675	2.757	2.809
H(2)···F(1)	2.422	2.555	2.533
H(25)···F(5)	2.669	2.530	2.540
C(27)-Pt(1)-N(1)	88.24(13)	86.48	85.99
N(1)-Pt(1)-N(2)	95.03(12)	97.53	97.52
C(26)-Pt(1)-N(2)	80.59(14)	79.60	80.65
C(26)-Pt(1)-C(27)	95.51(15)	96.03	95.57
N(3)-Pt(1)-N(1)	100.98(11)	101.12	101.41
N(3)-Pt(1)-N(2)	90.86(11)	89.00	87.94
N(3)-Pt(1)-C(26)	86.72(13)	83.80	83.94
N(3)-Pt(1)-C(27)	93.39(13)	94.39	94.48

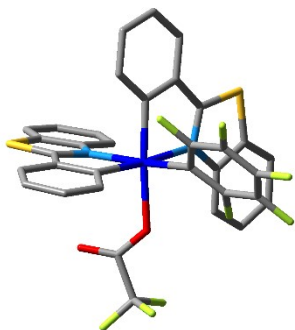
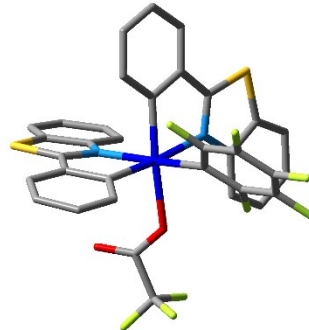
	2^+		
	S_0		T_1
Pt(1)-N(1)	-	2.289	2.290
Pt(1)-N(2)	-	2.202	2.203
Pt(1)-C(26)	-	2.043	2.041
Pt(1)-C(27)	-	2.064	2.064
Pt(1)-C(13)	-	2.046	2.049
Pt(1)-N(3)	-	2.284	2.255
C(7)-C(8)	-	1.450	1.451
C(20)-C(21)	-	1.448	1.448
C(27)-Pt(1)-N(1)	-	86.19	86.27
N(1)-Pt(1)-N(2)	-	97.82	97.66
C(26)-Pt(1)-N(2)	-	79.62	79.63
C(26)-Pt(1)-C(27)	-	96.03	96.08
N(3)-Pt(1)-N(1)	-	101.58	101.27
N(3)-Pt(1)-N(2)	-	88.62	88.90
N(3)-Pt(1)-C(26)	-	83.52	83.84
N(3)-Pt(1)-C(27)	-	94.42	94.44

3⁺			
	S ₀	T ₁	
X-Ray		S ₀	T ₁
Pt(1)-N(1)	-	2.288	2.262
Pt(1)-N(2)	-	2.202	2.214
Pt(1)-C(26)	-	2.042	2.044
Pt(1)-C(27)	-	2.065	2.063
Pt(1)-C(13)	-	2.045	2.042
Pt(1)-N(3)	-	2.282	2.291
C(7)-C(8)	-	1.450	1.378
C(20)-C(21)	-	1.448	1.448
C(27)-Pt(1)-N(1)	-	86.09	85.81
N(1)-Pt(1)-N(2)	-	97.95	98.25
C(26)-Pt(1)-N(2)	-	79.64	79.47
C(26)-Pt(1)-C(27)	-	96.00	96.20
N(3)-Pt(1)-N(1)	-	101.22	100.99
N(3)-Pt(1)-N(2)	-	88.21	88.01
N(3)-Pt(1)-C(26)	-	83.90	83.22
N(3)-Pt(1)-C(27)	-	94.61	94.80

4⁺			
	S ₀	T ₁	
			
	X-Ray	S ₀	T ₁
Pt(1)-N(1)	2.192(5)	2.289	2.289
Pt(1)-N(2)	2.130(5)	2.201	2.204
Pt(1)-C(26)	2.018(6)	2.042	2.042
Pt(1)-C(27)	2.055(5)	2.065	2.064
Pt(1)-C(13)	2.033(6)	2.046	2.047
Pt(1)-N(3)	2.180(5)	2.273	2.272
C(7)-C(8)	1.430(9)	1.450	1.450
C(20)-C(21)	1.422(9)	1.448	1.448
C(38)-C(39)	1.317(11)	1.349	1.466
C(27)-Pt(1)-N(1)	86.4(2)	86.22	86.15
N(1)-Pt(1)-N(2)	80.5(2)	97.81	97.96
C(26)-Pt(1)-N(2)	80.5(2)	79.64	79.64
C(26)-Pt(1)-C(27)	96.3(2)	96.00	95.91
N(3)-Pt(1)-N(1)	102.92(19)	101.04	101.15
N(3)-Pt(1)-N(2)	89.22(18)	88.41	88.59
N(3)-Pt(1)-C(26)	85.2(2)	83.94	83.88
N(3)-Pt(1)-C(27)	93.3(2)	94.66	94.58
C(38)-C(39)-C(40)	127.13	126.32	125.03
C(37)-C(38)-	176.41	179.66	93.36
C(39)-C(40)			

	5⁺	S ₀	T ₁
	X-Ray	S ₀	T ₁
Pt(1)-N(1)	-	2.289	2.290
Pt(1)-N(2)	-	2.202	2.203
Pt(1)-C(26)	-	2.043	2.042
Pt(1)-C(27)	-	2.065	2.064
Pt(1)-C(13)	-	2.045	2.047
Pt(1)-N(3)	-	2.288	2.266
C(7)-C(8)	-	1.450	1.450
C(20)-C(21)	-	1.448	1.448
C(38)-C(39)	-	1.221	1.266
C(40)-C(41)	-	1.221	1.263
C(27)-Pt(1)-N(1)	-	86.15	86.18
N(1)-Pt(1)-N(2)	-	97.85	97.77
C(26)-Pt(1)-N(2)	-	79.65	79.64
C(26)-Pt(1)-C(27)	-	96.04	96.07
N(3)-Pt(1)-N(1)	-	101.57	101.37
N(3)-Pt(1)-N(2)	-	88.46	88.67
N(3)-Pt(1)-C(26)	-	83.54	83.74
N(3)-Pt(1)-C(27)	-	94.38	94.37
C(38)-C(39)-C(40)-C(41)	-	14.40	20.86

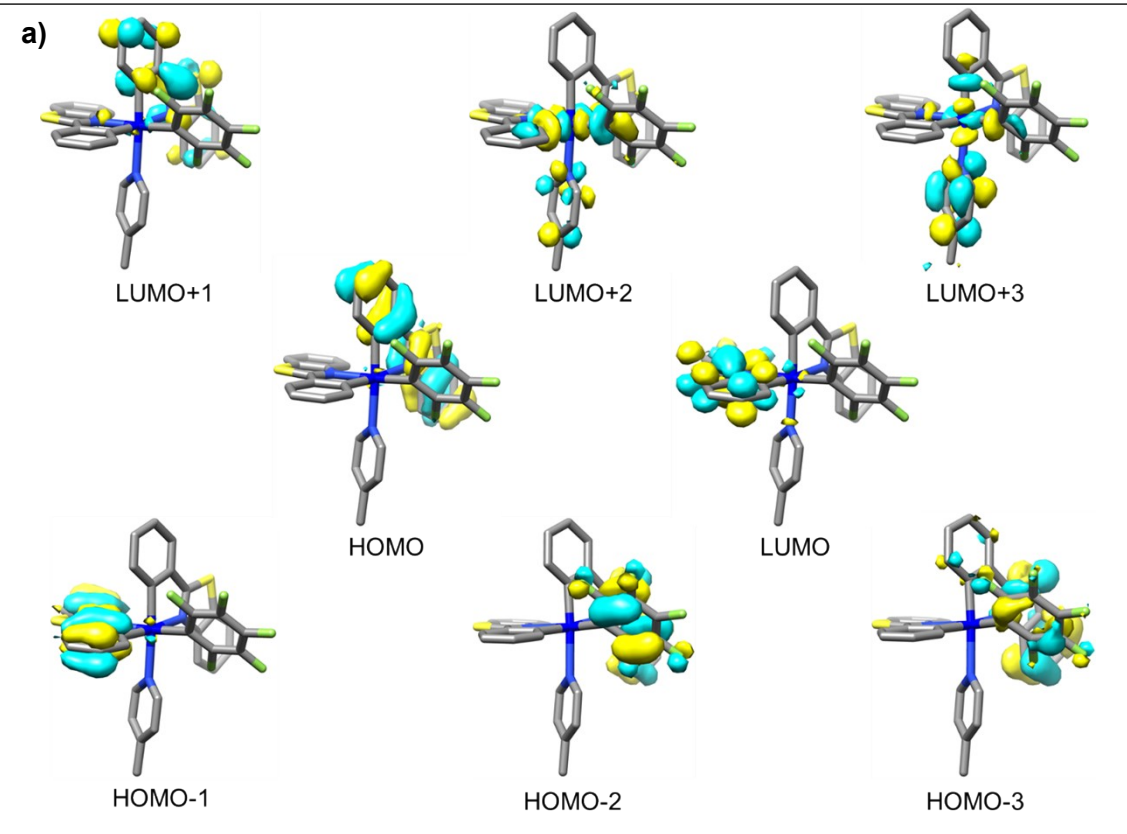
6

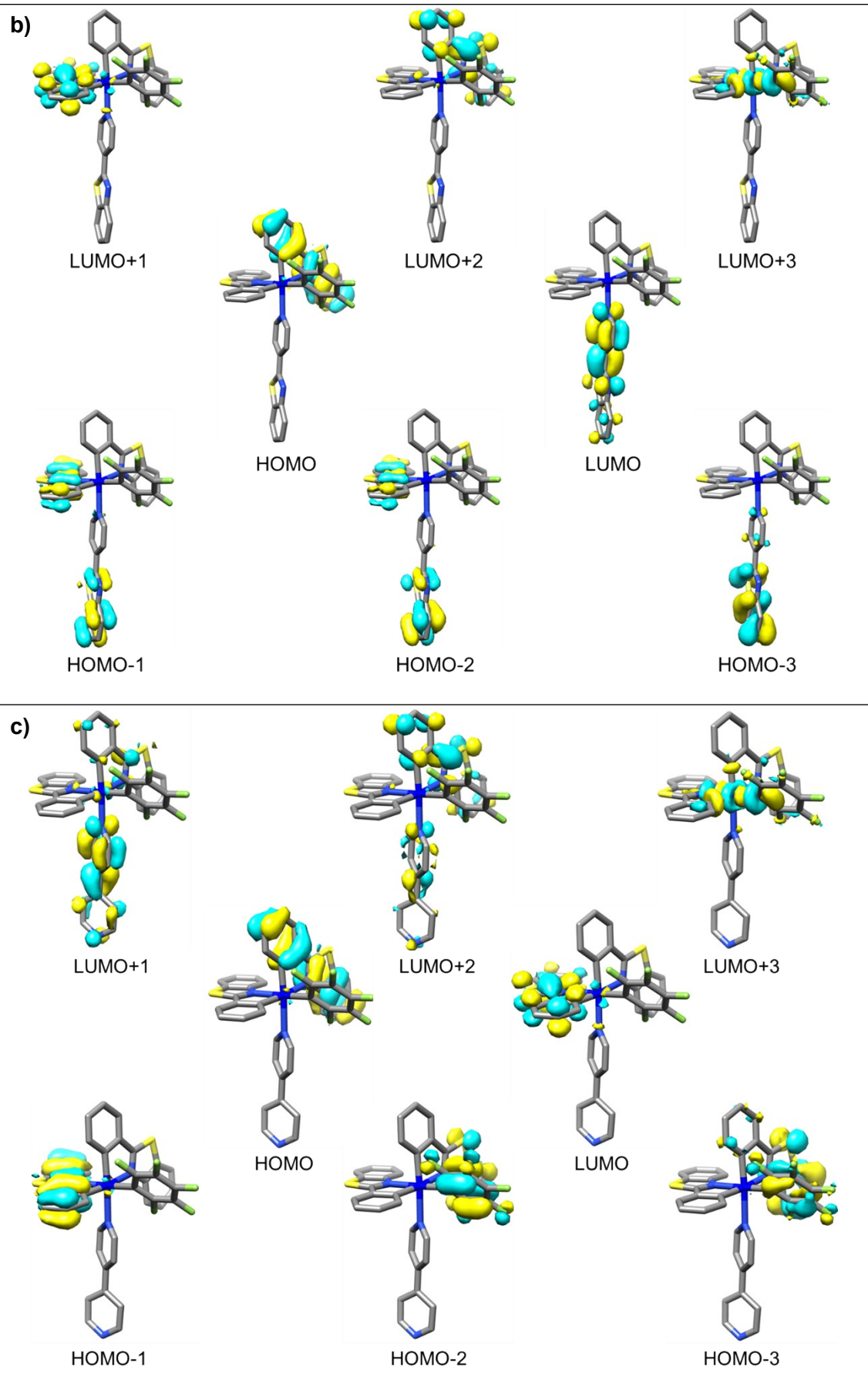
S₀T₁

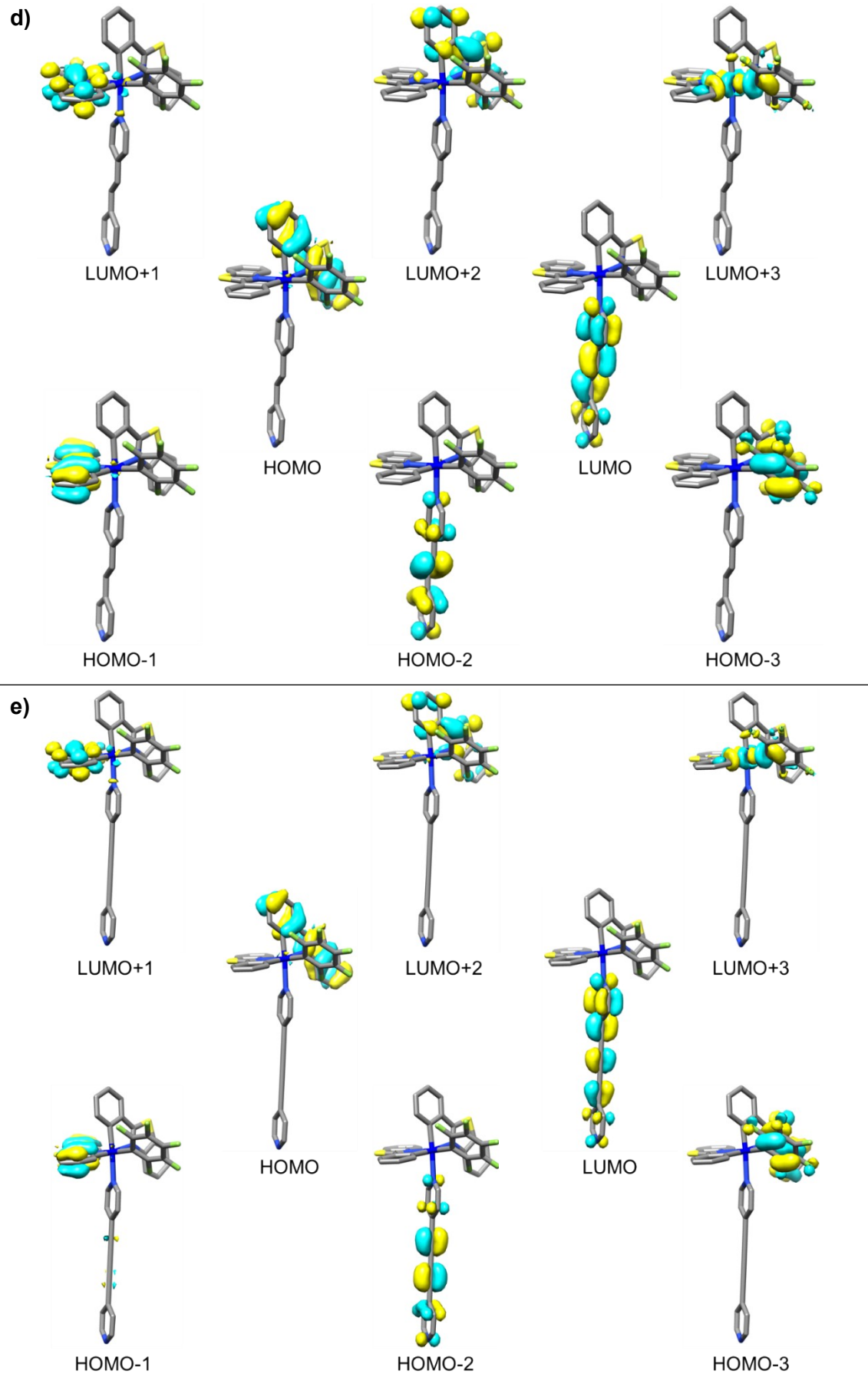
	X-Ray	S ₀	T ₁
Pt(1)-N(1)	2.301(6)	2.2541	2.2665
Pt(1)-N(2)	2.121(5)	2.2007	2.1810
Pt(1)-C(26)	2.172(7)	2.0350	2.0330
Pt(1)-C(27)	2.052(7)	2.0627	2.0633
Pt(1)-C(13)	1.879(7)	2.0410	2.0406
Pt(1)-O(1)	2.022(5)	2.1977	2.2033
C(7)-C(8)	1.534(12)	1.4515	1.4519
C(20)-C(21)	1.551(11)	1.4477	1.3798
C(27)-Pt(1)-N(1)	93.3(2)	87.869	88.002
N(1)-Pt(1)-N(2)	91.6(2)	97.181	96.797
C(26)-Pt(1)-N(2)	86.0(3)	79.615	80.291
C(26)-Pt(1)-C(27)	89.0(3)	95.074	94.658
O(1)-Pt(1)-N(1)	87.2(2)	95.399	95.524
O(1)-Pt(1)-N(2)	86.8(2)	94.893	94.293
O(1)-Pt(1)-C(26)	95.9(2)	88.210	88.386
O(1)-Pt(1)-C(27)	95.1(2)	89.052	89.172

7^{2+}			
	S_0	T_1	
Pt(1)-N(1A)	-	2.286	2.293
Pt(1)-N(2A)	-	2.200	2.201
Pt(1)-C(26A)	-	2.043	2.042
Pt(1)-C(27A)	-	2.065	2.065
Pt(1)-C(13A)	-	2.045	2.046
Pt(1)-N(3A)	-	2.290	2.279
C(7A)-C(8A)	-	1.450	1.450
C(20A)-C(21A)	-	1.448	1.448
C(38A)-C(39A)	-	1.220	1.265
Pt(2)-N(1B)	-	2.286	2.293
Pt(2)-N(2B)	-	2.200	2.201
Pt(2)-C(26B)	-	2.043	2.042
Pt(2)-C(27B)	-	2.065	2.065
Pt(2)-C(13B)	-	2.045	2.046
Pt(2)-N(3B)	-	2.290	2.279
C(7B)-C(8B)	-	1.450	1.450
C(20B)-C(21B)	-	1.448	1.448
C(38B)-C(39B)	-	1.220	1.265
C(27A)-Pt(1)-N(1A)	-	86.16	86.06
N(1A)-Pt(1)-N(2A)	-	97.85	97.87
C(26A)-Pt(1)-N(2A)	-	79.68	79.61
C(26A)-Pt(1)-C(27A)	-	95.99	96.12
N(3A)-Pt(1)-N(1A)	-	101.46	101.50
N(3A)-Pt(1)-N(2A)	-	88.30	88.53
N(3A)-Pt(1)-C(26A)	-	83.69	83.89
N(3A)-Pt(1)-C(27A)	-	94.54	94.36
C(27B)-Pt(2)-N(1B)	-	86.16	86.06
N(1B)-Pt(2)-N(2B)	-	97.85	97.87
C(26B)-Pt(2)-N(2B)	-	79.68	79.61

C(26B)-Pt(2)-C(27B)	-	95.99	96.12
N(3B)-Pt(2)-N(1B)	-	101.46	101.50
N(3B)-Pt(2)-N(2B)	-	88.30	88.53
N(3B)-Pt(2)-C(26B)	-	83.69	83.89
N(3B)-Pt(2)-C(27B)	-	94.54	94.36







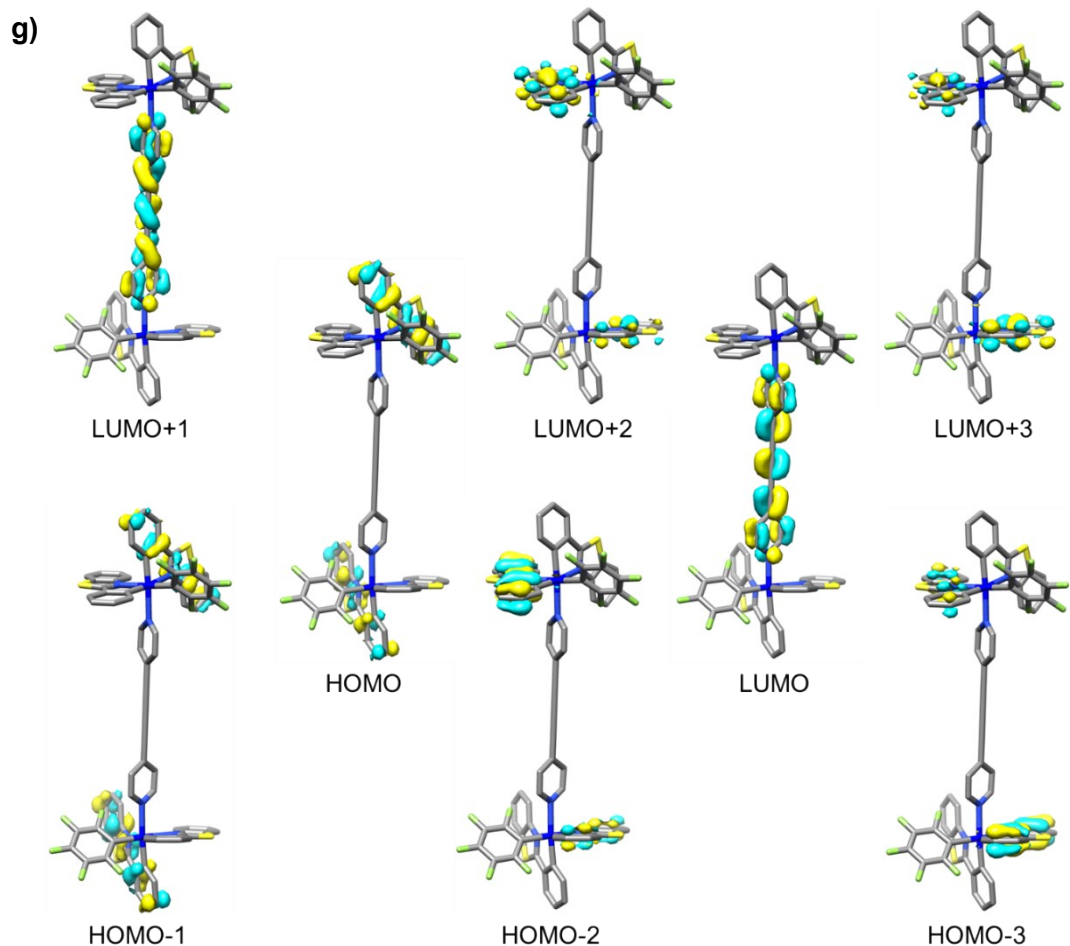
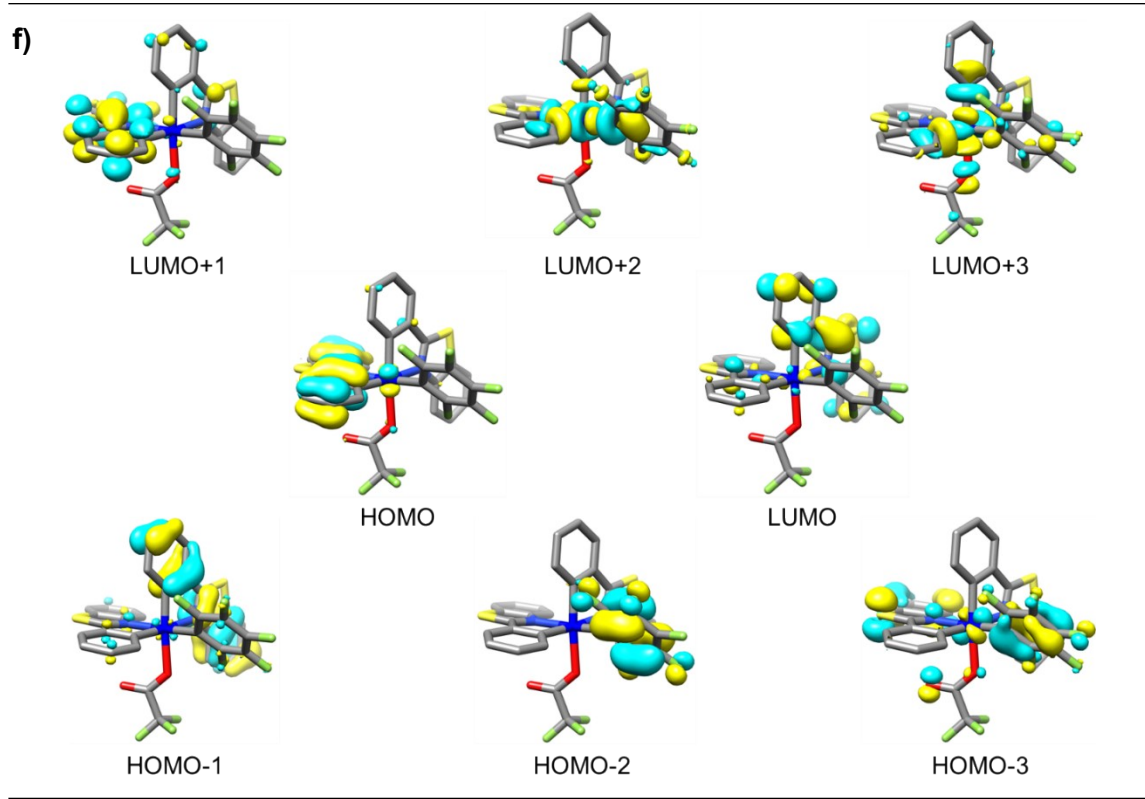


Fig. S13 Selected frontier Molecular Orbitals for a) 1^+ , b) 2^+ , c) 3^+ , d) 4^+ , e) 5^+ , f) 6 and g) 7^{2+} in the ground state.

Table S5. Selected vertical excitation energies singlets (S_0) and first triplets computed by TD-DFT/SCRF (CH_2Cl_2) with the orbitals involved.

	State	λ/nm	f	Transition (% Contribution)
1⁺	T ₁	464.04	-	H-1→LUMO (86%)
	T ₂	458.26	-	HOMO→L+1 (82%)
	S ₁	349.96	0.0163	HOMO→LUMO (95%)
	S ₂	339.12	0.2464	H-1→LUMO (88%)
	S ₃	332.64	0.3161	HOMO→L+1 (88%)
2⁺	T ₁	479.76	-	H-3→LUMO (15%). H-2→LUMO (34%). H-1→LUMO (37%)
	T ₂	464.69	-	H-2→L+1 (39%). H-1→L+1 (46%)
	T ₃	458.35	-	HOMO→L+2 (82%)
	S ₁	357.06	0.0131	HOMO→LUMO (95%)
	S ₄	351.17	0.0229	H-1→LUMO (21%), HOMO→L+1(66%)
	S ₅	342.86	0.8535	H-3→LUMO (37%). H-2→LUMO (25%). H-1→LUMO (18%)
	S ₆	339.48	0.2525	H-2→L+1 (33%). H-1→L+1 (40%)
3⁺	S ₇	331.96	0.4031	HOMO→L+2 (83%)
	T ₁	464.64	-	H-1→LUMO (86%)
	T ₂	458.25	-	HOMO→L+1 (22%). HOMO→L+2 (61%)
	S ₁	351.21	0.0147	HOMO→LUMO (95%)
	S ₂	339.62	0.2453	H-1→LUMO (88%)
4⁺	S ₃	334.57	0.2266	HOMO→L+1 (67%). HOMO→L+2 (20%)
	T ₁	534.87	-	H-2→LUMO (89%)
	T ₂	464.17	-	H-1→L+1 (85%)
	T ₃	458.21	-	HOMO→L+2 (82%)
	S ₁	352.56	0.0096	HOMO→LUMO (93%)
	S ₄	339.24	0.2974	H-1→L+1 (87%)
	S ₅	333.32	0.2293	H-2→LUMO (20%). HOMO→L+2 (69%)
5⁺	S ₆	328.28	1.4438	H-2→LUMO (73%). HOMO→L+2 (20%)
	T ₁	539.55	-	H-2→LUMO (80%)
	T ₂	464.81	-	H-1→L+1 (78%)
	T ₃	458.47	-	HOMO→L+2 (82%)
	S ₁	371.64	0.1756	HOMO→LUMO (89%)
	S ₃	367.19	0.9358	H-2→LUMO (48%). H-1→LUMO (31%)
	S ₄	364.16	0.1459	H-2→LUMO (37%). H-1→LUMO (61%)
6	S ₉	332.65	0.2983	HOMO→L+2 (76%)
	T ₁	462.95		HOMO→LUMO (11%). HOMO→L+1 (66%)
	T ₂	459.73		H-1→LUMO (64%). H-1→L+1 (11%)
	S ₁	340.72	0.0563	HOMO→LUMO (92%)
	S ₂	335.99	0.1238	H-1→LUMO (10%). HOMO→L+1 (78%)
7²⁺	S ₃	332.83	0.3845	H-1→L+1 (81%). HOMO→L+1 (10%)
	T ₁	501.88	-	H-17→L+1 (14%). H-14→LUMO (59%). H-12→LUMO (12%)
	T ₂	465.18	-	H-3→L+3 (17%). H-2→L+2 (20%). H-2→L+3 (40%)
	T ₃	465.16	-	H-3→L+2 (39%). H-3→L+3 (20%). H-2→L+2 (18%)
	T ₄	458.06	-	H-1→L+4 (37%). HOMO→L+5 (32%)
	S ₁	383.80	0.0083	HOMO→LUMO (94%)
	S ₆	356.81	0.6137	H-17→L+1 (15%). H-14→LUMO (54%). H-12→LUMO (11%)
	S ₈	352.42	0.0256	H-1→L+3 (45%). HOMO→L+2 (43%)

Table S6. Composition (%) of Frontier MOs in terms of ligands and metals in the ground state in CH₂Cl₂.

1 ⁺						
MO	eV	Pt	pbt(1)	pbt(2)	C ₆ F ₅	Mepy
LUMO+5	-1.19	1	3	4	1	91
LUMO+4	-1.59	24	16	17	6	37
LUMO+3	-1.84	18	9	13	12	48
LUMO+2	-2.01	29	21	12	19	20
LUMO+1	-2.48	3	6	90	1	0
LUMO	-2.65	4	90	4	2	1
HOMO	-6.74	2	0	94	4	0
HOMO-1	-6.85	2	97	1	0	0
HOMO-2	-7.05	0	1	30	69	0
HOMO-3	-7.12	1	1	71	28	0
HOMO-4	-7.18	6	56	6	31	0
HOMO-5	-7.26	4	44	17	35	1

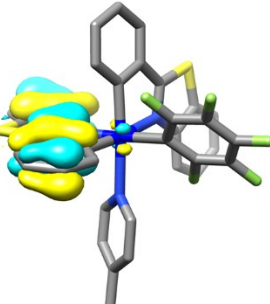
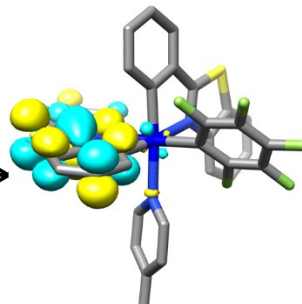
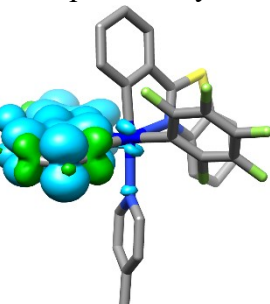
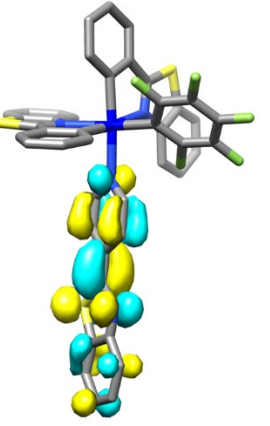
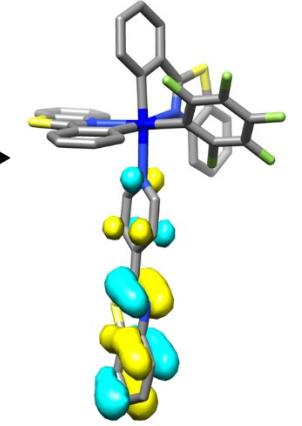
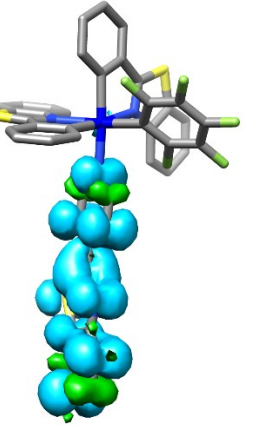
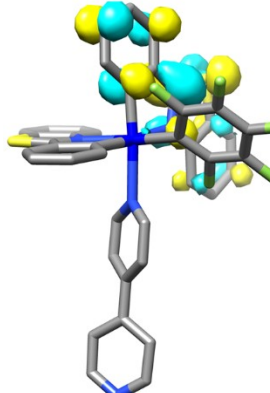
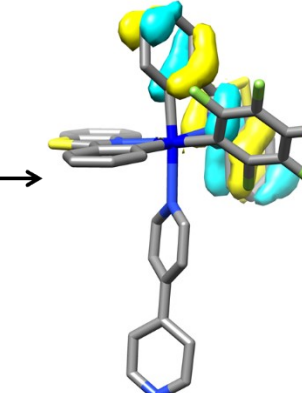
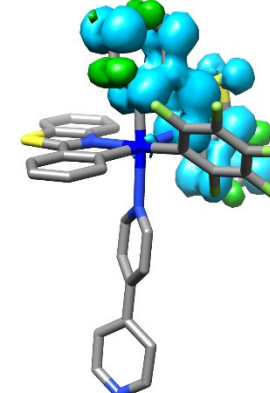
2 ⁺						
MO	eV	Pt	pbt(1)	pbt(2)	C ₆ F ₅	pybt
LUMO+5	-1,35	1	2	2	1	94
LUMO+4	-1,72	35	22	27	8	8
LUMO+3	-1,97	32	24	14	27	3
LUMO+2	-2,48	3	6	90	1	0
LUMO+1	-2,66	4	89	4	2	2
LUMO	-2,84	2	0	1	0	97
HOMO	-6,74	2	1	94	4	0
HOMO-1	-6,85	1	52	1	0	46
HOMO-2	-6,86	1	44	0	0	55
HOMO-3	-6,92	0	1	0	0	98
HOMO-4	-7,05	0	0	31	68	0
HOMO-5	-7,12	1	1	69	29	0

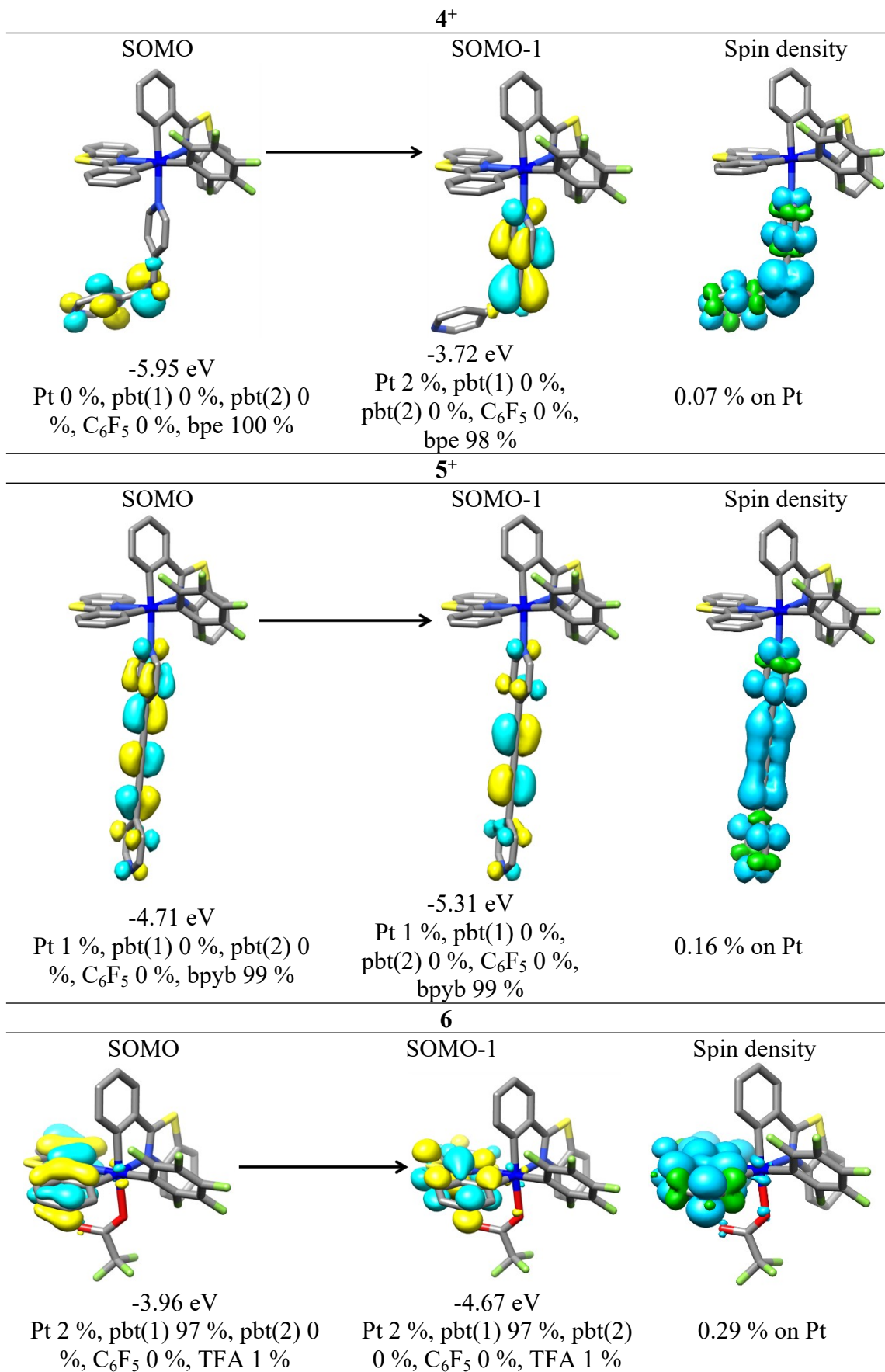
3⁺						
MO	eV	Pt	pbt(1)	pbt(2)	C ₆ F ₅	4,4'-bipy
LUMO+5	-1,38	1	2	2	1	95
LUMO+4	-1,73	34	22	26	8	9
LUMO+3	-1,98	32	23	14	27	4
LUMO+2	-2,48	1	3	69	0	26
LUMO+1	-2,53	4	3	23	1	69
LUMO	-2,67	4	90	3	2	1
HOMO	-6,75	2	0	94	4	0
HOMO-1	-6,87	2	97	1	0	0
HOMO-2	-7,06	0	0	34	65	0
HOMO-3	-7,13	1	1	66	32	0
HOMO-4	-7,2	5	57	7	30	0
HOMO-5	-7,27	4	42	19	34	1
4⁺						
MO	eV	Pt	pbt(1)	pbt(2)	C ₆ F ₅	bpe
LUMO+5	-1,24	1	3	3	1	92
LUMO+4	-1,7	34	21	27	9	9
LUMO+3	-1,97	33	25	13	27	3
LUMO+2	-2,48	3	5	91	1	0
LUMO+1	-2,66	4	90	3	2	1
LUMO	-2,82	2	0	1	0	98
HOMO	-6,74	2	1	94	4	1
HOMO-1	-6,86	2	95	1	0	2
HOMO-2	-6,92	1	2	1	0	96
HOMO-3	-7,05	0	0	30	69	0
HOMO-4	-7,12	1	1	70	28	0
HOMO-5	-7,19	6	52	8	34	0

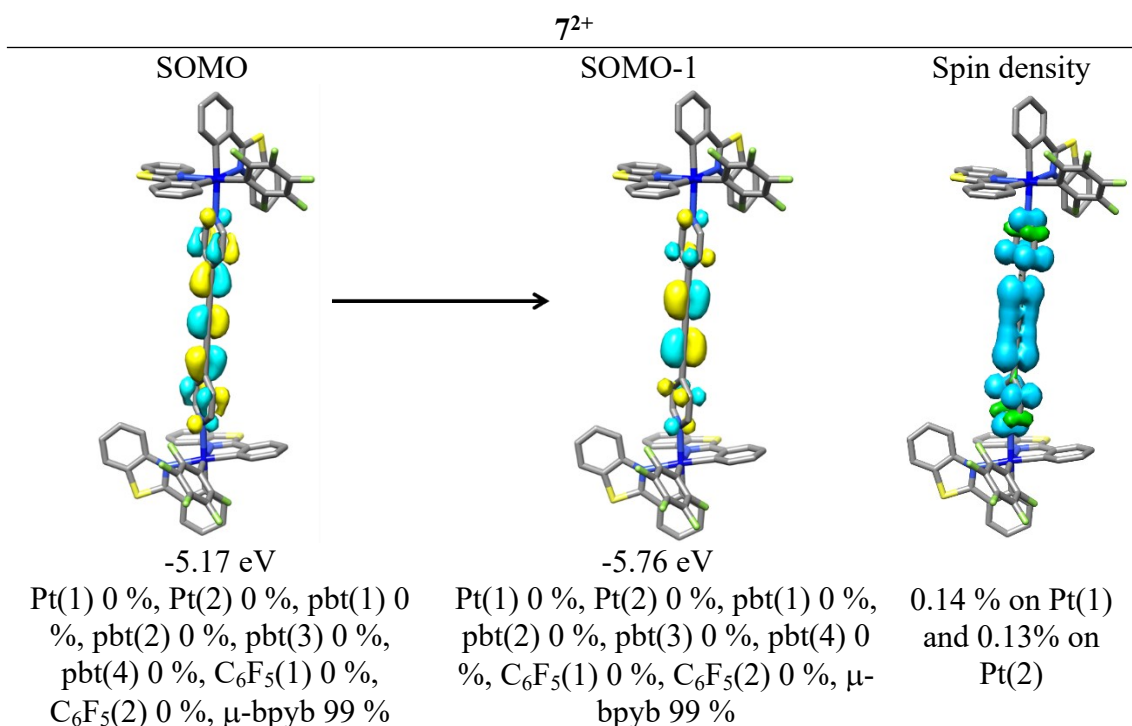
5⁺						
MO	eV	Pt	pbt(1)	pbt(2)	C ₆ F ₅	bpyb
LUMO+5	-1,55	5	4	3	1	86
LUMO+4	-1,77	31	18	24	8	19
LUMO+3	-2	32	24	14	27	3
LUMO+2	-2,49	3	6	90	1	0
LUMO+1	-2,68	4	89	4	2	2
LUMO	-3,02	1	0	0	0	98
HOMO	-6,75	2	1	94	4	1
HOMO-1	-6,86	1	87	1	0	10
HOMO-2	-6,89	1	10	1	0	89
HOMO-3	-7,06	0	0	33	66	0
HOMO-4	-7,13	1	1	67	31	0
HOMO-5	-7,2	5	60	6	29	0
6						
MO	eV	Pt	pbt(1)	pbt(2)	C ₆ F ₅	TFA
LUMO+5	-0,47	1	30	68	0	0
LUMO+4	-0,6	2	69	29	0	0
LUMO+3	-1,2	36	22	26	10	7
LUMO+2	-1,41	34	23	12	30	0
LUMO+1	-2,15	2	81	15	1	1
LUMO	-2,17	3	15	82	1	0
HOMO	-6,39	4	83	11	1	1
HOMO-1	-6,43	1	13	80	5	0
HOMO-2	-6,67	0	0	9	90	0
HOMO-3	-6,76	7	50	4	32	7
HOMO-4	-6,79	1	7	67	20	5
HOMO-5	-6,83	4	20	37	22	18

MO	eV	γ^{2+}								
		Pt (1)	Pt (2)	pbt (1)	pbt (2)	pbt (3)	pbt (4)	C ₆ F ₅ (1)	C ₆ F ₅ (2)	μ -bpyb
LUMO+5	-2,58	1	1	3	47	3	44	0	0	1
LUMO+4	-2,58	1	1	3	44	3	47	0	0	0
LUMO+3	-2,77	3	1	59	2	30	1	1	1	2
LUMO+2	-2,77	1	3	30	1	59	2	1	1	2
LUMO+1	-2,81	1	1	0	1	0	1	0	0	96
LUMO	-3,26	1	1	0	0	0	0	0	0	98
HOMO	-6,84	1	1	0	53	0	41	2	2	0
HOMO-1	-6,84	1	1	0	41	0	53	2	2	0
HOMO-2	-6,96	1	1	67	1	30	0	0	0	0
HOMO-3	-6,96	1	1	30	0	67	1	0	0	0
HOMO-4	-7,15	0	0	0	12	0	21	25	42	0
HOMO-5	-7,15	0	0	0	21	0	12	42	25	0
HOMO-12	-7,43	1	1	4	24	4	23	13	13	16
HOMO-14	-7,46	1	1	0	10	0	10	1	1	76
HOMO-17	-7,65	0	0	1	1	1	1	0	0	97

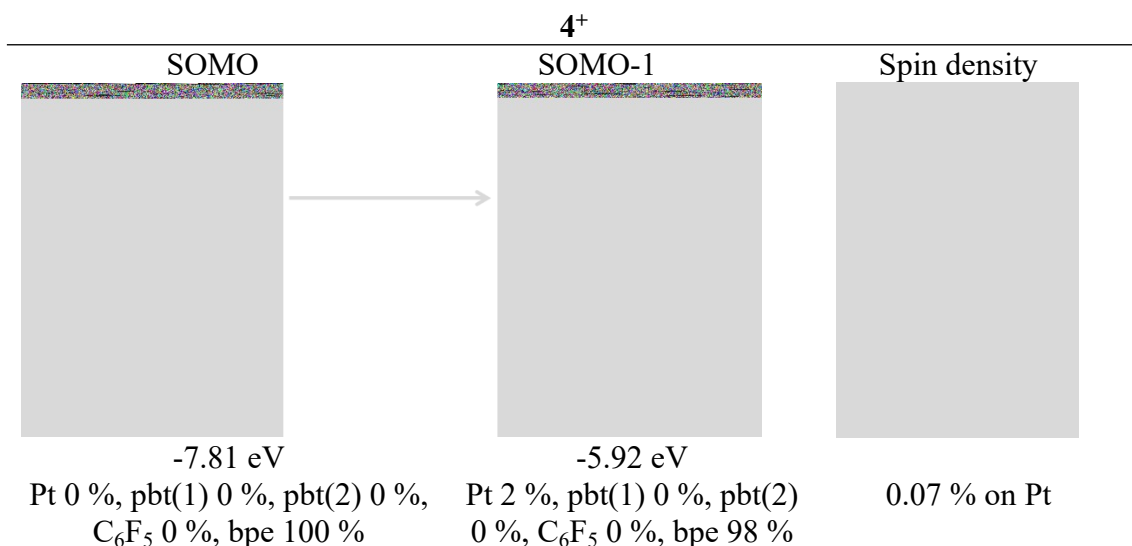
Table S7. Plots and composition (%) of the frontier MOs and spin density of the first triplet state in CH_2Cl_2 .

1^+		
SOMO	SOMO-1	Spin density
		
-4.42 eV Pt 2 %, pbt(1) 97 %, pbt(2) 0 %, C_6F_5 0 %, 4-Mepy 1 %	-5.17 eV Pt 1 %, pbt(1) 98 %, pbt(2) 0 %, C_6F_5 0 %, 4-Mepy 0 %	0.33 % on Pt
2^+		
SOMO	SOMO-1	Spin density
		
-4.61 eV Pt 1 %, pbt(1) 0 %, pbt(2) 0 %, C_6F_5 0 %, pybt 99 %	-5.14 eV Pt 1 %, pbt(1) 0 %, pbt(2) 0 %, C_6F_5 0 %, pybt 99 %	0.19 % on Pt
3^+		
SOMO	SOMO-1	Spin density
		
-4.30 eV Pt 2 %, pbt(1) 1 %, pbt(2) 97 %, C_6F_5 0 %, 4,4'-bipy 0 %	-5.06 eV Pt 1 %, pbt(1) 0 %, pbt(2) 98 %, C_6F_5 1 %, 4,4'-bipy 0 %	0 % on Pt





Plots and composition (%) of the frontier MOs and spin density of the first triplet state of **4** in gas phase.



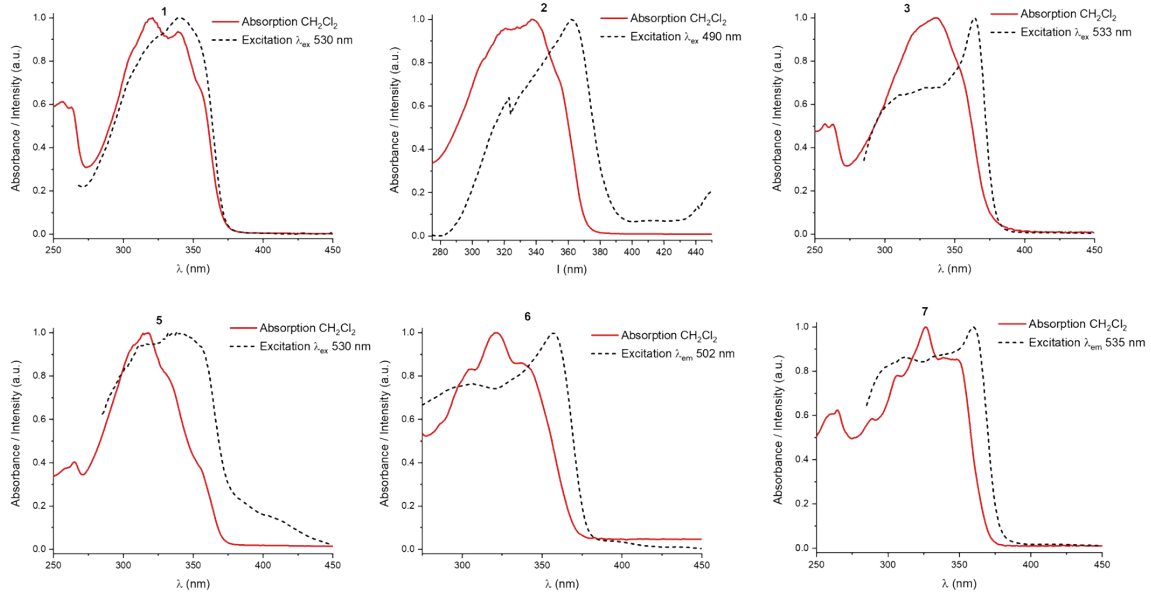
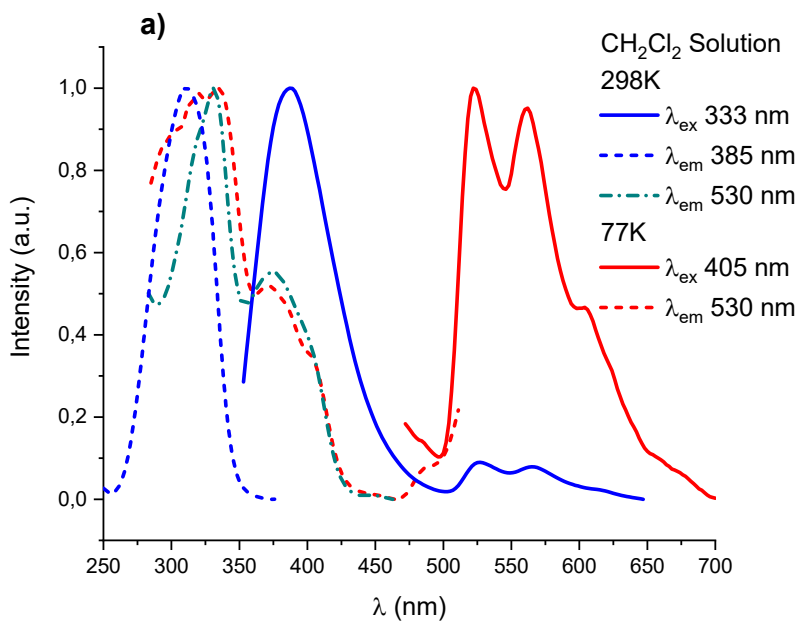


Fig. S14 Overlaid UV-Vis absorption and excitation spectra of complexes **1–3** and **5–7** in CH_2Cl_2 solution (5×10^{-5} M) at 298 K.



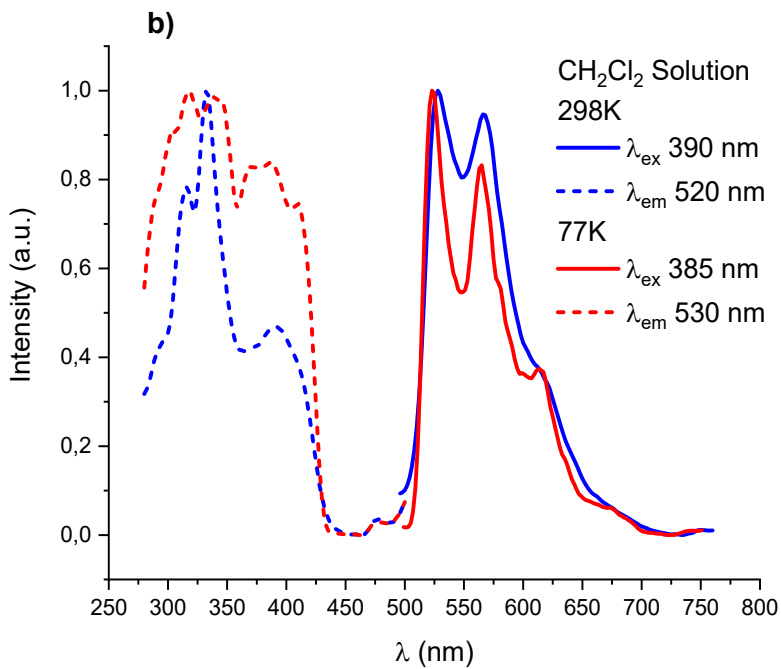


Fig. S15 Emission spectra of the free ligands: a) 4-pyridylbenzothiazole (pybt), b) 1,4-bis-(pyridyl)-butadiyne (bpyb).

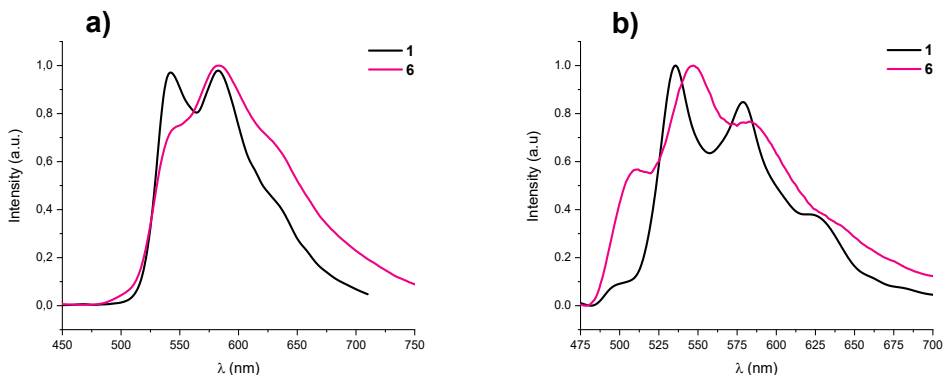


Fig. S16 Emission spectra complexes **1** and **6** in the solid state at a) 298 K and b) 77 K.

Singlet Oxygen Measurements

The singlet oxygen quantum yield was measured evaluating the phosphorescence of ${}^1\text{O}_2$ at 1274 nm with an Edinburgh FLS1000 spectrofluorimeter equipped with Xe lamp and a NIR detector (900 – 1800 nm). The absorbance was detected with a Hewlett Packard 8453 spectrophotometer. For each sample, the emission spectra were recorded upon excitation at 365 nm. As a reference the whole procedure was repeated for the known standard phenalenone (PN). The area below the signal was integrated with Origin Pro2018. The respective singlet oxygen quantum yield $\phi({}^1\text{O}_2)$ was calculated and

referenced against the literature reported value for the phenalenone $\phi = 1$ in acetonitrile,¹² following the next equation:

$$\Phi_C = \Phi_R \cdot \frac{A_R}{A_C} \cdot \frac{I_C}{I_R} \quad (eq. 1)$$

In this equation ϕ_C is the $^1\text{O}_2$ quantum yield of the compound and ϕ_R is the $^1\text{O}_2$ quantum yield of the reference (phenalenone), A_C the absorbance of the compound and A_R the absorbance of reference, I_C the area of the singlet oxygen emission of the compound and I_R the area of the singlet oxygen emission of the reference.

5.- Biological Studies

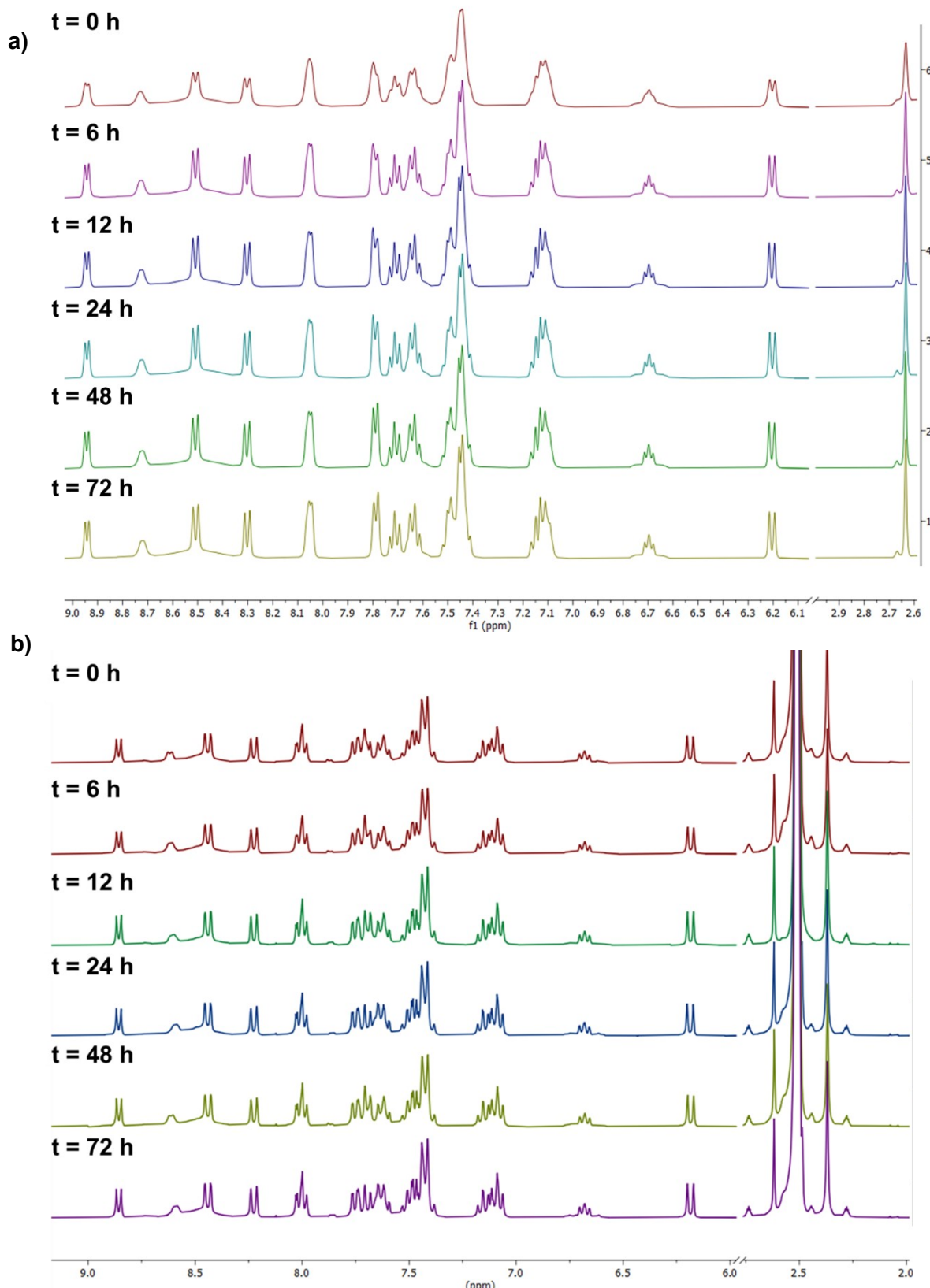


Fig. S17 Stability of **1** monitored by ^1H NMR at several times (0–72 h) recorded in a) DMSO- d^6 , b) DMSO- $\text{d}^6/\text{D}_2\text{O}$ (9/1).

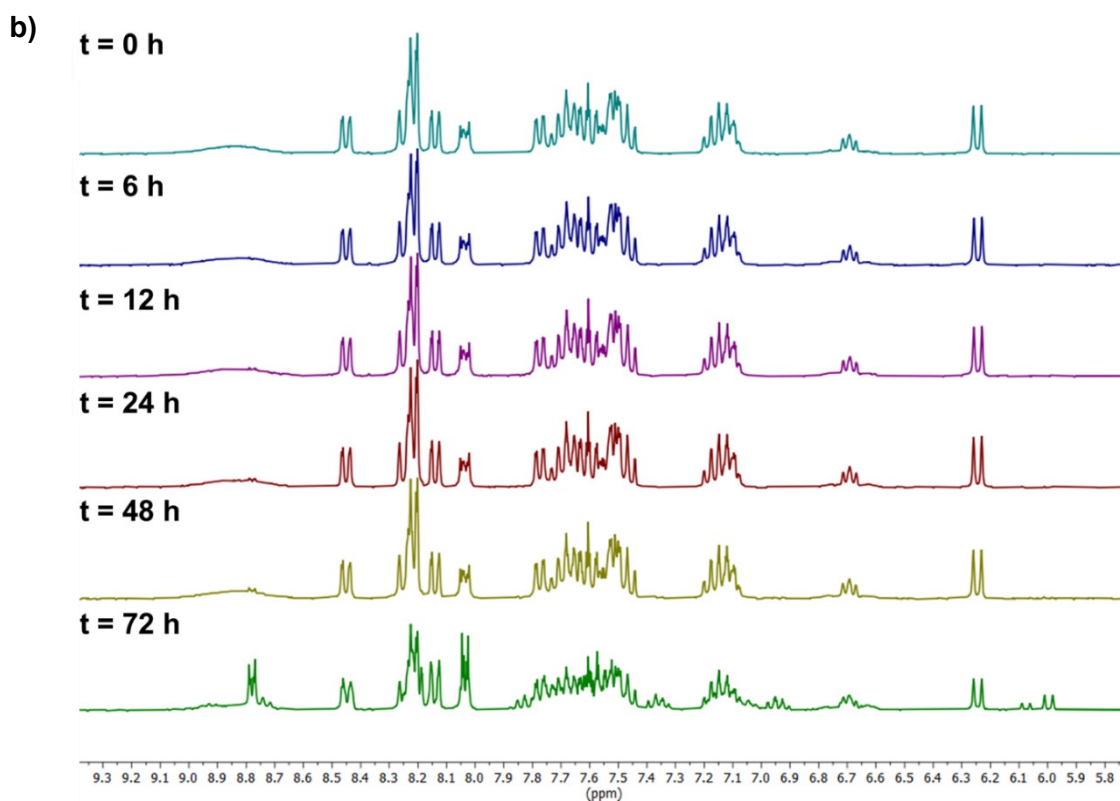
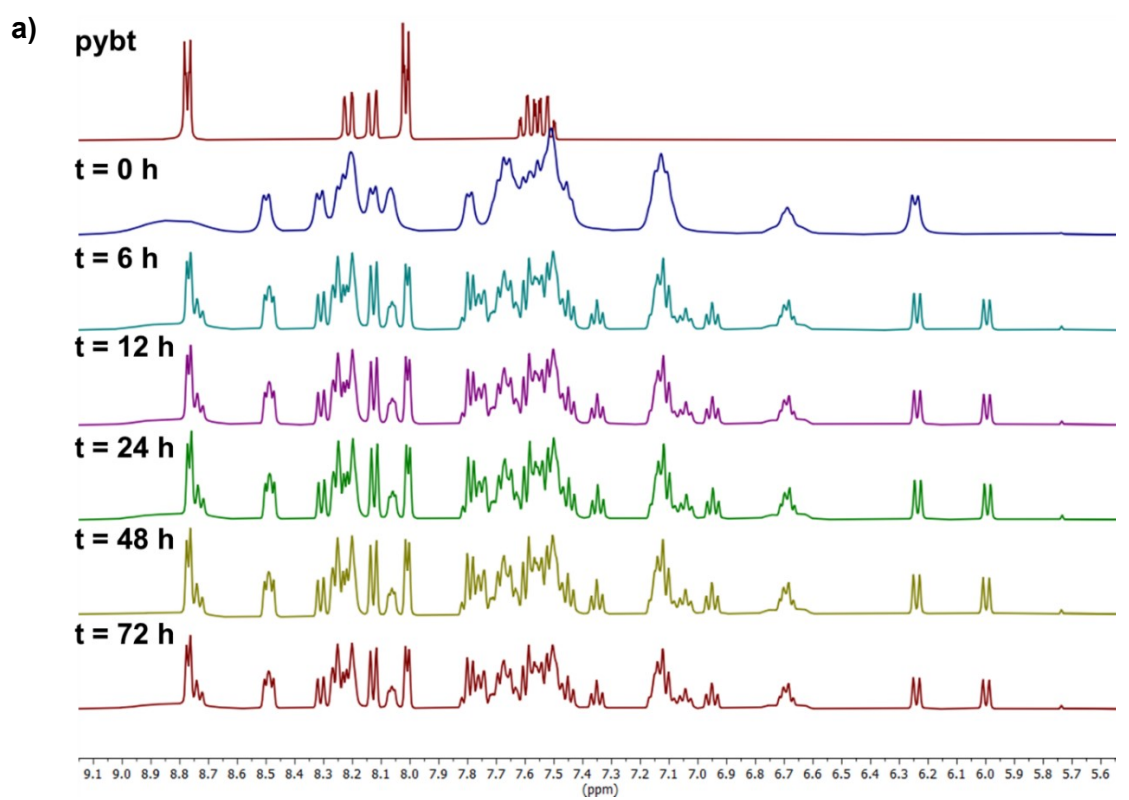


Fig. S18 Stability of **2** monitored by ^1H NMR at several times (0–72 h) together with the free ligand pybt, recorded in a) DMSO-d⁶, b) DMSO-d⁶/D₂O (9/1).

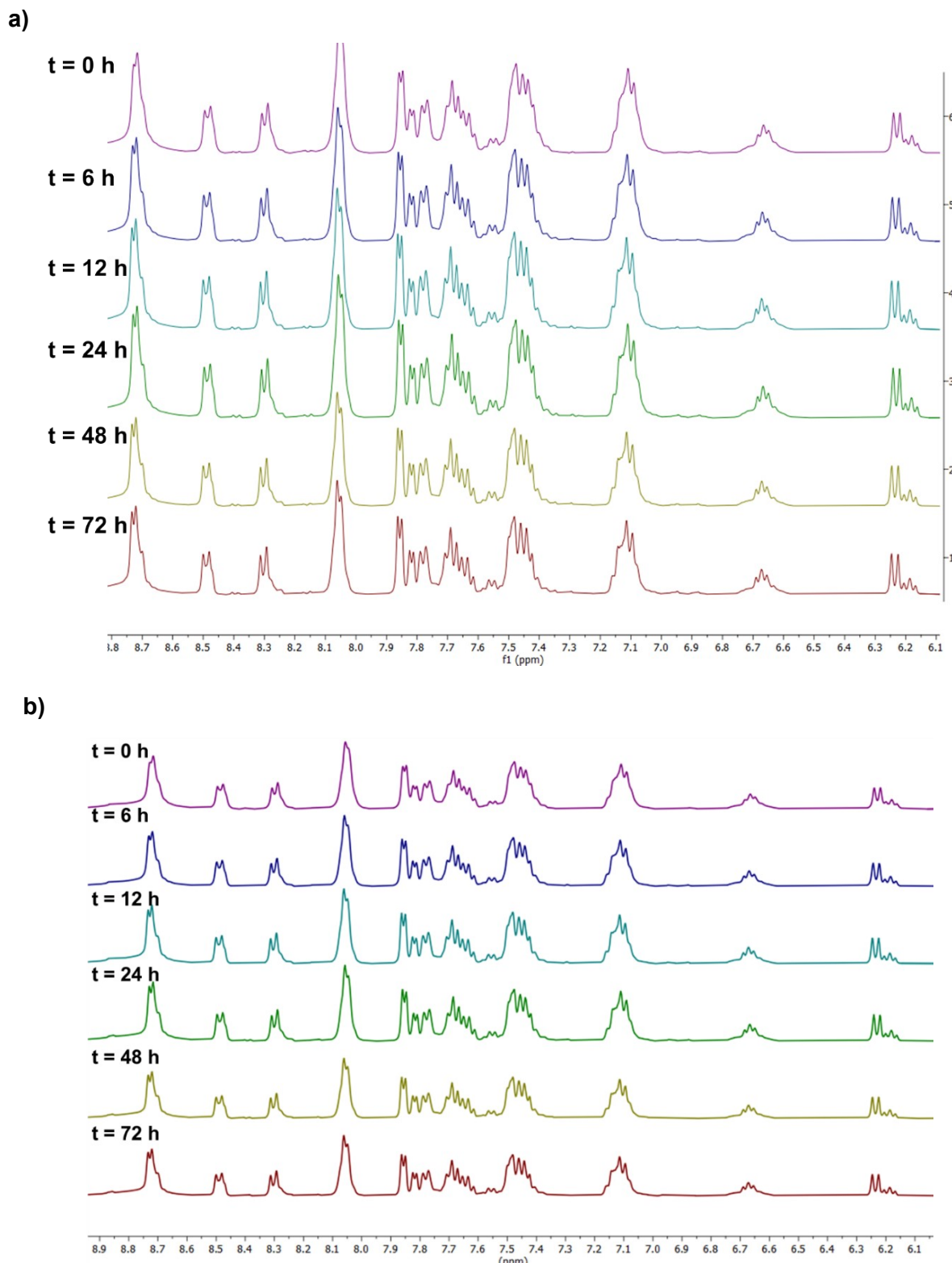
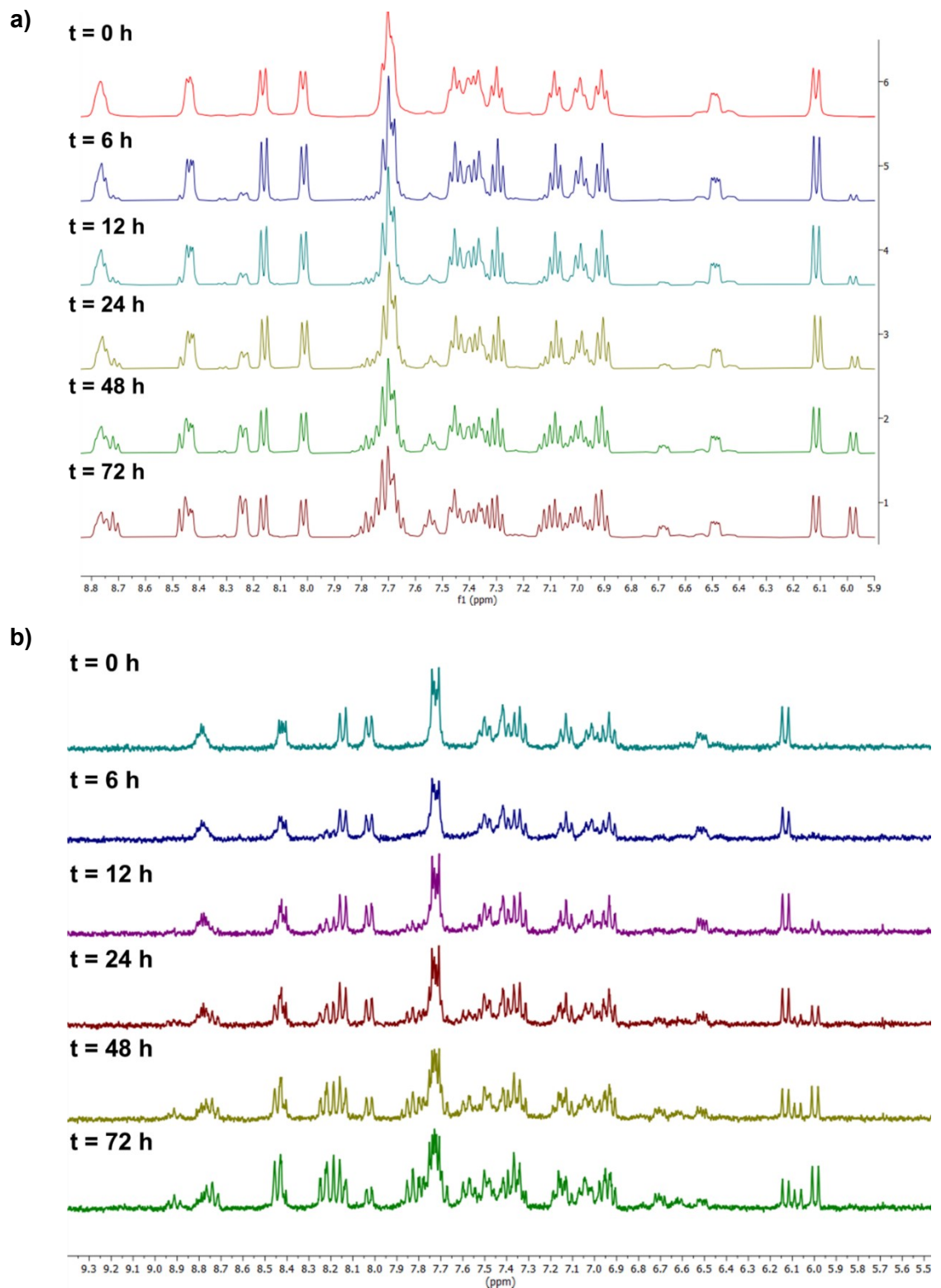


Fig. S19 Stability of **3** monitored by ^1H NMR at several times (0–72 h) recorded in a) DMSO-d⁶, b) DMSO-d⁶/D₂O (9/1).



c)

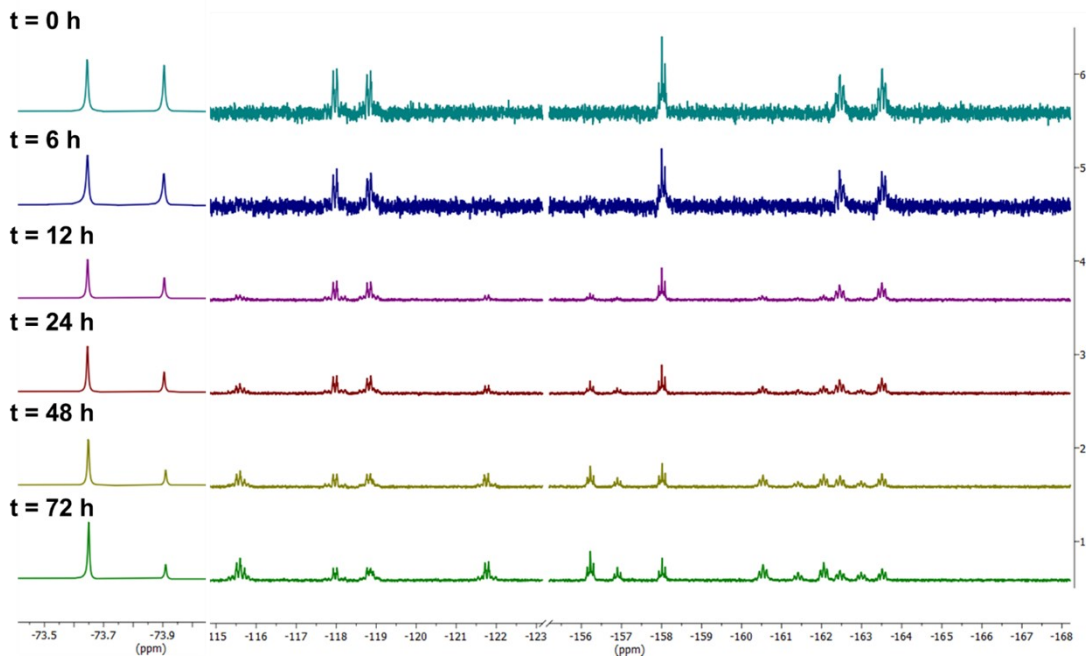


Fig. S20 Stability of **6** monitored by a) ^1H NMR recorded in DMSO-d^6 , b) ^1H and c) $^{19}\text{F}\{^1\text{H}\}$ NMR recorded in $\text{DMSO-d}^6/\text{D}_2\text{O}$ (9/1) at several times (0–72 h.).

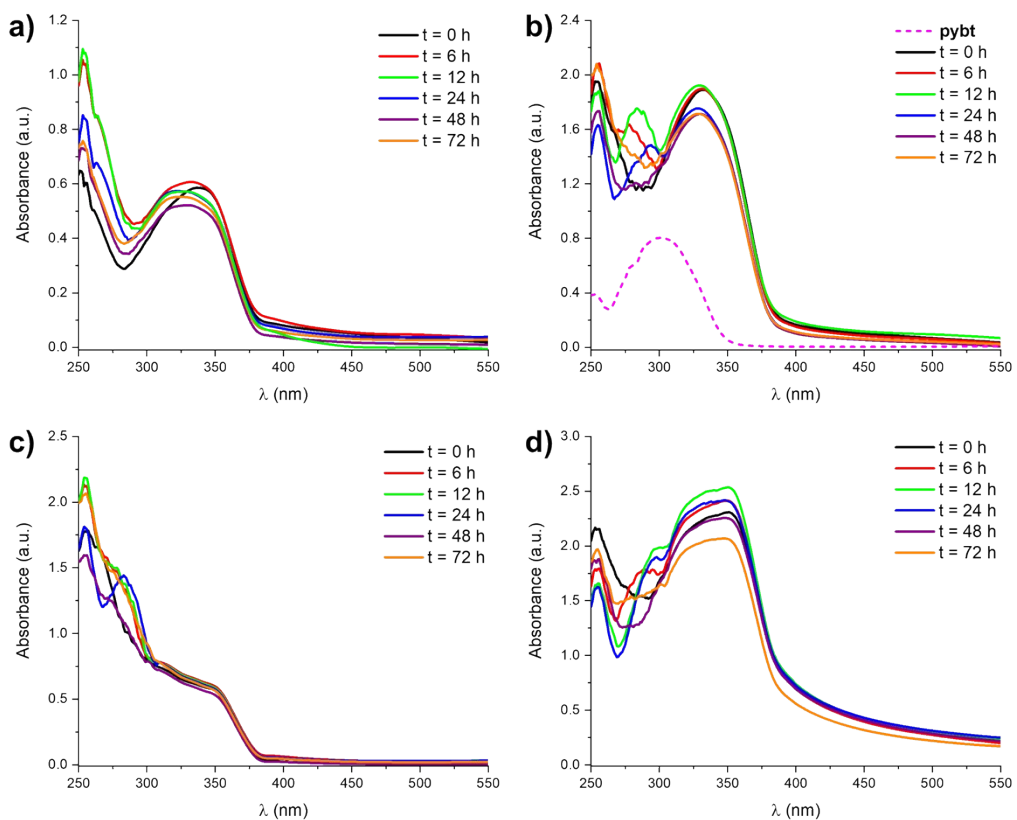


Fig. S21 UV-Vis absorption spectra of a) **1**, b) **2** and **pybt** ligand, c) **3** and d) **6** (5×10^{-5} M) recorded in DMSO (<1%)-cellular medium after been kept at room temperature from 0 to 72 h (intervals in legends).

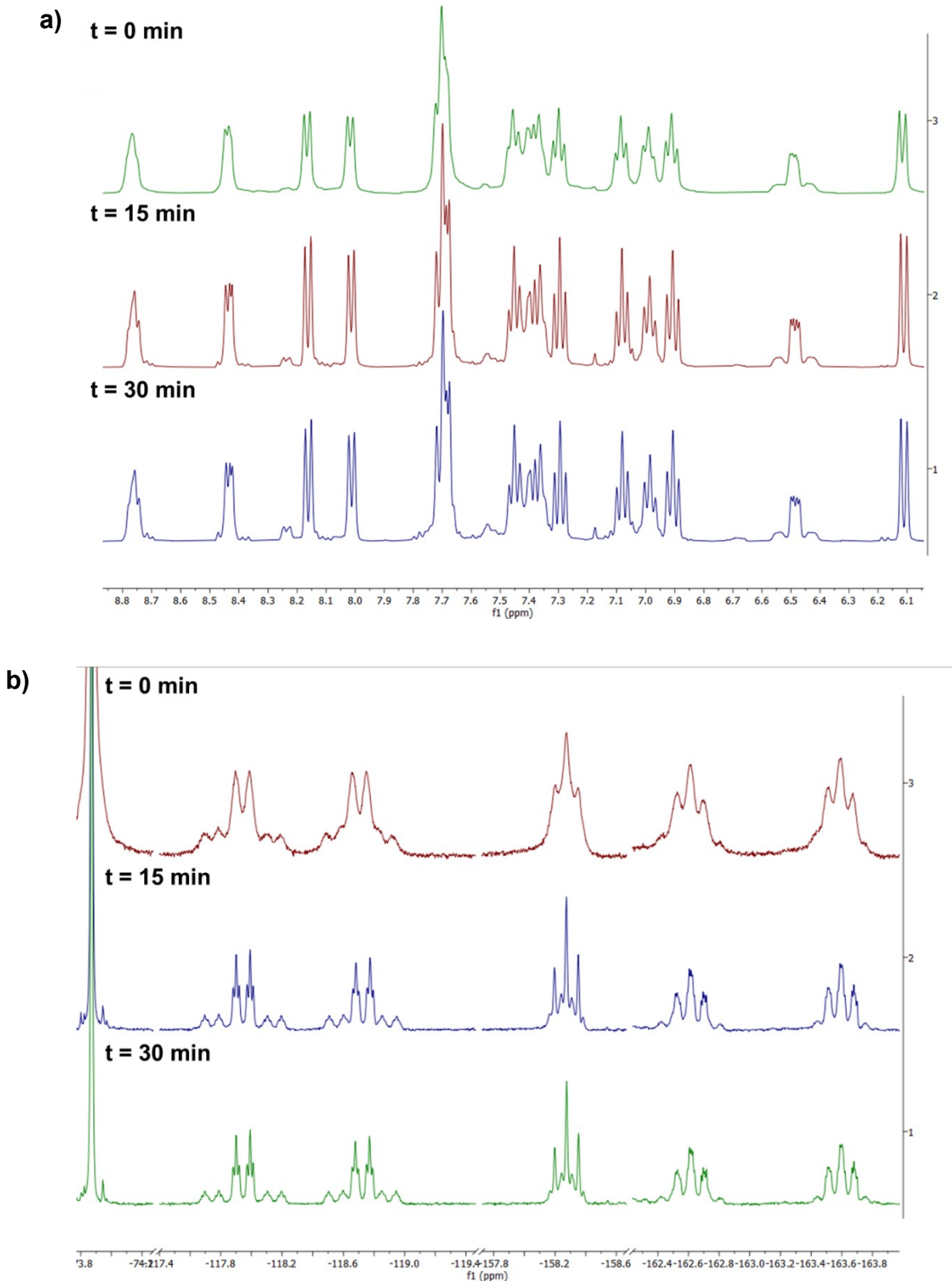
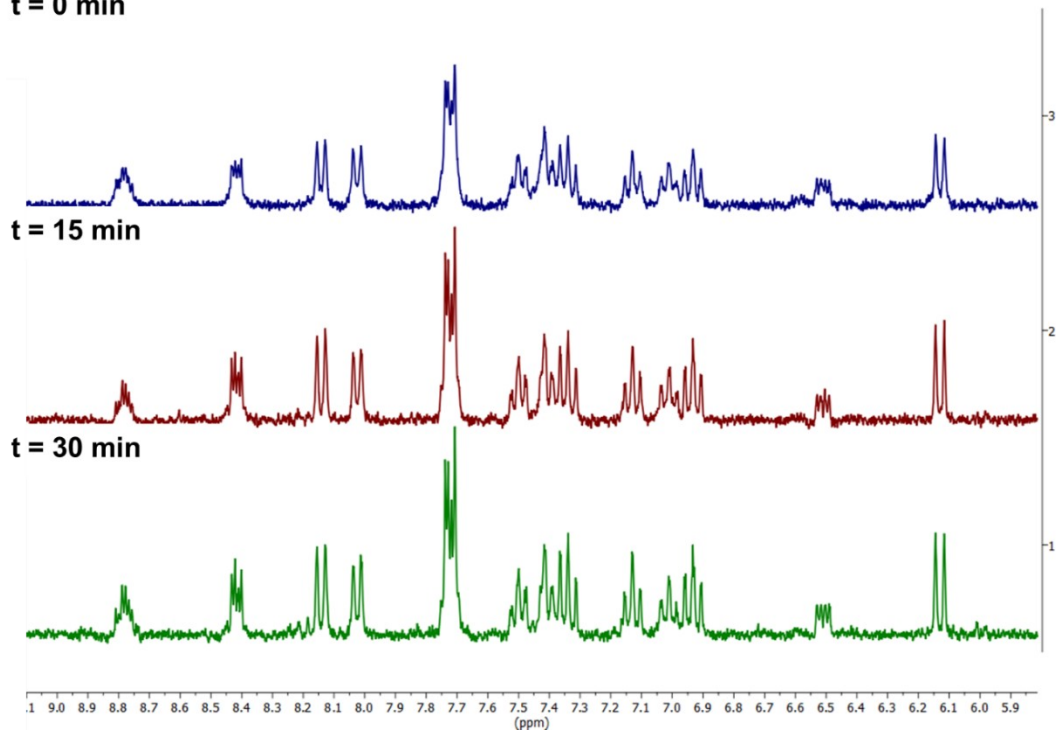


Fig. S22 Photostability of **6** monitored by a) ^1H and b) $^{19}\text{F}\{^1\text{H}\}$ NMR recorded in DMSO-d^6 irradiated at several times (0, 15, 30 min.) with a $\lambda = 396$ nm (15 W).

a) $t = 0 \text{ min}$



b) $t = 0 \text{ min}$

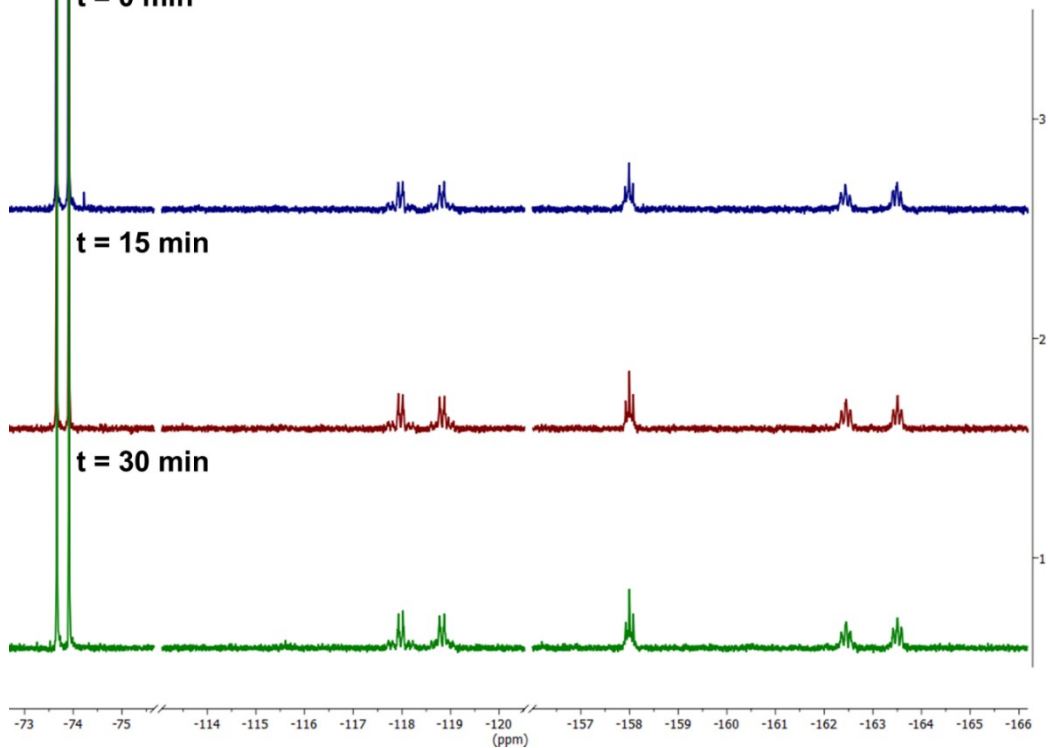


Fig. S23 Photostability of **6** monitored by a) ^1H and b) $^{19}\text{F}\{^1\text{H}\}$ NMR recorded in DMSO- $\text{d}^6/\text{D}_2\text{O}$ (9/1) irradiated at several times (0, 15, 30 min.) with a $\lambda = 396 \text{ nm}$ (15 W).

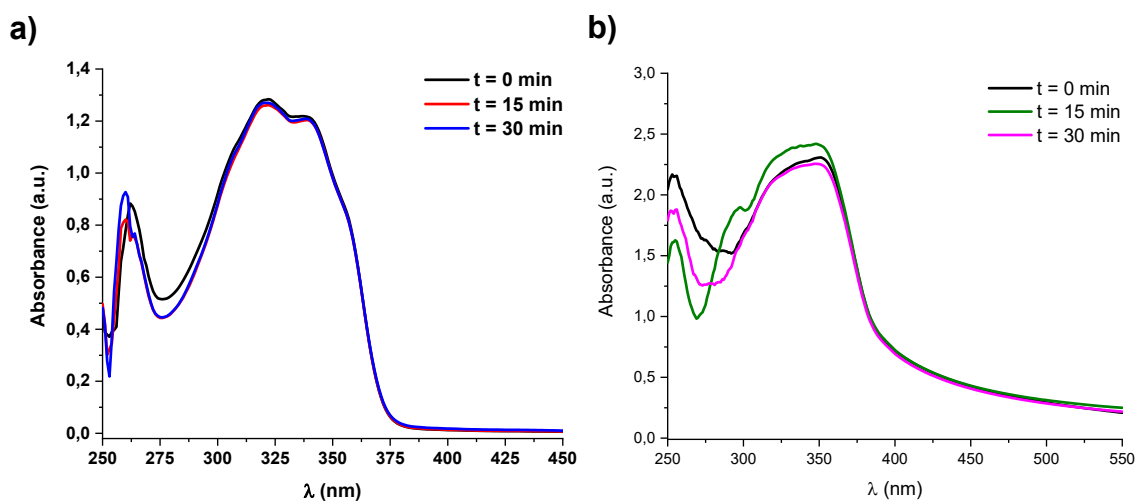


Fig. S24 Photostability of **6** monitored by UV-vis absorption spectra recorded in a) DMSO ($5 \times 10^{-5} \text{ M}$), b) in DMSO (<1%) - cellular medium, irradiated at several times (0, 15, 30 min.) with a $\lambda = 396 \text{ nm}$ (15W).

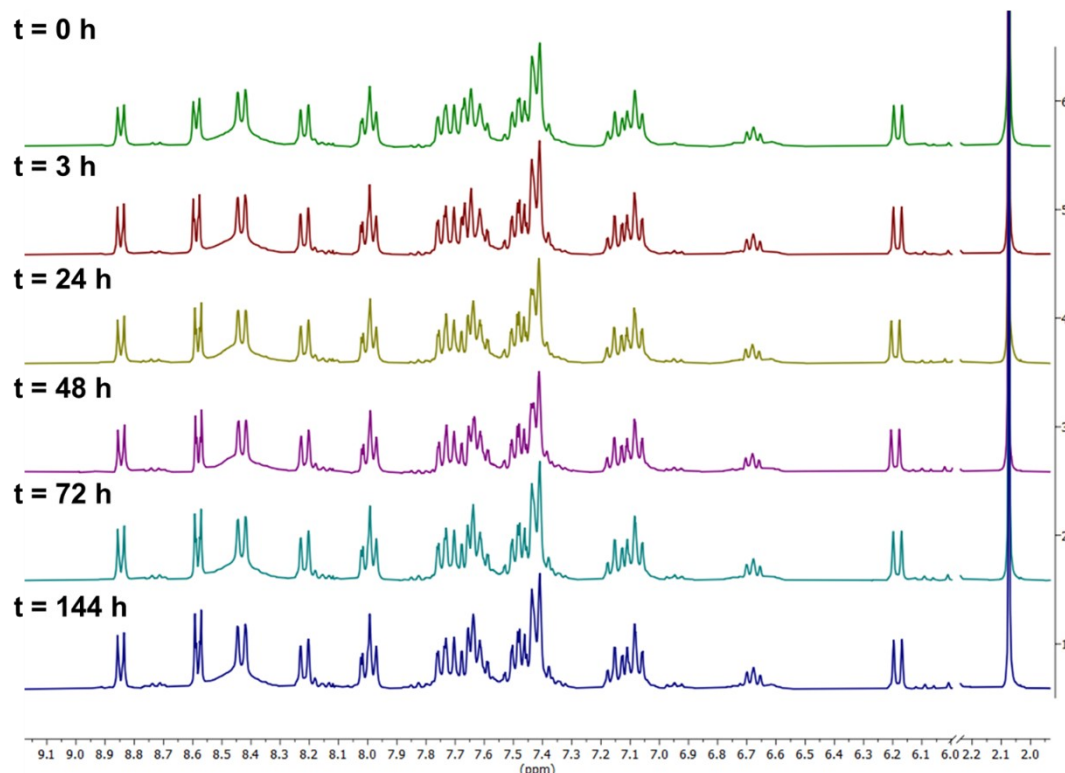


Fig. S25 ^1H NMR spectrum of a solution of complex **1** and ascorbic acid (1:10 molar ratio) in DMSO- $\text{d}^6/\text{D}_2\text{O}$ (9/1) freshly prepared, and after 3 h, 24 h, 2, 3 and 6 days of storage at 298 K.

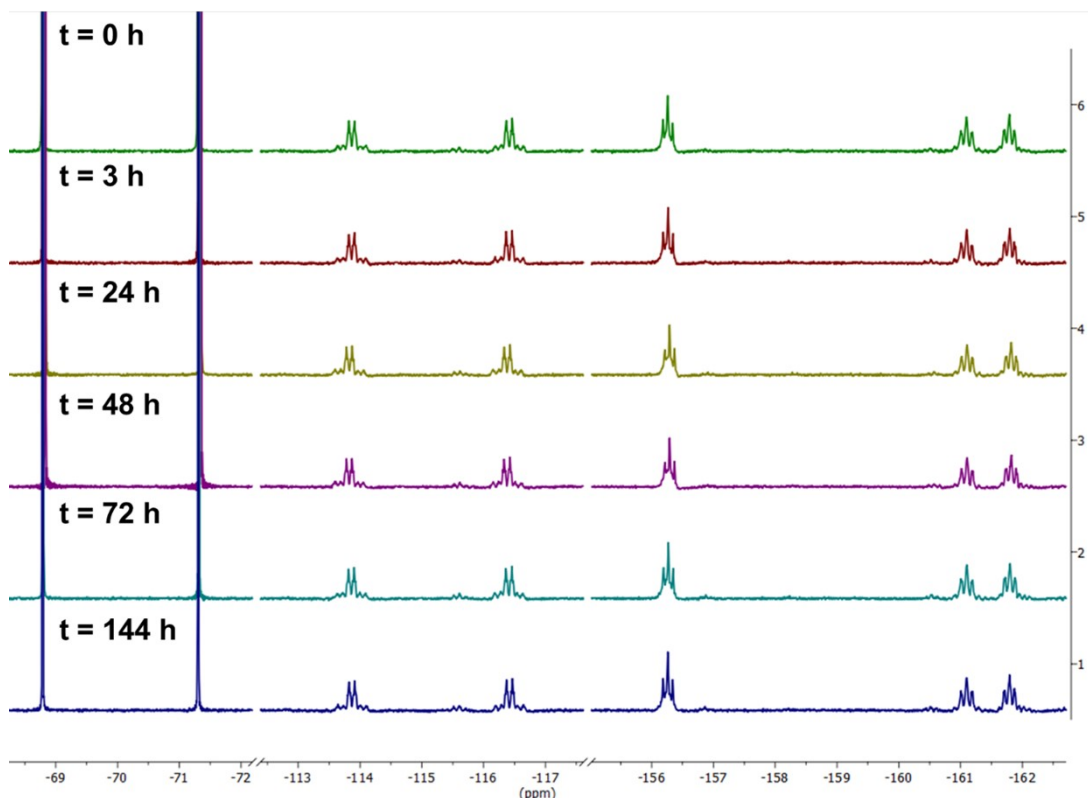


Fig. S26 $^{19}\text{F}\{^1\text{H}\}$ NMR spectrum of a solution of complex **1** and ascorbic acid (1:10 molar ratio) in $\text{DMSO-d}_6/\text{D}_2\text{O}$ (9/1) freshly prepared, and after 3 h, 24 h, 2, 3 and 6 days of storage at 298 K.

Cell lines and Culture Conditions

Two different human tumor cell lines: A549 (lung carcinoma) and HeLa (cervix carcinoma), as well as one nontumor human cell line BEAS-2B (bronchial epithelium), were cultured following the American Type Culture Collection (www.atcc.org) recommendations and standard methods, as previously described.¹³ Cells were maintained in RPMI 1640 with L-glutamine medium, supplemented with 10% fetal bovine serum (FBS), penicillin (100 U/mL) and streptomycin (100 µg/mL), kept under a humidified atmosphere of 95% air/5% CO₂ at 37°C, and sub-cultured before they get confluent using a 0.25% trypsin-EDTA solution.

Cytotoxicity Assay

The 3-(4,5-dimethylthiazol-2-yl)-5-(3-carboxymethoxyphenyl)-2-(4-sulfophenyl)-2H-tetrazolium (MTS) hydrolysis method (MTS-based CellTiter® 96. AQueous Assay; Promega Corp., Madison, WI) was used to determine the cell viability as an indicator of A549, HeLa and BEAS-2B cells sensitivity to the complexes as previously reported.¹⁴

Briefly, 50 µL of exponentially growing cells were seeded at a density of 1.5x10³ (A549 and HeLa) and 6.0 x 10³ (BEAS-2B) cells per well, in a 96-well flat-bottomed microplate in growing media, with reduced concentrations of FBS (5%) in case of A549. 24 h later, they were incubated for 72 h with the complexes that were dissolved in DMSO at 16 mM (**1**, **2** and **3**) or 8 mM (**6** and **pybt**). Cisplatin (Alfa Aesar, Karlsruhe, Germany) as a reference was dissolved at 6.4 mM in a saline solution.¹⁵ These stock solutions were kept frozen until they were dissolved in a test medium as nine 1:3.5, 1:2.5, 1:1.2 or 1:1.5 serial dilutions for the three cell lines, as required. A total of 50 µL of each dilution or complete medium alone was added to the growing cells in the 96-well plate designed as previously recommended.¹⁶ Final range concentrations in sextuplicate were: from 200 to 7.8 µM (1:1.5 dilutions) for **6** (A549 and BEAS-2B) and **pybt** (A549 and BEAS-2B); from 150 to 0.59 µM (1:1.2 dilutions) for **pybt** (HeLa); for **6** (HeLa); from 65 to 0.04 µM (1:2.5 dilutions) for **3** (HeLa); from 16 to 0.0007 µM (1:3.5 dilutions) for **3** (A549); from 15 to 0.1 µM (1:2.5 dilutions) for **1** (A549 and BEAS-2B) and **2** (A549, HeLa and BEAS-2B); from 12.5 to 0.05 µM (1:2 dilutions) for **1** (HeLa); and from 12 to 0.008 µM (1:2.5 dilutions) for **3** (BEAS-2B). In the case of cisplatin, serial dilutions were 1:1.5 ranging from 40 to 1.56 µM for A549 cells¹⁴ and 1:2 ranging from 200 to 0.78 µM for HeLa cells.¹⁵ For BEAS-2B cells, cisplatin serial dilutions were 1:2.5 ranging from 100 to 0.07 µM. After 72 h at 37 °C, 20 µL of MTS was added and plates were incubated for 1 h (A549 and HeLa) or 2 h (BEAS-2B) at 37 °C. Finally, the optical density was measured at 490 nm using a 96-well multiscanner autoreader (POLARstar Omega; BMG Labtech, Offenburg, Germany). Each experiment was repeated three times. The IC₅₀ (drug concentration that produced 50% inhibition of cell proliferation) was calculated by plotting the percentage of growing inhibition versus log of the drug concentration using the GraphPad Prism 6 (La Jolla, CA) software.

Selectivity Index

The selectivity index (SI) was calculated according to the following equation: SI = IC₅₀ non-tumor cell (BEAS-2B)/IC₅₀ tumor cells (A549 or HeLa), as previously reported.^{13a} Non-tumor BEAS-2B epithelial lung cells served as the selectivity reference to match the same tissue origin of A549 lung carcinoma (epithelial origin) cells, as suggested.¹⁷

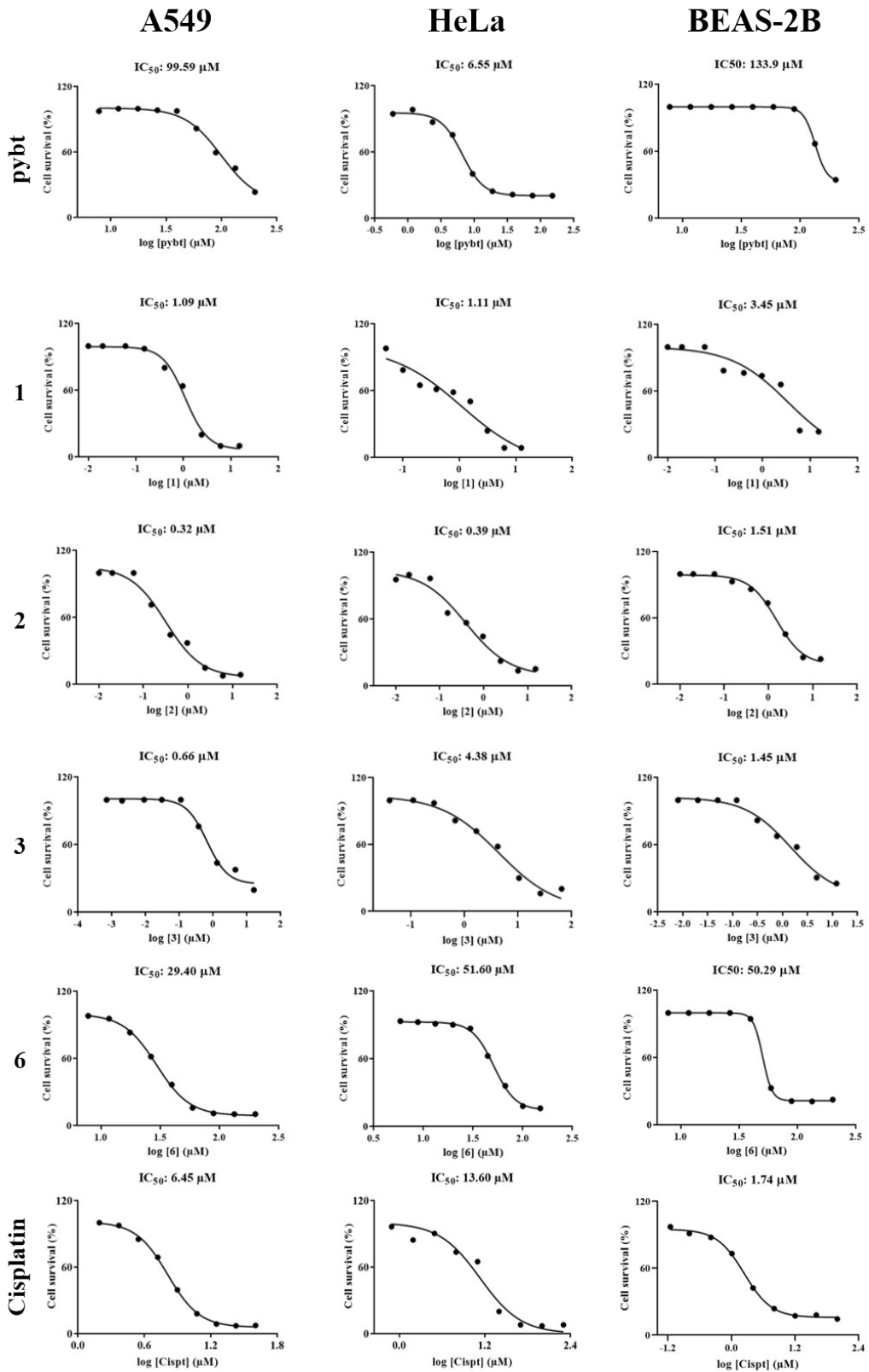


Fig. S27 Dose-response curves for determination of the IC_{50} cytotoxicity values of all compounds tested. IC_{50} cytotoxicity values of **pybt**, **1**, **2**, **3** and **6** complexes, as well as **cisplatin** in A549, HeLa and BEAS-2B cell lines. The IC_{50} values correspond to the dose required to inhibit 50% cellular growth after cellular exposure to complexes for 72 h.

***In vitro* Photocytotoxicity Testing**

Induction of phototoxicity in cultured cells was performed following previous reports, with modifications.^{13b} A549 cell were seeded in 96-well plates as described above for the MTS assay. 24 h later, cells were washed with HBSS (Hank's Balanced Salt Solution) (with 1 g/L glucose, without phenol red and pyruvate) and incubated in 50 µL sextuplicates of HBSS alone or in 1:2.5 nine serial dilutions of complex **6** ranged from 200 to 0.13 µM in HBSS for 1 h at 37°C in a 5% CO₂ atmosphere. After 1 h of exposure to the complex, plates were laid 91 mm under a LED lamp (λ_{max} 396 nm; Onforu 15W IP66) and irradiated (“photoinduced” plate) for 15 min under room normoxic atmosphere. Meanwhile, an equivalent control non-irradiated plate was manipulated in the same way (“nonphotoinduced” plate). After, cells were washed with HBSS, added 100 µL of complete medium and further incubated for 72 h at 37°C in a 5% CO₂ atmosphere. Finally, 20 µL of MTS was added to each well, plates were incubated for 1 h at 37°C and the optical density was measured at 490 nm using a 96-well multi-scanner auto reader. Each experiment was repeated three times. The IC₅₀ was calculated as described above under the Cytotoxicity Assay section.

Lipophilicity Determinations

Relative Lipophilicity measurements by RP-UPLC were performed using a Waters Acquity UPLC system (Waters, Milford, MA, USA), which was interfaced to quadrupole, high resolution, TOF mass spectrometer (micrOTOF-Q Bruker, Bremen, Germany), using an ESI interface operating in positive ion mode. The UPLC separation was performed using an Acquity UPLC BEH C18 1.7 µm particle size analytical column 100 mm × 2.1 mm (Waters) at a flow rate of 0.35 mL/min. The mobile phases used were A = H₂O with 0.1% HCOOH and B = acetonitrile with 0.1% HCOOH. The percentage of organic modifier (B) was changed linearly as follows: 0 min, 50%; 9.5 min, 99%; 11.5 min, 99%; 12 min, 20%; 12.5 min, 20%. Nitrogen (from a nitrogen generator) was used as the drying gas and nebulizing gas (2 Bar). The column temperature was set to 30°C. MS data were acquired over an m/z range of 50–3300. A capillary voltage of 4.5 kV, set end plate offset -500 V, dry gass of 7.0 L/min and set dry heater of 190° were used. Calibrations were conducted from m/z 50 to 3300 with a HCOONa solution (15 mg) in 100 mL of water. MS data were acquired in centroid mode and were processed by the DataAnalysis application manager (within Compass Data Analysis 4.2 SR2; Bruker Corporation). Samples were dissolved in 10% v/v methanol in water, ~10 µM.

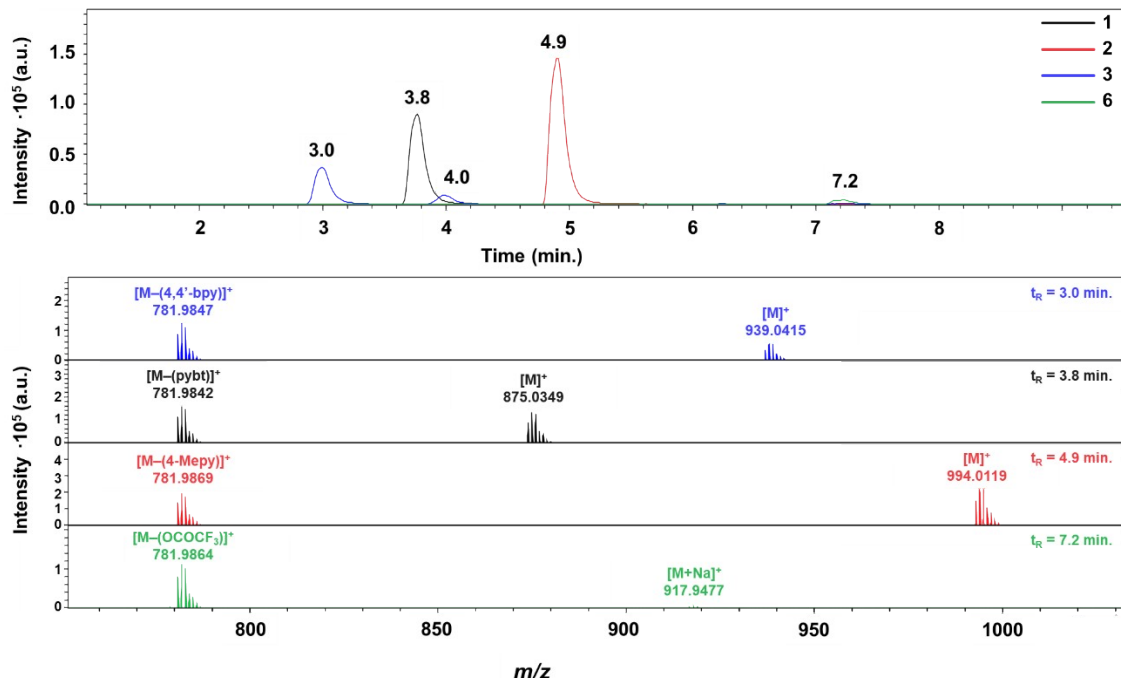


Fig. S28 RP-UPLC chromatograms with UV detection at 320 nm of 1 ppm **1-3** and **6** solutions in mobile phase, indicating the retention time for each. An Acquity UPLC BEH C18 1.7 μ m particle size analytical column 100 mm \times 2.1 mm (Waters) was used. The mobile phases used were A = acetonitrile with 0.1% HCOOH and B = H₂O with 0.1% HCOOH. The percentage of organic modifier (A) was changed linearly as follows: 0 min, 50%; 9.5 min, 99%; 11.5 min, 99%; 12 min, 50%; 12.5 min, 50%. ESI(+) Mass Spectra for UPLC fractions are shown for all complexes (m/z 875 [M]⁺ **1**, 994 [M]⁺ **2**, 939 [M]⁺ **3**, 917 [M+Na]⁺ **6** and for all 782 [M-L]⁺).

Interaction of Complexes with DNA

The interaction between complexes and cisplatin with pBR322 plasmid DNA was studied by gel electrophoresis (mobility shift assay) as previously described.^{13a, 18} The amount of DNA was kept constant (200 ng), while the concentrations of the compounds were varied to obtain increasing molar ratios with respect to plasmid DNA base pairs (0.25:1, 0.5:1, 1:1, 2:1 and 4:1). Aliquots of 2 μ L of pBR322 plasmid DNA were mixed either alone or with 0.25, 0.5, 1, 2 or 4 μ L of each compound solution (300 μ M), respectively, in a 10 μ L final volume of interaction buffer (50 mM NaClO₄, 5 mM Tris-HCl, pH 7.5). Mixtures were incubated at 37 °C for 20 h in the dark and, after the addition of 2 μ L of loading dye, were loaded onto 1% (w/v) agarose gels made in Trisacetate/ ethylenediaminetetraacetic acid (EDTA) buffer (TAE) and separated by electrophoresis for 4 h at 70 V in TAE. Finally, gels were dyed for 30 min by immersion in a 3X solution of GelRed nucleic acid gel stain (Biotium Inc., Fremont, CA) diluted in 100 mM NaCl and images registered using a Gel-Doc System with the help of Quantity One software (BioRad, Hercules, CA).

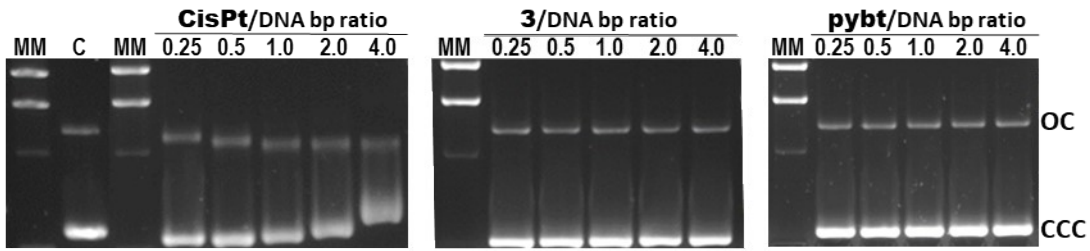


Fig. S29 Electrophoresis mobility shift assay for cisplatin and complexes **3** and **pybt**. C, control lane, DNA without compound; **CisPt**, cisplatin; MM, λ HindIII DNA molecular marker; Numbers refer to complex/plasmid DNA (pBR322); base pairs (bp) increasing ratios; OC, open circular (relaxed) plasmid DNA form; CCC, covalently closed circular (supercoiled) plasmid DNA form (as described in Ref. ^{13a}).

References

1. N. Giménez, R. Lara, M. T. Moreno and E. Lalinde, *Chem. Eur. J.*, 2017, **23**, 5758-5771.
2. D.-F. Shi, T. D. Bradshaw, S. Wrigley, C. J. McCall, P. Lelieveld, I. Fichtner and M. F. G. Stevens, *J. Med. Chem.*, 1996, **39**, 3375-3384.
3. L. D. Ciana and A. Haim, *J. Heterocycl. Chem.*, 1984, **21**, 607.
4. G. M. Sheldrick, *Acta Crystallogr., Sect. A: Found. Crystallogr.*, 2015, **71**, 3-8.
5. L. J. Farrugia, *Appl. Crystallogr.*, 1999, **32**, 837-838.
6. G. Sheldrick, *Acta Crystallogr., Sect. C*, 2015, **71**, 3-8.
7. M. J. Frisch, G. W. Truks, H. B. Schlegel, G. E. Scuseria, M. A. Robb, J. R. Cheeseman, G. Scalmani, V. Barone, G. A. Petersson, H. Nakatsuji, X. Li, M. Caricato, A. V. Marenich, J. Bloino, B. G. Janesko, R. Gomperts, B. Mennucci, H. P. Hratchian, J. V. Ortiz, A. F. Izmaylov, J. L. Sonnenberg, D. Williams-Young, F. Ding, F. Lipparini, F. Egidi, J. Goings, B. Peng, A. Petrone, T. Henderson, D. Ranasinghe, V. G. Zakrzewski, J. Gao, N. Rega, G. Zheng, W. Liang, M. Hada, M. Ehara, K. Toyota, R. Fukuda, J. Hasegawa, M. Ishida, T. Nakajima, Y. Honda, O. Kitao, H. Nakai, T. Vreven, K. Throssell, J. A. Montgomery, Jr., J. E. Peralta, F. Ogliaro, M. J. Bearpark, J. J. Heyd, E. N. Brothers, K. N. Kudin, V. N. Staroverov, T. A. Keith, R. Kobayashi, J. Normand, K. Raghavachari, A. P. Rendell, J. C. Burant, S. S. Iyengar, J. Tomasi, M. Cossi, J. M. Millam, M. Klene, C. Adamo, R. Cammi, J. W. Ochterski, R. L. Martin, K. Morokuma, O. Farkas, J. B. Foresman, and D. J. Fox, Gaussian 16, Revision A.03, Inc., Wallingford CT, 2016.
8. (a) A. D. Becke, *J. Chem. Phys.*, 1993, **98**, 5648-5652; (b) A. D. Becke, *Phys. Rev. A*, 1988, **38**, 3098-3100.
9. W. R. Wadt and P. J. Hay, *J. Chem. Phys.*, 1985, **82**, 284-298.
10. V. Barone and M. Cossi, *J. Phys. Chem. A*, 1998, **102**, 1995-2001.

11. N. M. O'Boyle, A. L. Tenderholt and K. M. Langner, *J. Comput. Chem.*, 2008, **29**, 839-845.
12. R. Schmidt, C. Tanielian, R. Dunsbach and C. Wolff, *J. Photochem. Photobiol. A: Chem.*, 1994, **79**, 11-17.
13. (a) G. Millán, N. Giménez, R. Lara, J. R. Berenguer, M. T. Moreno, E. Lalinde, E. Alfaro-Arnedo, I. P. López, S. Piñeiro-Hermida and J. G. Pichel, *Inorg. Chem.*, 2019, **58**, 1657-1673; (b) R. Lara, G. Millán, M. T. Moreno, E. Lalinde, E. Alfaro-Arnedo, I. P. López, I. M. Larráyoz and J. G. Pichel, *Chem. Eur. J.*, 2021, **27**, 15757-15772.
14. J. R. Berenguer, J. G. Pichel, N. Giménez, E. Lalinde, M. T. Moreno and S. Piñeiro-Hermida, *Dalton Trans.*, 2015, **44**, 18839-18855.
15. E. Lalinde, M. T. Moreno, R. Lara, I. P. López, E. Alfaro-Arnedo, J. G. Pichel and S. Piñeiro-Hermida, *Chem. Eur. J.*, 2018, **24**, 2440-2456.
16. OECD. 2010. Guidance Document on using Cytotoxicity Tests to Estimate Starting Doses for Acute Oral Systemic Toxicity Tests. No. 129, París, France. Available at: [<http://www.oecd.org/env/testguidelines>].
17. M. López-Lázaro, *Oncoscience*, 2015, **2**, 91-98.
18. M. Frik, J. Jimenez, V. Vasilevski, M. Carreira, A. de Almeida, E. Gascon, F. Benoit, M. Sanau, A. Casini and M. Contel, *Inorg. Chem. Front.*, 2014, **1**, 231-241.